UNIVERSITY OF SOUTHAMPTON

SINGLE FREQUENCY AND HIGH POWER OPERATION OF DIODE-PUMPED SOLID-STATE LASERS

by Anthony Brian Neilson

A thesis submitted for the Degree of Doctor of Philosophy

FACULTY OF SCIENCE

OPTOELECTRONICS RESEARCH CENTRE

December 1993

UNIVERSITY OF SOUTHAMPTON

ABSTRACT

FACULTY OF SCIENCE

OPTOELECTRONICS RESEARCH CENTRE

Doctor of Philosophy

SINGLE FREQUENCY AND HIGH POWER OPERATION OF DIODE-PUMPED SOLID-STATE LASERS

by Anthony Brian Neilson

In recent years, advances made in semiconductor diode lasers have led to a resurgence in the development of solid-state lasers. Diode-pumped solid-state lasers (DPSSLs) are typically more compact, efficient, reliable and economical than alternative laser sources. In this thesis two areas of research in the field of DPSSLs have been investigated, namely single frequency ring lasers and high power diode bar pumped solid-state lasers.

Single frequency laser sources are important in a wide range of applications, and a number of methods are available for producing single frequency operation. In this work an acousto-optic modulator was used in a ring laser cavity to enforce unidirectional operation, which in turn can produce single frequency output. Acousto-optic devices can provide a simple, low-loss means of enforcing unidirectional operation in ring lasers, compared to other methods. Previously, the means by which this was accomplished was not understood. Here, two distinct mechanisms are described that can be used to enforce unidirectional operation, experimental verification is provided, and the implications that this has for the development of single frequency sources are discussed. Ring lasers were also constructed which operated at wavelengths of 1.3μm and 2μm, using acousto-optic modulators to produce unidirectional operation.

Diode bar lasers have recently emerged as one of the most economical pump sources for solid-state lasers, and are capable of producing high output powers in side-pumping geometries. In this thesis, the use of diode bars in end-pumping configurations is explored, as such systems potentially offer much higher efficiencies than side-pumping, and should be more suitable for output powers up to a few tens of watts. A significant problem with diode bar end-pumped systems is that the dimensions of the diode bar (10mm x 1μm) make it difficult to effectively couple their output into the lasing mode of a solid-state laser. In this thesis, initial attempts to end-pump lasers are described. Some degree of success was obtained. Also presented is a novel optical arrangement that manipulates the diode bar output to produce a beam with a much higher degree of symmetry, and hence, suitability for end-pumping. This system, using just two mirrors to chop up and rearrange the diode beam, has applications in a wide variety of situations involving laser beams with a large difference in dimensions and divergence properties in two orthogonal directions, and should allow diode bars to be effectively used for end-pumping solid-state lasers. Preliminary results for end-pumping a solid-state laser are presented, which offer great promise for optimised laser systems.

to Paula...

Table of Contents

ACKNOWLEDGEMENTS

CHAPTER 1 INTRODUCTION

1.1 Background 1
1.2 Diode-Pumped Solid-State Lasers 3
1.2.1 History 3
1.2.2 Basic Properties of Diode Lasers 5
1.2.3 Advantages of Diode Laser Pumped Solid-State Lasers 7
1.2.4 Diode Laser Coupling Schemes 9
1.2.5 Laser-diode end-pumping of solid-state lasers 11
1.3 Outline of Thesis 15

References 16

CHAPTER 2 ACOUSTO-OPTICALLY INDUCED UNIDIRECTIONAL OPERATION OF RING LASERS

2.1 Introduction 17
2.2 Spatial Hole Burning 22
2.3 The Acousto-Optic Effect 28
2.4 Intrinsic Mechanism for Unidirectional Ring Laser Operation 38
2.4.1 Theory 38
2.4.2 Experimental Verification 45
2.4.3 Optimisation and Discussion 50
2.5 Feedback Mechanism for Unidirectional Operation 51
2.5.1 Theory 51
2.5.2 Experimental Verification 55
2.5.2.1 Effective Diffraction Loss 55
2.5.2.2 External Feedback Cavities 60
2.5.2.3 Self-feedback Cavities 64

2.6 A 1.3μm Unidirectional ring laser 66
2.6.1 Experimental Details 66
2.6.2 Results 68
2.6.3 Explanation of Two-Frequency Operation 72
2.6.4 Future Work 74
2.7 A 2μm Unidirectional Ring Laser 75
2.7.1 Introduction 75
2.7.2 Experimental 76
2.7.3 Results 78
2.7.4 Discussion 80
2.8 Future Work 81

References 82

CHAPTER 3 DIODE BAR PUMPED SOLID-STATE LASERS

3.1 Introduction 84
3.1.1 Fibre Bundles 87
3.1.2 Compound Lens Systems 88
3.1.3 Cylindrical Microlenses 89
3.1.4 Binary Optics Systems 91
3.1.5 Multi-Diode Bar End-Pumped Lasers 92
3.2 Initial Experimental Investigations 94
3.2.1 Nd:YAG Side-Pumped Laser 96
3.2.2 Nd:GGG Side-Pumped Laser 101
3.3 Diode Bar End-Pumping 106
3.3.1 Cylindrical Mirror End-Pumped Resonator 109
3.2.3 Variable Curvature Mirror End-Pumped Resonator 112

References 121

CHAPTER 4 DIODE BAR BEAM SHAPING TECHNIQUE

4.1 Introduction 124

4.2 Beam Shaping Technique 129

4.3 Experimental Implementation 136

4.3.1 Introduction 136

4.3.2 Pumping Scheme 139

4.3.3 End-Pumping Performance 149

4.3.4 System Improvements 152

4.4 Discussion 155

References 159

CHAPTER 5 CONCLUSIONS AND FUTURE WORK 160

APPENDIX A: FABRY-PEROT ANALYSIS OF FEEDBACK MECHANISM 163

APPENDIX B: PUBLISHED PAPERS 169

ACKNOWLEDGEMENTS

I would first like to express my sincere thanks to my supervisor, Professor David Hanna, for his guidance and assistance during the course of this PhD, and his helpful approach to many of the problems I have encountered, both in the lab and out. Special thanks are also due to Dr Andrew Clarkson, for his guidance in the labs, and many useful discussions and thoughts throughout my research.

Many thanks also to those friends in the department who helped me in many other ways, especially golf, and who made sure that I didn't acquire an English accent in my time spent here.

As a non-E.C. based student, much financial support has been necessary to enable me to complete my studies. Initial funding from Rotary International, in the form of a Rotary Foundation Scholarship, enabled me to complete my first year here. Ongoing support from Telecom Australia Research Labs for conferences, fees and living expenses have made it possible to continue in my second and third years, as have an Overseas Research Studentship awarded by the Committee of Vice-Chancellors and Principals, and a University of Southampton Research Studentship. The assistance of Mr Bruce Chisholm from TRL in obtaining ongoing support is greatly appreciated.

The support of my family (at long distance) has also been invaluable and much appreciated, as has the love and support of Paula, who has helped me get through the last three years by always being there. Finally, thanks to James, for sleeping through the nights, and for showing me that some things in life are even better than lasers!

Chapter 1
INTRODUCTION

1.1 Background

Diode-pumped solid-state lasers have been a major area of growth in laser physics in recent years. The development of more efficient and reliable diode lasers, coupled with novel solid-state laser designs has led to the opening up of many new areas of research. Two areas in particular have aroused much interest, with many potential applications in each. These areas, high power diode bar pumped solid-state lasers, and single frequency ring lasers, are explored in this thesis, with emphasis on the means of implementing them in practical systems.

The advent of high power diode-laser structures in the form of linear arrays (or *bars*) which offer tens of watts of output power from an active area only 1cm wide has offered the promise of solid-state laser performance with powers an order of magnitude greater than with conventional diode lasers. These devices are by far the cheapest source of laser photons for pumping solid-state lasers, in terms of price/Watt, and the ability to use them efficiently and effectively is becoming more important as researchers seek higher powers for a variety of applications. These diode bars pose some difficulties when it comes to using them to end-pump solid-state lasers, and in this thesis a number of means of efficiently exploiting their high power output are explored, with a novel, and we believe, highly useful method being described in Chapter 4. We expect that this method could be used to improve the performance of many conventional diode end-pumped laser systems, and may lead to diode bars becoming a more attractive pump source for solid-state lasers.

A second area of much interest is the development of single frequency sources for applications such as laser radar, micromachining, injection seeding, remote sensing, gravitational wave detection, and as pump sources for non-linear systems. Unless special steps are taken, most lasers tend to oscillate on more than one axial mode,

which leads to instabilities in the output power and wavelength. There are a number of ways of removing these extra axial modes to achieve single frequency operation. In solid-state lasers, a common way of doing this is to eliminate spatial hole burning in the gain medium, which provides gain for additional axial modes to lase. This is accomplished by constructing a ring laser which is made to oscillate unidirectionally, hence removing standing waves in the cavity and thereby the spatial hole burning that accompanies them. Unidirectional operation is enforced by some form of optical diode, and in this thesis we describe how the acousto-optic effect can be used to implement an optical diode. Previously, it had been observed that using an acousto-optic modulator in a ring laser could lead to unidirectional operation, but no explanation of the underlying mechanism responsible was available. In this thesis we describe the physical basis responsible for unidirectional operation via the acousto-optic effect, and in fact we describe two distinct mechanisms that we have identified. We also present a number of applications of the acousto-optic effect to particular solid-state ring laser systems.

These two themes of solid-state laser development have been examined separately in this thesis, and at first appear to be totally distinct areas of study. However, we expect that the diode bar end-pumping scheme we describe should be suitable to pump a ring laser. This would ultimately enable us to construct a high-power, diode-bar pumped single frequency ring laser, for which a number of uses can be anticipated, with a particular interest being pumping a cw optical parametric oscillator.

1.2 Diode Pumped Solid-State Lasers

In recent years diode-pumped solid-state lasers have emerged as efficient, stable, compact and versatile sources of laser radiation. Advances made in semiconductor diode lasers in the last decade have made this possible, with much improved reliability, cost and performance providing an ideal pump source for many solid-state lasers. A number of extensive reviews on this subject have been written, e.g. [Byer, 1988], [Fan, 1988], [Malcolm, 1991], [Hughes, 1992] and the reader is referred to these for a detailed overview of this field. In this section an introduction to the main points of interest for the work presented in the following chapters will be given.

1.2.1 History

Diode lasers were first produced over 30 years ago [Hall, 1962], [Nathan, 1962], [Holonyak, 1962]. It was realised from the outset that the emission from GaAs or GaAlAs diodes, which is around 800nm would overlap with a strong absorption band of the trivalent ion of the rare earth element Neodymium (Nd^{3+}), as shown in Figure 1.1(a) and (b). Newman [1963] was the first to show that the output from a GaAs diode (LED as opposed to laser) could excite fluorescence near 1.06μm in Nd^{3+} doped $CaWO_4$. Keyes and Quist [1964] demonstrated the first diode laser pumped solid-state laser, using a GaAs laser to pump $CaF_2:U^{3+}$, and suggested that a GaAs diode would be ideal for pumping a Nd^{3+} laser. The first diode-pumped Nd:YAG laser was then constructed by Ross [1968], where a number of comments made about its performance still hold true today. After noting that 1.2mJ of flashlamp pump was required for lasing, compared with only 0.06mJ of diode laser power (with the diode cooled to 170K), he commented that "..a YAG laser acts as a temporary energy storage device so that many pulses from many semiconductor diode lasers can be collected together and emitted as one giant pulse ... the YAG laser acts as an energy director ... the spectral width of the YAG laser is many times narrower than semiconductor lasers". All these are still very important reasons for the use of diode-pumped solid-state lasers today.

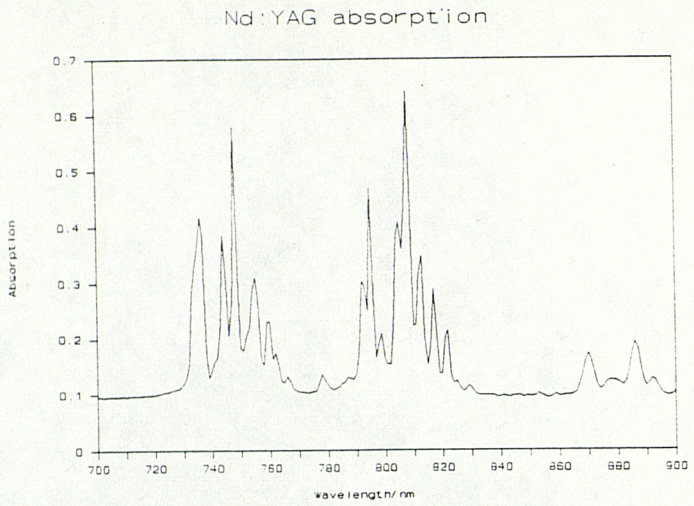

Fig 1.1(a) The absorption spectrum of Nd^{3+} in Yttrium Aluminium Garnet (YAG) crystal shows a very strong peak around 807nm.

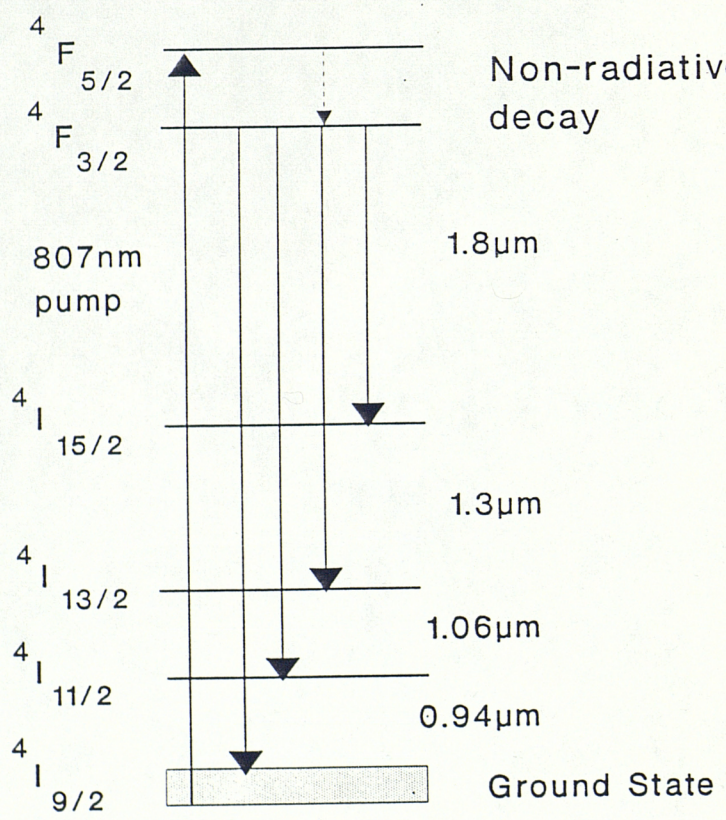

Fig 1.1(b) Energy bands in Nd^{3+}. Pumping at around 807nm excites electrons to the $^4F_{5/2}$ level, where rapid non-radiative decay to the upper laser level ($^4F_{3/2}$) occurs. The strongest lasing transition is to the $^4I_{11/2}$ level, which corresponds to a wavelength around 1.06 μm.

After further work on diode-pumped lasers, including room temperature operation of a Nd:YAG laser [Ostermayer, 1971], the use of diode pumping did not advance as rapidly as might have been expected, mainly due to the short operating lifetime of diode lasers and the low powers available from them. Advances made in fabrication techniques during the 1980's has led to what has been termed a renaissance of solid-state lasers, due to the availability of cheap, reliable, compact diode laser sources with output powers continuing to rise year by year, with an increasing number of different diode laser devices. Since the mid 1980's, when highly efficient miniature diode end-pumped Nd:YAG lasers were demonstrated [Zhou, 1985], [Sipes, 1985], the performance of diode-pumped solid-state lasers has continued to improve, driven by the development of ever more powerful and sophisticated diode laser sources.

1.2.2 Basic Properties of Diode lasers

While semiconductor diode lasers have been in existence for over 30 years, it is only relatively recently that significant advances in their performance have been made, with new structures being manufactured, resulting in vastly increased output powers and a greater variety of devices being available. The basic principle of operation remains the same: light is generated in an active region by the recombination of electron-hole pairs after charge injection across a forward biased p-n junction. The laser cavity is defined by the cleaved ends of the semiconductor material (e.g. GaAlAs, InGaAs, AlGaInP), where the reflectivity is sufficient to enable lasing to occur, although the rear facet can be made into a high reflector with appropriate dielectric coatings. It is the nature of the junction formed that has undergone the greatest change, with more complex and miniaturised structures resulting in more efficient devices. These changes have been made possible by advances in fabrication techniques such as molecular beam epitaxy (MBE) and metal-organic chemical vapour deposition (MOCVD).

The evolution of diode lasers has followed the path from single heterostructures, where the active region of GaAs is bounded on the p-side by a GaAlAs layer, to double heterostructure where the active region is bounded on both sides by a material of different composition, to double heterostructures with smaller active regions. Reducing

the dimensions of the active region lowers the threshold current for lasing, which has led to the development of quantum well lasers, where the active layer thickness is less than 30nm, of the order of the de Broglie wavelength of the electron. Typically, quantum well lasers are configured as either multiple quantum well (MQW), graded-index separate confinement heterostructures (GRINSCH) or single quantum well, separate confinement heterostructures (SQW-SCH). These devices can have overall electrical to optical conversion efficiencies exceeding 50%, which has led to them becoming the preferred pump source for solid-state lasers.

The operating wavelength of diode lasers can be changed by altering the composition of the materials used, thus changing the size of the bandgap at the junction. For example, in diode lasers around 800nm, the material used is $Ga_{1-x}Al_xAs$, where $x \simeq 0.09$ for devices operating on the 807nm Nd:YAG absorption line. By varying the aluminium concentration the emission wavelength can be tuned over the range 680-900nm [Striefer, 1988], although the performance and lifetime drops sharply at the extremes of this range, and commercial devices are usually in the range 780-860nm. Changing the material entirely allows different wavelength ranges to be accessed, e.g., InGaAs for 900nm-1.1μm and AlGaInP for 630-690nm. At present, much work is devoted to achieving reliable room-temperature blue wavelength diodes, as these would allow much greater densities to be achieved in optical storage systems, but commercial products have not yet been realised. Fine tuning of the lasing wavelength can then be achieved by varying the operating temperature of the diode. For GaAlAs lasers the wavelength is tuned by approximately 0.25nm/°C. Typically, Peltier coolers can provide a 40° temperature range, resulting in a wavelength tuning range of 10nm. This easily allows the diode output to be accurately matched to the peak of the solid-state laser absorption.

Other factors which make diode lasers attractive in many applications include their long lifetimes (in excess of 10^5 hours extrapolated from elevated temperature tests), ease of production (e.g. for the many millions of compact disc players, optical storage devices and laser printers), ability to modulate them at high frequencies ($>$ 10GHz), compactness and versatility of devices available. To illustrate the range of semiconductor diode lasers commercially available (let alone those that exist only in

laboratories), the following list presents a selection of diodes currently in the marketplace (Spectra Diodes Labs 1993 Catalogue) :

GaAlAs Diode lasers (780-860nm)

20W cw diode bar (10mm x 1μm emitting region)

100W quasi-cw diode array (10mm x 1μm)

5000W quasi-cw stacked array (10mm x 19.6mm)

3W diode array (500μm x 1μm)

100mW single longitudinal and axial mode

10W cw fibre coupled diode lasers

4W cw high brightness (500μm x 1μm, single emitting area)

InGaAs Diode lasers (910-1020nm)

1W cw diode array (100μm x 1 μm)

60W quasi-cw linear array (10mm x 1μm)

360W quasi-cw stacked array (10mm x 2mm)

1W cw single transverse and axial mode master oscillator/power amplifier (MOPA) monolithically integrated laser package.

ALGaInP Visible Diode laser (670-690nm)

500mW cw (250μm x 1 μm)

3W cw fibre couple diode laser bar (400μm fibre diameter)

1.2.3 Advantages of Diode laser Pumped Solid-State Lasers

It is worthwhile to briefly consider why diode-pumped solid-state lasers are used rather than just the diode laser itself, which would be much more efficient, and why they are preferred to flashlamp pumped lasers, which have been extensively used for the last 30 years. To address the second point, the output from diode lasers is in a relatively narrow spectral band (2-3nm) and can be readily tuned to overlap the absorption bands of many solid-state laser materials. This can lead to very efficient

optical pumping whereas the broad band output of flashlamps is not absorbed very well, which can result in low efficiency and excess heat generation. Total electrical to optical conversion of up to 15.8% [Fields, 1988] with diode-pumped solid-state lasers has been reported, compared to 8% in a lamp-pumped system [Mak, 1984], which was an atypical configuration. More typical lamp-pumped systems give around 5% efficiency. The water cooling required for flashlamp pumped systems increases the technical noise of the system, which means that the laser linewidth is greater than that of diode-pumped systems. Whilst flashlamps have traditionally been used for very high power operation of solid-state lasers, rapid recent advances in diode laser technology has meant that diode-pumped systems with in excess of 1kW cw powers [Comaskey, 1993] have been developed, so that the potential exists for similar output powers to that obtained by all but the largest flashlamp pumped systems.

While diode lasers provide a cheap source of "raw" photons for pumping solid-state lasers and are compact, robust, efficient and reliable devices, the output from them is often not suitable to use directly. Emission from diode lasers is typically only partially coherent, has a large frequency spectrum compared to solid-state lasers, poor spatial properties and they are restricted in the maximum output available. By pumping a solid-state laser we can achieve a number of significant improvements over using just the diode laser, as the following points outline:

(a) The output will usually be in a diffraction limited beam, thus improving the spatial quality.

(b) We can increase the output power by either coupling the output from many diode lasers into a single laser rod or by using the long upper laser level lifetimes of solid-state materials to store energy from the diode pump and releasing it as high power Q-switched pulses.

(c) Diode lasers are restricted in the range of frequencies that can be produced, but using different solid-state lasers allows a much wider choice of frequencies to be selected.

(d) The fundamental limit on laser linewidths is given by the Schawlow-Townes equation [Schawlow, 1958]:

$$\Delta\nu = \frac{h\nu}{2\pi\tau_c^2 P} \qquad (1.1)$$

where $\Delta\nu$ is the linewidth in Hertz, τ_c is the cavity decay time, $h\nu$ the photon energy and P the laser output power. For diode-pumped solid-state lasers the fundamental linewidth limit is less than 1Hz for 1mW output [Zhou, 1985]. Diode lasers, on the other hand, have fundamental linewidths some 6 orders of magnitude greater, due to the short length of their cavities and low reflectivity of their facets which gives a cavity decay time 10^{-3} times that of solid-state lasers.

In summary, diode laser-pumped solid-state lasers can provide spectral and spatial brightness "amplification" of the diode lasers, and operate more economically and efficiently than any flashlamp-pumped system.

1.2.4 Diode laser Coupling Schemes

An important issue to resolve with the use of diode lasers is the best way to efficiently collect and couple their output into the lasing mode of the solid-state laser. Diode lasers almost always have different dimensions in the x and y planes, and hence different beam properties in these two directions. A typical single-stripe device could have an emitting region with dimensions 3 μm x 1 μm, leading to an elliptical output beam which would usually need to be circularised to match the lasing mode. One way of doing this is to first collimate the output, either with a single spherical lens or compound lens, and then use an anamorphic prism beam expander to magnify the beam in one direction so that the two dimensions are equalised. Such an expander can produce a magnification of 3-7 times in one direction. The same technique can be used for larger diode laser arrays, although further elements such as crossed pairs of cylindrical lenses may be necessary to equalise the x and y spot sizes. If the lenses and prisms used are antireflection coated at the diode wavelength, the throughput can be very high, at least 90%.

If the requirements for equal spot sizes do not have to be met, a simpler and more compact means of collecting and focusing the diode output may be to use a

gradient-index (GRIN) lens [Zhou, 1985]. There may be some loss in overall efficiency due to the mismatch of pump and laser mode sizes in one dimension, but the simplicity of the laser system (Fig 1.2) may be attractive in some applications.

An alternative method is to use an optical fibre to collect the output, and then deliver this to a remote laser. Multimode fibre (with, say, 100-400 μm core diameter) placed close to the diode laser facet can collect around 50% of the output. While not as efficient, such systems are convenient to use, and are particularly suited for fibre laser and medical applications. This approach has also been used for diode laser bars where a separate fibre is used to collect the output of each emitting region. The fibres are bundled together to circularise the output and then focused down. This method is inefficient (around 50% throughput in commercial devices) and produces a highly divergent output beam.

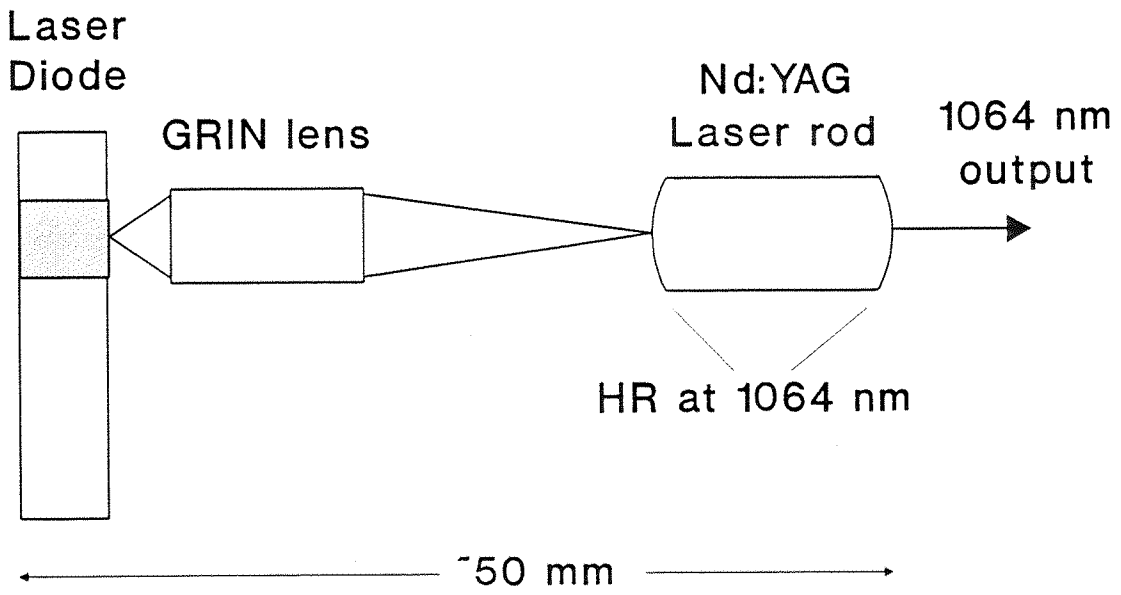

Fig 1.2 Schematic of laser as used by Zhou [1985]. The diode laser output is collected and focused by the GRIN lens, which pumps a monolithic Nd:YAG laser, to give TEM_{00} output at 1.064 μm. The monolithic laser has curved ends which have a highly reflecting dielectric coating applied to them.

1.2.5 Laser-diode end-pumping of solid-state lasers

In the work described in later sections of this thesis, most of the systems use diode lasers to end-pump (or "longitudinally-pump") solid-state lasers. In this section some of the basic properties of such systems are considered, with reference to lasing threshold, slope efficiency and output beam quality. As most pump bands in solid-state laser materials can be well matched to diode laser wavelengths, thermal problems only arise for high power operation, and will not be considered at this stage. A schematic of a typical laser-diode end-pumped solid-state laser is shown in Fig 1.3. Other configurations are also widely used, e.g. using the laser rod as the cavity itself, as shown in Fig 1.2 above, but the example shown here is of the general type used in much of the work described in this thesis.

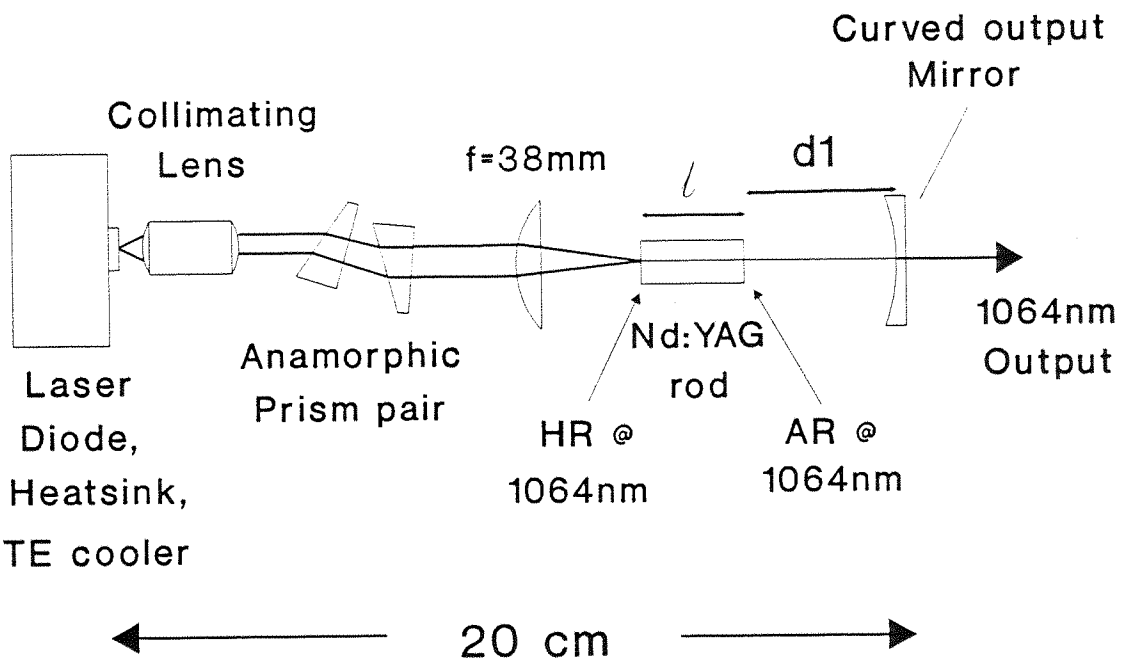

Fig 1.3 Diode laser end-pumping. The output from the diode, which is mounted on a heatsink and cooled with a thermo-electric (TE) cooler, is first collimated and then expanded up by the anamorphic prism pair, finally being focused into the laser rod. The laser cavity comprises a dielectric mirror coated on one end of the laser rod, which is highly reflecting at the lasing wavelength and transmits the pump, and an output coupler.

The first point to consider is the nature of the lasing mode in this resonator. The lasing mode can in general be a combination of higher order transverse Hermite-Gaussian modes, but the best spatial properties are obtained for the lowest order mode, i.e. the TEM_{00} mode, which has a purely Gaussian profile. It is this mode of operation that we seek to establish in our diode-pumped lasers. Misalignment of the pump beam with the lasing mode, or having the laser's fundamental mode much smaller than the pump spot size can allow higher-order transverse modes to lase, but this can often be corrected. The lasing mode will propagate as a Gaussian beam, i.e. for a beam travelling in the z-direction, the beam radius w, will evolve as:

$$w(z)=w_0\left[1+\left(\frac{\lambda(z-z_0)}{\pi w_0^2}\right)^2\right]^{1/2} \qquad (1.2)$$

where λ is the laser wavelength, and w_0 is the laser waist size (radius) located at z_0, the waist position (i.e. where the beam wavefront is plane), which will be located at the plane mirror in the rod and be given by:

$$w_0^2=\frac{\lambda}{\pi}\sqrt{d(R-d)} \qquad (1.3)$$

where R is the radius of curvature of the output coupler and d the effective length of the cavity. The effective length is the sum of the free-space cavity length and equivalent length of the laser rod in air, which is ℓ/n, where ℓ is the physical length of the rod, and n is the refractive index of the medium. The effective length of the rod is used, as the wavelength of the laser beam is reduced by 1/n in the medium, and hence the diffraction of the beam is reduced by the same amount. This then determines the Gaussian beam propagation. Referring to Fig 1.2, the effective length of the cavity is $d=\ell/n+d_1$.

Knowing the lasing mode size we then need to match the focused spot-size of the diode laser pump to it to achieve as efficient operation as possible. As shown by Clarkson [1989], the threshold (P_{th}) and slope efficiency (η), just above threshold, for end-pumped 4-level laser systems are given by

$$P_{th}=\frac{\pi h\nu_p L}{4\sigma_f\tau_f\alpha_p\eta}\left[\int_0^{\ell}\frac{\exp(-\alpha_p z)\,dz}{(w_{px}^2+w_{Lx}^2)^{1/2}(w_{py}^2+w_{ly}^2)^{1/2}}\right]^{-1} \tag{1.4}$$

and

$$\eta=\frac{T\nu_L}{L\nu_p}[1-\exp(-\alpha_p\ell)]\eta_q\eta_{pl} \tag{1.5}$$

where ν_p is the pump frequency,

ν_L is the lasing frequency,

L is the round trip loss in the cavity,

T is the output coupler transmission,

τ_f is the fluorescence lifetime of the upper laser level,

α_p is the absorption coefficient of the pump in the laser medium,

ℓ is the length of the laser medium, and

η_q is the pumping quantum efficiency, i.e. the fraction of the absorbed pump photons producing upper state population of the laser.

The pump and laser spot sizes in the x and y planes, $w_{px}(z)$, $w_{py}(z)$, $w_{Lx}(z)$, $w_{Ly}(z)$ can in general be different and have a z-dependence, and are assumed to be Gaussian beams (TEM_{00}). The η_{pl} term in the slope efficiency is given by the effective overlap of the pump beam with the lasing mode inside the medium:

$$\eta_{pl}=\frac{w_{Lx}w_{Ly}(2w_{px}^2+w_{Lx}^2)^{\frac{1}{2}}(2w_{py}^2+w_{Ly}^2)^{\frac{1}{2}}}{(w_{px}^2+w_{Lx}^2)(w_{py}^2+w_{Ly}^2)} \tag{1.6}$$

If we take the simple case of $w_{Lx} = w_{px}$ and $w_{Ly} = w_{py}$ (i.e. matching pump dimensions to lasing mode) then $\eta_{pl}=0.75$, and further assuming that the w's have no z-dependence (reasonable for large mode sizes over an absorption length), (1.4) and (1.5) reduce to

$$P_{th} = \frac{2\pi h\nu_p L}{4\sigma\tau_f\eta_q(1-\exp(-\alpha_p\ell))} w_{Lx} w_{Ly} \qquad (1.7)$$

and

$$\eta = \frac{3T\nu_L\eta_q}{4L\nu_p}(1-\exp(-\alpha_p\ell)) \qquad (1.8)$$

Generally, with diode end-pumped lasers, the length of the laser medium is chosen to be of the order of 1 or 2 pump absorption lengths long, as pump light which diverges more rapidly than the fundamental lasing mode can excite higher order transverse lasing modes. With these relationships for threshold pump power and slope efficiency it is possible to optimise the design of miniature diode-pumped solid-state lasers, by, for example, changing the output coupling (T) or reducing the net loss in the cavity (L). Reducing the lasing mode size may help to reduce threshold, but the diode laser pump is usually limited in the extent to which it can be focused down to match the lasing mode, due to its poor spatial properties (as will be explained further in section 4.1). If the lasing mode is too small, the effective overlap η_{pl} will reduce, thus degrading the laser's performance. Compromises therefore have to be made in cavity design, but because it is larger power diodes that are generally more difficult to focus to smaller sizes, the increase in threshold is compensated by the greater amount of pump power available and hence greater overall output will be obtained from the laser.

1.3 Outline of Thesis

After this brief introduction to diode pumped solid-state lasers, two main subjects will be considered in the remainder of this thesis. In Chapter 2 the use of unidirectional ring lasers as single frequency sources will be discussed, with particular reference to the use of the acousto-optic effect to enforce unidirectional operation. The underlying mechanisms responsible for this behaviour will be described, and details of experimental verification and applications of these techniques are described. The use of diode bars as pump sources will be discussed in Chapters 3 and 4. In Chapter 3 an introduction to the use of these devices will be given, along with initial experiments that sought to end-pump solid-state lasers. Chapter 4 describes a novel beam shaping system that allows the output from diode bars to be focused to spot sizes that can readily be used by conventional end-pumped systems and presents results using this system.

The work described in this thesis has been carried out under the supervision of Professor D.C. Hanna and Dr W.A. Clarkson. Whilst a substantial part of this thesis is my own original work, much of the work described in Chapter 2 was in collaboration with Dr Clarkson, as this was a continuation of work he was already engaged in, and is still working on. Chapters 3 and 4 feature much work that is my own, but input from Dr Clarkson in a supervisory role has been given.

References

Byer, R.L., Science, **239**, 742 (1988)

Clarkson, W.A. and Hanna, D.C., J. Mod. Opt., **36**, 483 (1989)

Comaskey, B., Albrecht, G., Beach, R., Sutton, S., Mitchell, S., CLEO '93 Technical Digest, paper CWI5, Baltimore, MA (1993).

Fan, T.Y. and Byer, R.L., IEEE J. Quantum Electron., **24**, 895 (1988)

Fields, R.A., Birnbaum, M. and Fincher, C.L., Tech. Dig. CLEO (Anaheim, CA) Paper PD3 (1988)

Hall, R.N., Fenner, G.E., Kingsley, J.D., Soltys, T.J. and Carlson, R.O., Phys. Rev. Lett., **9**, 366 (1962)

Holonyak, N. and Bevacqua, S.F., Appl. Phys. Lett., **1**, 82 (1962)

Hughes, D.W. and Barr, J.R.M., J. Phys. D: Appl. Phys., **25**, 563 (1992)

Keyes, R.J. and Quist, T.M., Appl. Phys. Lett., **4**, 50 (1964)

Leger, J.R., IEEE J. Quantum Electron, **28**, 1088 (1992)

Mak, A.A., Fromzel, N.A. and Shcherbakov, A.A., Izv. Akad. Nauk. SSSR, Ser Fiz, **48**, 1466 (1984)

Malcolm, G.P.A. and Ferguson, A.I., Contemporary Physics, **32**, 305 (1991)

Nathan, M.I., Dumke, W.P., Burns, G., Dill, F.H. and Lasher, G.J., Appl. Phys. Lett., **1**, 62 (1962)

Newman, R., J. Appl. Phys., **34**, 437 (1963)

Ostermayer, F.W., Appl. Phys. Lett., **18**, 93 (1971)

Ross, M., Proc. IEEE, **56**, 196 (1968)

Schawlow, A.L., and Townes, C.H., Phys. Rev., **112**, 1940 (1958)

Sipes, D.L., Appl. Phys. Lett., **47**, 74 (1985)

Striefer, W., Scifres, D.R., Harnagel, G.L., Welch, D.F., Berger, J. and Sakamoto, M., IEEE J. Quantum Electron., **24**, 883 (1988)

Zhou, B., Kane, T.J., Dixon, G.J. and Byer, R.L., Opt. Lett., **10**, 62 (1985)

Chapter 2
ACOUSTO-OPTICALLY INDUCED UNIDIRECTIONAL OPERATION OF RING LASERS

2.1 Introduction

In the previous chapter we saw how diode-end-pumped solid-state lasers can produce fundamental transverse mode (TEM_{00}) lasing output. However, many lasers will still oscillate on a number of axial modes as the frequency separation of adjacent cavity modes is less than the laser gain bandwidth. In many solid-state lasers the phenomenon of *spatial hole burning* (see next section) allows axial modes to access regions of undepleted gain in the laser medium, leading to multimode operation. In standing wave lasers frequency selective elements such as etalons [Carr, 1985] or thin metallic films [Culshaw, 1971] can be used to enforce operation on one axial mode, but this can be very lossy and not suitable for low-gain lasers.

It is usually preferable to construct a ring laser that would normally operate in both counter-propagating directions, and then use some means of forcing it to oscillate in one direction only. When operating unidirectionally there will be travelling wave rather than standing wave oscillation, which ,in homogeneously broadened solid-state laser media, can eliminate spatial hole burning and allow single frequency operation to occur. Since unidirectional ring lasers saturate the gain medium more uniformly, with no spatial nodes along the axial direction, they can extract more power in a single mode. Ring lasers can also offer scope for greater flexibility in cavity design, as well as reduced sensitivity to external back reflections. The main disadvantages are the increase in system complexity and the fact that the gain medium is accessed only once per round trip, as opposed to twice for a standing wave cavity, which can result in lower output from low-gain systems, where the reduced gain requires a smaller transmission from the output coupler.

A number of methods can be used to enforce unidirectional operation of ring lasers. The simplest is probably to use an auxiliary external mirror to reflect back one of the counter-propagating beams and return it to the main cavity, thus leading to preferential lasing in the opposite direction (Fig 2.1). However the other lasing direction is generally not completely suppressed since it is this wave which is fed back

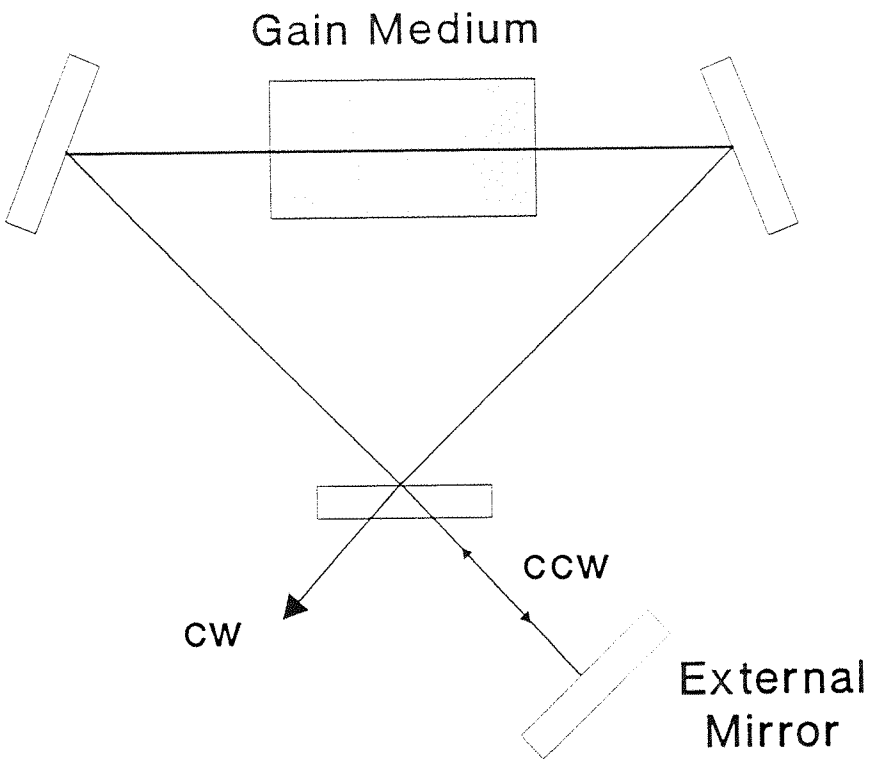

Fig 2.1 Ring laser in which unidirectional operation is encouraged by use of an external mirror. Any counter-clockwise (ccw) oscillation is fed back, enhancing clockwise (cw) operation.

by the external mirror. So this method may not be suitable for achieving true single frequency operation [Faxvog, 1980]. It is much more usual to employ some form of "optical diode" within the ring cavity. This diode is used to produce a "non-reciprocal" loss, i.e. a different loss for the two propagation directions, and hence force the laser to oscillate in one direction only. The optical diode most commonly used is shown in Fig 2.2, of which the principle element is a Faraday rotator. A plane-polarized wave passing through the rotator has its plane of polarization rotated in a sense which is different according to whether the light propagation is parallel or antiparallel to the dc magnetic field of the Faraday rotator. The optically active element, e.g. a quartz polarizer, cancels out the Faraday rotation for one direction of propagation through the optical diode, which means that the beam can pass through the Brewster plate unattenuated. A beam propagating in the opposite direction will have a net polarization change through the rotator and polarizer and experience a loss at the Brewster plate. From a detailed analysis of the polarisation changes at all elements and surfaces, one can derive the eigenpolarisations for the counter-propagating waves, their net round trip loss and hence their loss-difference. From this it can be determined if unidirectional operation will occur. Systems such as these have been implemented in a number of ring lasers, including monolithic structures [Kane, 1985], [Trutna, 1987], Q-switched rhomb-ring cavities [Clarkson, 1989], intracavity frequency doubled ring lasers [Scheps, 1990] and they perform well. There are a number of drawbacks however, in that additional birefringent components in the cavity (e.g. frequency doubling crystals and laser media such as Nd:YLF) alter the polarisation properties of the beam, Faraday rotators with large Verdet constants (i.e. large polarization rotation for a given d.c. magnetic field) also tend to be highly absorbing at optical wavelengths, and the additional components increase the complexity of the ring laser system. Other mechanisms that have been described include using a Kerr lens and slit in a ring cavity [Heatley, 1993], where the counter-propagating beams have different waist positions and beam widths, and the non-linear Kerr lens introduces a non-reciprocity in the net loss in the cavity. Another non-reciprocal device is a pair of counter-acting frequency shifters with a Fabry-Perot filter inserted between them [Sabert, 1993]. The transmission through the filter is frequency dependent, and the counter-propagating beams will have different frequencies between the two frequencies shifters, leading to a non-reciprocal transmission through the system. In some ways this has similarities to

the scheme we describe in section 2.5, where an acousto-optic Q-switch acts as a frequency shifter, and an external Fabry-Perot ring cavity acts as a frequency filter. With our scheme, only one frequency shifting device is required, as the output from the frequency filter is fed back to the to the opposite side of the Q-switch, giving a second frequency shift that cancels the first exactly.

An important alternative means of implementing an optical diode is to use a travelling wave acousto-optic modulator in the ring cavity [Golyaev, 1987], [Roy, 1987], [Neev, 1988]. Initially the mechanism responsible for enforcing unidirectional operation was not known, which meant that there was no logical strategy for optimising the device. Work carried out during the course of this PhD has revealed that two mechanisms are responsible for unidirectional operation, and these are discussed in sections 2.4 and 2.5. First, in section 2.2 the role of spatial hole burning is discussed in more detail, and then the acousto-optic effect is introduced in section 2.3. Application of this technique to particular ring laser systems is given in sections 2.6 and 2.7.

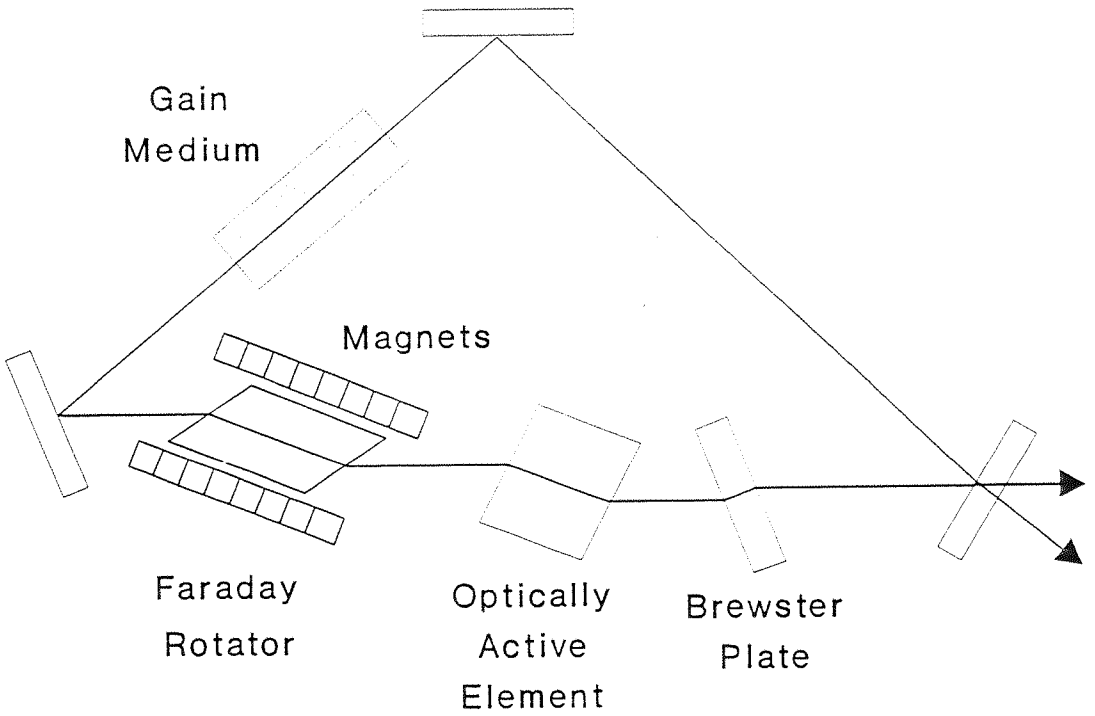

Fig 2.2 Ring laser incorporating Faraday rotator as non-reciprocal optical diode.

2.2 Spatial Hole Burning

In most solid-state laser media the transition linewidth is homogeneously broadened, i.e. the gain profile of every atom in the material is the same, which gives rise to a Lorentzian gain profile. In contrast, for inhomogeneously broadened lasers the individual atoms will in general have different gain profiles. A simple example of the latter arises from the different thermal velocities of molecules in a gas laser and the consequent Doppler broadening of their gain profiles. As we shall not be dealing with inhomogeneously broadened laser systems, only homogeneously broadened lasers will be considered further in this section.

To illustrate our discussion of a homogenously broadened laser medium, we show a schematic gain profile in Fig 2.3 below. Here we also show a number of adjacent cavity axial modes falling within the gain bandwidth of the transition. Axial modes have a frequency separation given by

$$\Delta \nu = \frac{c}{2L} \tag{2.1}$$

where L is the optical length of the laser cavity. For example, in Nd:YAG miniature diode-pumped lasers, the gain bandwidth at 1.064μm is around 156GHz [Danielmeyer, 1971] whilst the axial mode spacing will typically be of the order of a few GHz. Above threshold, in the steady-state, the net gain of the highest gain axial mode will be unity, so that the other axial modes, having lower net gain, are below threshold. We could then expect single axial mode operation to result, on the highest gain axial mode.

However, in standing wave lasers, not all the gain available is used by the highest gain axial mode, due to spatial hole burning. This phenomenon occurs as a result of the interference of waves travelling in opposite directions in the gain medium. If we consider two waves with different amplitudes, E_1 and E_2, with the same frequency ω, travelling in the opposite direction, the resultant total field strength will be:

$$\epsilon(z,t) = \mathrm{Re}[E_1(z)\exp i(\omega t - kz) + E_2(z)\exp i(\omega t + kz)] \tag{2.2}$$

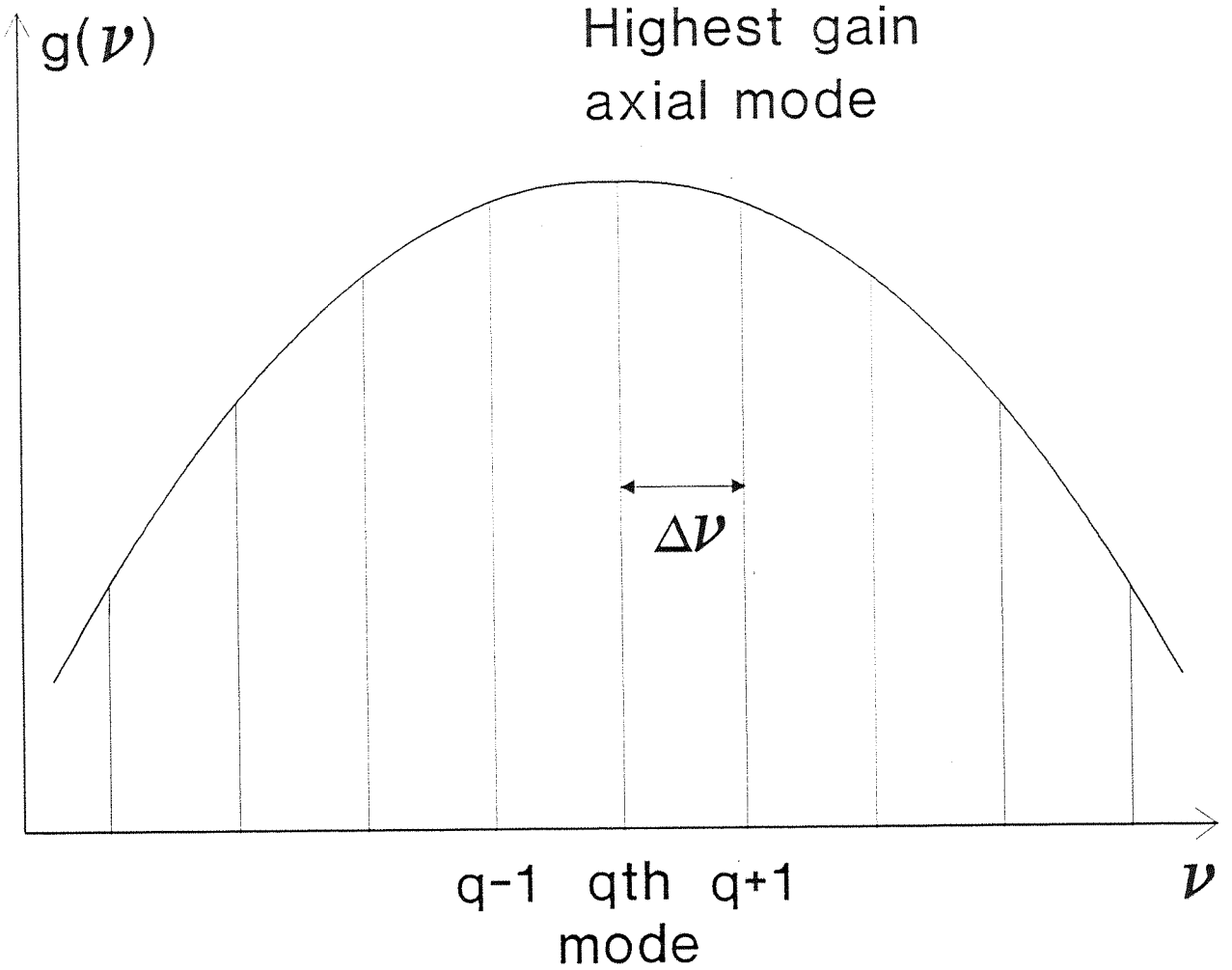

Fig 2.3 Homogenously broadened gain profile, g(ν),with a number of laser axial modes superimposed. The highest gain axial mode is the first to lase.

Now, in the gain medium, the stimulated rate of emission is proportional to the energy density of the stimulating radiation, which in this case is given by the proportionality

$$\begin{aligned} \text{Energy Density} &\propto |\epsilon(z,t)|^2 \\ &= |E_1(z)|^2 + |E_2(z)|^2 \\ &+ E_1^*(z)E_2(z)\exp i(2kz) + \text{c.c.} \end{aligned} \tag{2.3}$$

If we were considering one oscillating wave only in the gain medium, the energy density would be essentially uniform. However, when two counter-propagating waves interact in the gain medium, the spatial modulation resulting from the interaction of the waves is important. The spatial variation in the total energy density field is given by a standing wave of the form

$$I(z) = I_1(z) + I_2(z) + 2\sqrt{I_1 I_2}\cos(2kz+\phi) \tag{2.4}$$

where I_1 and I_2 are the intensities of the two waves independently and ϕ is the relative phase of the two waves. This is shown in Fig 2.4(a)

Now, in an homogeneously broadened laser medium, this standing wave will produce a spatially varying gain saturation of the medium, given by [Siegman, 1986]

$$\frac{\Delta N(z)}{\Delta N_0} = \frac{1}{1 + \dfrac{I(z)}{I_{sat}}} \tag{2.5}$$

where ΔN_0 is the initial population inversion before lasing commences and I_{sat} is the saturation intensity for the laser medium (i.e. the intensity at which the gain coefficient is reduced to half its small-signal value). In this expression the total intensity, I(z), is proportional to the energy density, and has the same spatial variation. This periodic depletion of the gain medium is referred to as *spatial hole burning* and is shown schematically in Fig 2.4(b). Thus there are regions in the gain medium where there is still significant gain available to other laser modes. As shown in Fig 2.5, if the q^{th} axial mode is the first to oscillate, then the $(q+1)^{th}$ mode can significantly overlap regions of undepleted gain, thus reducing gain competition between the modes, and may allow

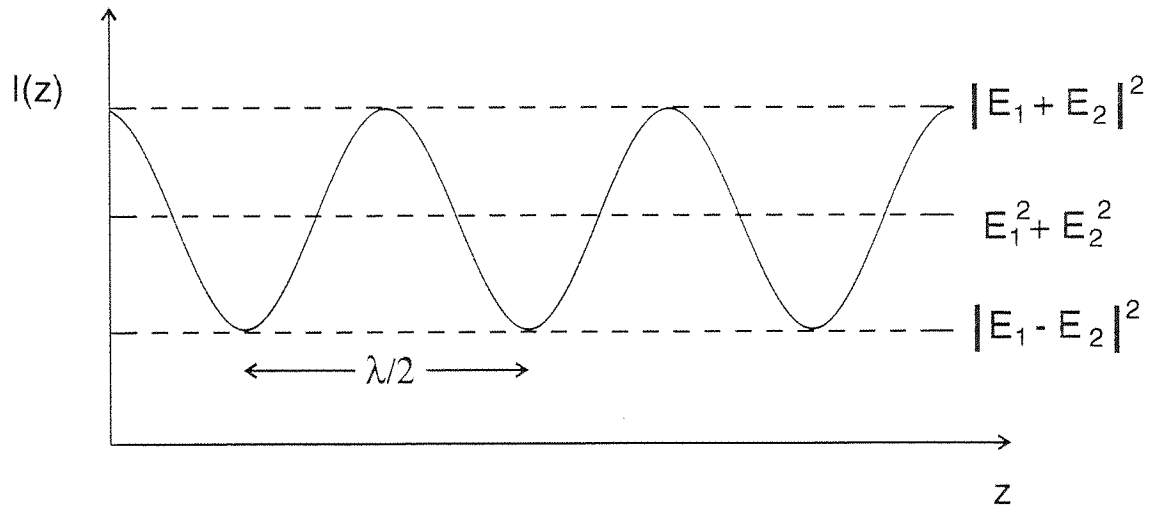

Fig 2.4(a) Standing wave spatial intensity field in the gain medium of a standing wave laser that arise from the interference between two oppositely travelling waves with the same frequency.

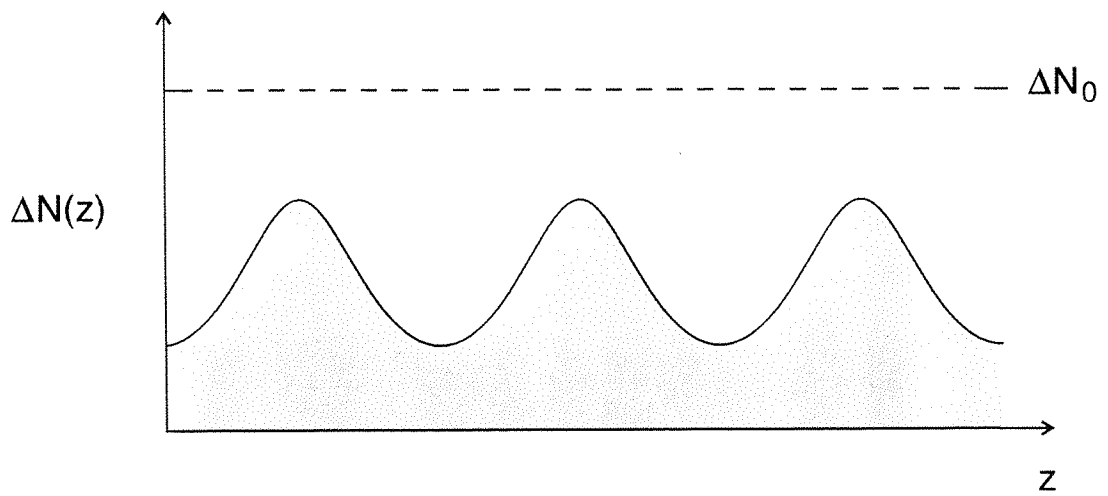

Fig 2.4(b) Spatial hole burning in the laser inversion that results from the above standing wave.

both modes to lase. When the $(q+1)^{th}$ (or indeed $(q-1)^{th}$) mode lases, further spatial hole burning results, reducing the available gain, but there may still be sufficient gain for other axial modes to lase.

We have seen, therefore, that the existence of standing waves in the gain medium can lead to spatial hole burning in homogeneously broadened lasers, which in turn can result in more than one axial mode lasing. The elimination of standing waves by creating a travelling wave unidirectional ring laser can produce single axial mode operation, which is preferable in many applications. The complete analysis of spatial hole burning is rather more complex than that outlined here, and depends on the particular laser resonator, the pump distribution (which determines the spatial distribution of gain in the medium), gain bandwidth, axial mode spacing, and spatial overlap of pump and laser beams. Further discussion of spatial hole burning is to found in, for example, [Danielmeyer, 1971] and [Clarkson, 1990], and also in sections 2.6 and 2.7 where we see some limitations in eliminating all spatial hole burning effects in ring lasers.

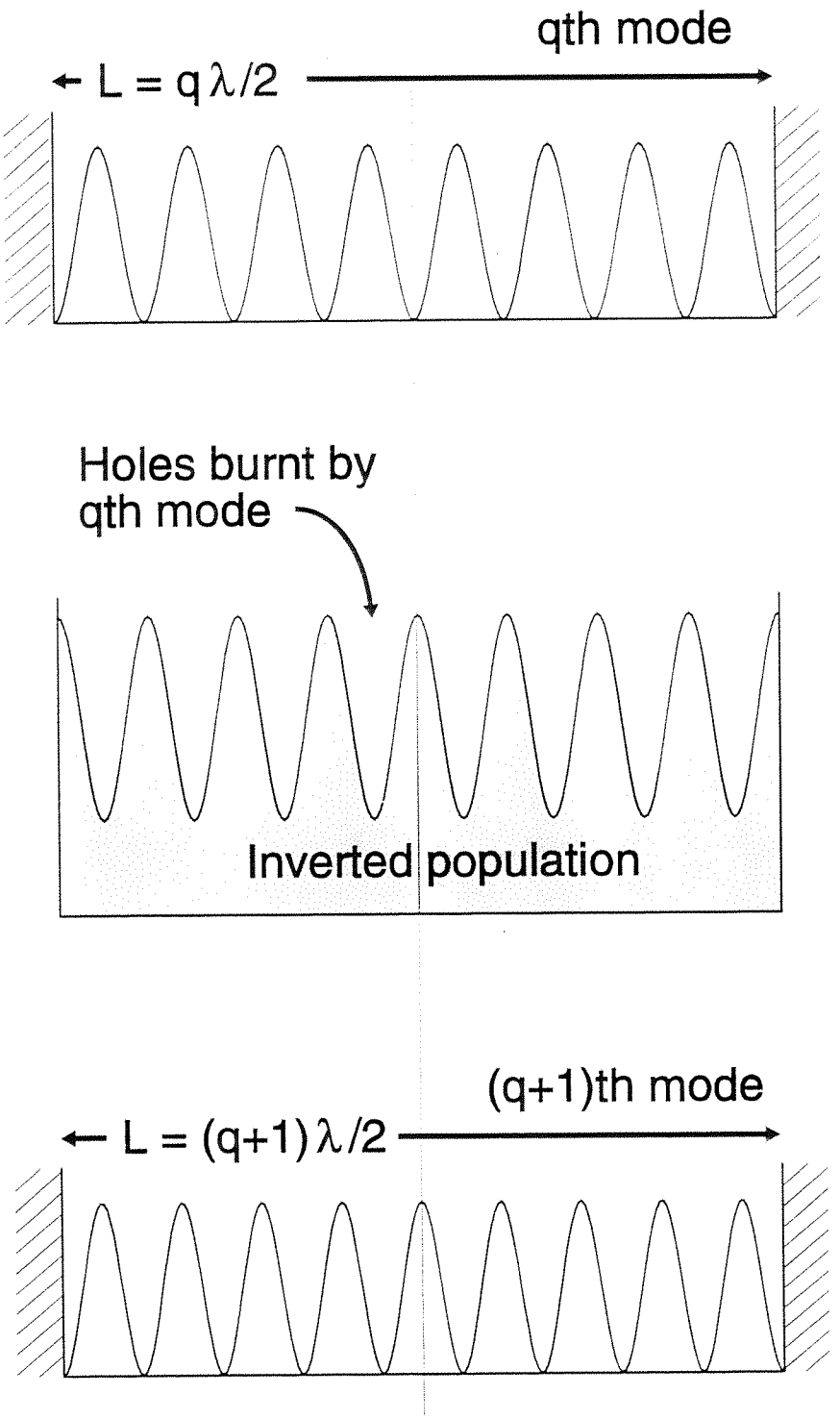

Fig 2.5 Schematic showing how adjacent axial modes can access the regions of undepleted gain caused by spatial hole burning. Here the entire laser cavity is depicted as being filled with the gain medium. In the centre of the cavity we see that the (q+1)th mode is out of phase with the qth mode, and is therefore able to access the undepleted gain.

2.3 The Acousto-Optic Effect

The interaction of light with acoustic waves in optical materials was predicted in 1922 [Brillouin, 1922] and verified 10 years later [Debye, 1932], [Lucas, 1932]. Although the acousto-optic (A-O) effect can be used for a number of applications including light modulators, beam deflectors, signal processors, tunable filters and spectrum analyzers [Adler, 1967], in this work we are primarily interested in the loss produced by diffraction of light in the acousto-optic medium and the effect this has on beam propagation in a ring laser cavity. In this section we shall introduce the standard analysis of the A-O effect with respect to diffraction, before pointing out how approximations made in this overlook effects which, in the case of ring lasers, significantly alter the lasing behaviour.

An acoustic wave in a medium consists of a sinusoidal strain field which in turn results in a variation in the refractive index, n, of the medium. This periodic refractive index variation for an acoustic wave of velocity v_s can be expressed as

$$\Delta n(z,t) = \Delta n \sin(\omega_s t - k_s z) \tag{2.6}$$

where $\omega_s = v_s k_s$ is the acoustic frequency and k_s the acoustic wavenumber $(2\pi/\lambda_s)$. The refractive index change (for isotropic media), Δn, is given by [Yariv, 1984]

$$\Delta n = -\tfrac{1}{2} n^3 \bar{p} \bar{S} \tag{2.7}$$

where $\bar{p}$ is the effective photoelastic constant and $\bar{S}$ the effective strain component.

Figure 2.6 shows a typical device used for A-O modulation of light. A piezo-electric transducer driven at r.f. frequencies (10's to 100's of MHz) generates sound waves which travel through the medium at that frequency (ν_s). In many A-O devices, and in particular for the modulators we have used in our ring lasers, the acoustic wave is a travelling wave. This is achieved by having an acoustic absorber at one end of the medium and also by cutting that face at an angle to the acoustic wave. Therefore the periodic variation in refractive index moves at the sound velocity, v_s, typically 1-10×10^3 ms^{-1}. As the velocity of light is some 5 orders of magnitude greater, the periodic variation can in effect (to a first approximation) be treated as a stationary

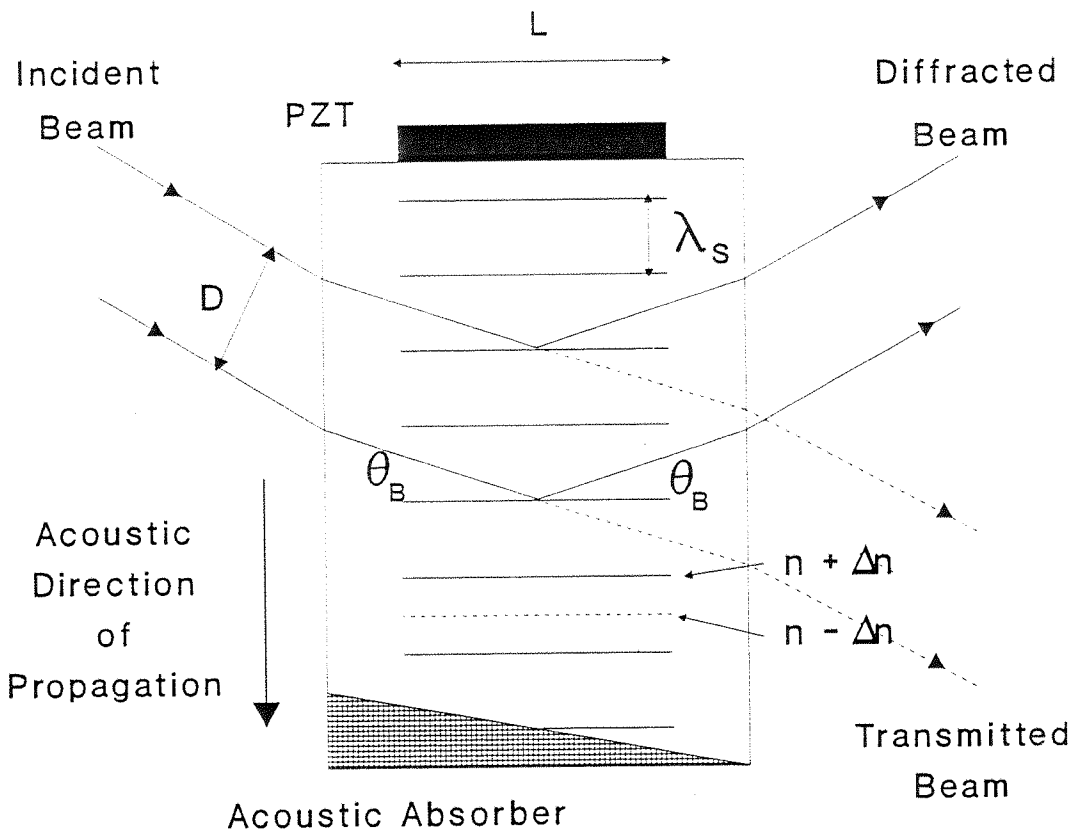

Fig 2.6 Travelling-wave acousto-optic modulator schematic. The modulators we used typically had a piezo electric transducer (PZT) of length 17mm (L), with the modulator itself being 10mm high by 4mm thick.

grating. We can then characterise the refractive index variation as a series of partially reflecting mirrors, separated by the sound wavelength λ_s. If we now consider a beam of light incident at angle θ_i to the acoustic wave (Figure 2.7), it will in general have a diffracted beam and a transmitted beam. This treatment is valid only when the diameter. D, of the light beam is at least of the order of several acoustic wavelengths ($D > 5\lambda_s$, [Sapriel, 1979]), which is the case in our experiments, where $D \simeq 400\mu m$, $\lambda_s \simeq 47\mu m$.

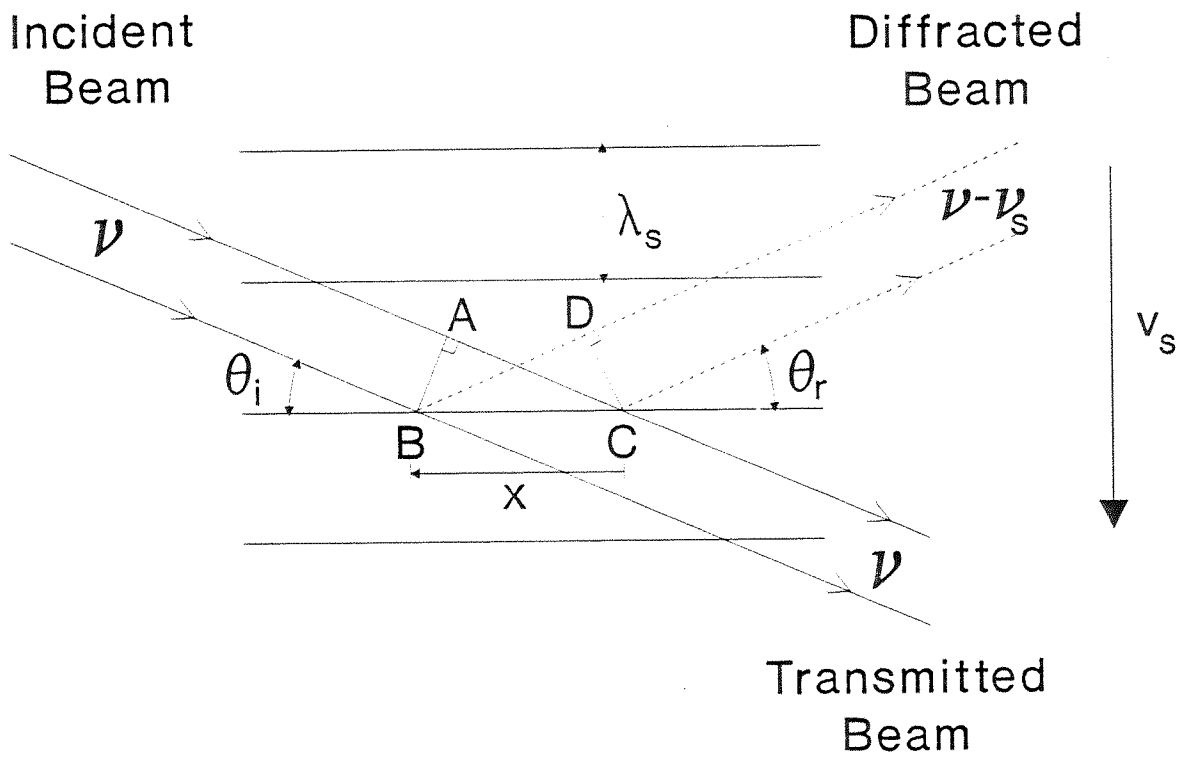

Fig 2.7 Schematic of diffraction from an acoustic wavefront along x. The light beam and acoustic waves are not drawn to scale.

The diffracted beam emerges at angle θ_r. For diffraction to occur in a given direction it is necessary that all points from an acoustic wavefront contribute in phase to diffraction in that direction. Thus from points such as B and C in Fig 2.7, the optical path difference AC-BD must be an integral multiple of λ/n, the optical wavelength in the medium. This means that

$$x(\cos\theta_i - \cos\theta_r) = \frac{m\lambda}{n} \quad ; \; m = 0, \pm 1, \pm 2, \ldots \tag{2.8}$$

For (2.8) to be satisfied along the plane, i.e. for any x, m must be 0, which means that $\theta_r = \theta_i$. In addition, we require that the reflection from all acoustic wavefronts also add in phase along the diffraction direction. As shown in Fig 2.8, the path difference between reflection from adjacent optical planes is AO+OB and this must be equal to λ/n. Simple trigonometry gives the condition that

$$\sin\theta_B = \frac{\lambda}{2n\lambda_s} \tag{2.9}$$

where $\theta_B = \theta_i = \theta_r$. This angle which satisfies the condition for peak diffraction is known as the *Bragg angle* (θ_B), because of the similarities with X-ray diffraction in crystals. This diffraction of light by sound waves is therefore known as Bragg diffraction. Lead molybdate ($PbMO_4$), an acousto-optic medium [Pinnow, 1969] which we use extensively in our experiments, has the following material properties: n = 2.3, $v_s = 3.75 \times 10^3$ ms^{-1}. Typically, we operated the modulator at a frequency of 80MHz, corresponding to $\lambda_s = 47\mu$m, and used 1.06μm lasers. This gives a Bragg angle (measured in the medium) of $\theta_B = 0.28°$, which, if measured in air is 0.65°.

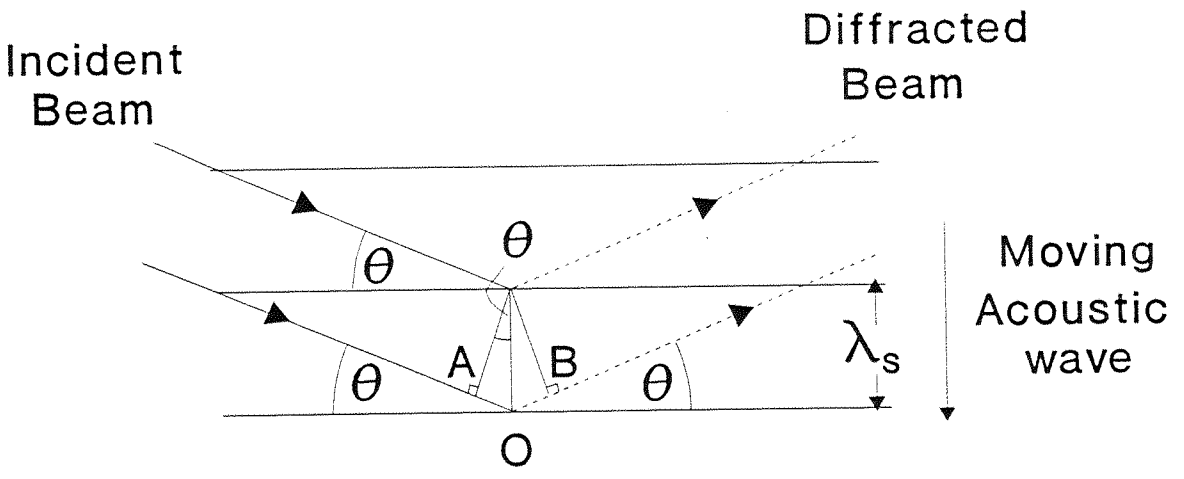

Fig 2.8 The path difference (AO+OB) for beams reflected from adjacent optical planes must be one optical wavelength to add up in phase.

It is also possible to describe acousto-optic diffraction using a particle model of light and sound. Here the light beam consists of photons with momentum $\hbar k$ and energy $\hbar\omega$. The acoustic wave can similarly be considered as being composed of phonons with momentum $\hbar k_s$ and energy $\hbar\omega_s$. The diffraction of light at incident frequency ω_i by an approaching phonon (frequency ω_s) is shown in the wavevector diagram of Fig 2.9(a). This can be considered as a collision of a photon in the light beam with a phonon in the acoustic wave. In this collision a single photon and single phonon are annihilated and a new (diffracted) photon is created, with frequency ω_d, which then propagates in the direction of the reflected beam. Conservation of momentum requires

$$\mathbf{k}_d=\mathbf{k}_i+\mathbf{k}_s \tag{2.10}$$

and energy conservation requires

$$\omega_d=\omega_i+\omega_s \tag{2.11}$$

Thus the diffracted beam is shifted in frequency by an amount equal to the acoustic frequency. In this case, the phonon energy is added to the photon energy (*frequency upshifted*). If the acoustic wave is receding from the light beam, then the situation is that a new photon and new phonon are created, with the incident photon annihilated (Fig 2.9(b)). Conservation of energy now gives

$$\omega_d=\omega_i-\omega_s \tag{2.12}$$

so the diffracted beam is *down-shifted* in frequency in this case. We can now derive the Bragg condition from the conservation of momentum requirement. Because $\omega_i \gg \omega_s$, then (2.11) and (2.12) reduce to $\omega_i \simeq \omega_d$. So

$$|\mathbf{k}_d| \simeq |\mathbf{k}_i| = k \tag{2.13}$$

From Figure 2.9, we can calculate the magnitude of the wave-vector as

$$k_s=2k\sin\theta \tag{2.14}$$

Substituting for k and k_s

$$\sin\theta_B=\frac{\lambda}{2n\lambda_s} \tag{2.15}$$

as before.

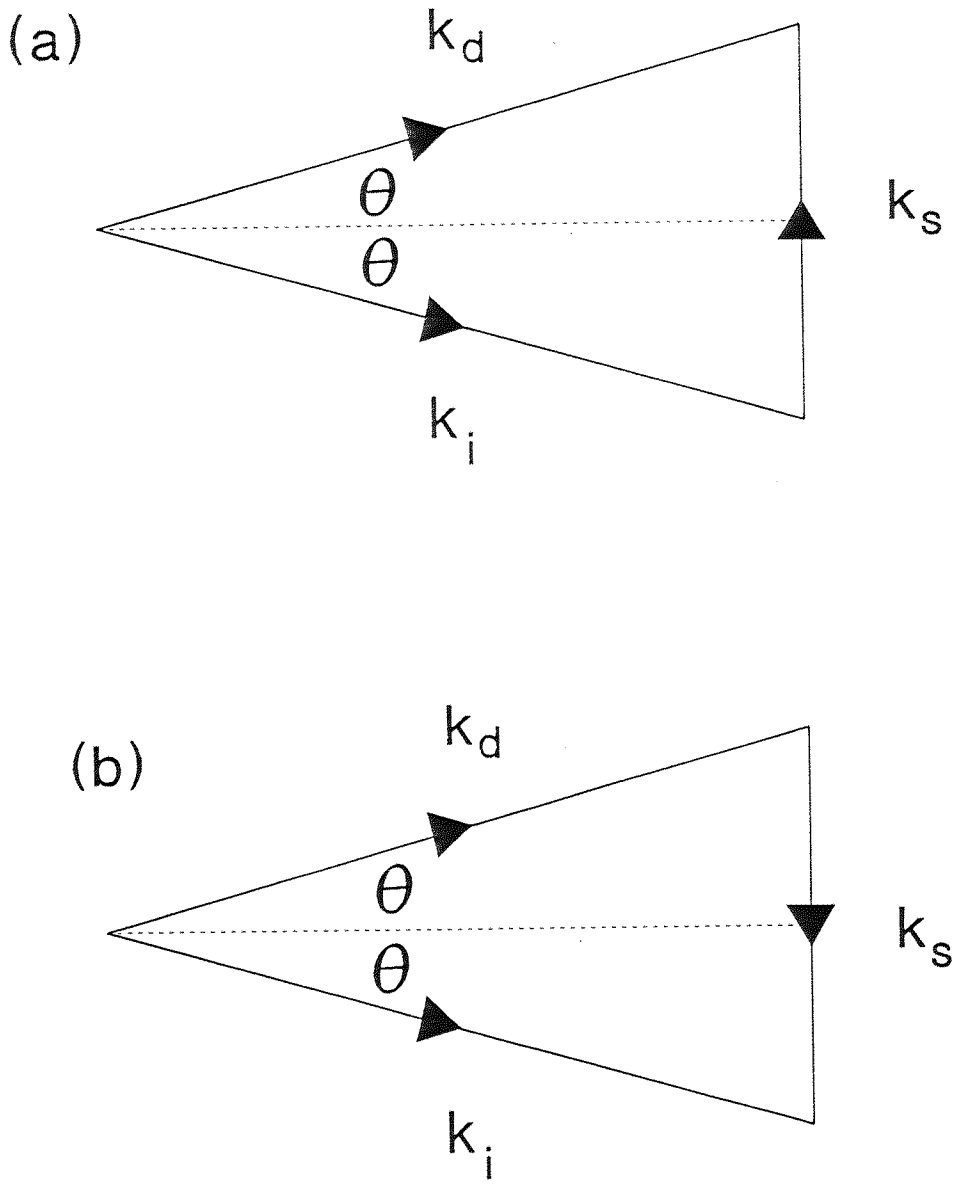

Fig 2.9 Wavevector diagrams showing incident photons with momentum k_i interacting with phonons of momentum k_s approaching **(a)** and receding **(b)** from the light beam to produce diffracted photons with momentum k_d.

In addition to knowing what the Bragg angle is for an acousto-optic modulator, of equal importance is the diffraction efficiency of the modulator, both at the Bragg angle, and at angles around this. The diffraction efficiency (at the Bragg angle) is derived by considering a coupled-mode analysis of the incident and diffracted beams, assuming an infinite plane wave and single frequency of both optical and acoustic beams [Yariv, 1984]. If multifrequency A-O interactions occur, then this analysis is insufficient, and an approach that has been used is to consider Feynman Diagrams of all the possible interactions [Xu, 1992]. The result obtained from coupled-mode analysis is

$$\frac{I_{diffracted}}{I_{incident}} = \sin^2 \kappa \ell \tag{2.16}$$

where ℓ is the interaction length between the acoustic and optical waves (in practice this is the length of the A-O transducer) and κ is a coupling constant given by

$$\kappa = \frac{\omega n^3}{4c} \bar{p} \bar{S} \tag{2.17}$$

where ω is the incident optical frequency, n the refractive index of the medium, $\bar{p}$ the effective photoelastic constant and $\bar{S}$ the effective strain component. Equations (2.16) and (2.17) can be reduced to more useful forms by using the relationship for acoustic intensity

$$I_{acoustic} = \frac{1}{2} \rho v^3 \bar{S}^2 \tag{2.18}$$

where ρ is the mass density of the medium and v is the acoustic phase velocity ("speed of sound in the medium"). Using the definition of the acousto-optic diffraction figure of merit:

$$M = \frac{n^6 \overline{p^2}}{\rho v^3} \tag{2.19}$$

and substituting it and (2.18) into (2.16) we get

$$\frac{I_{diffracted}}{I_{incident}} = \sin^2 \left(\frac{\pi \ell}{\sqrt{2} \lambda} \sqrt{M I_{acoustic}} \right) \tag{2.20}$$

and it is also apparent that the coupling constant κ can be rewritten as

$$\kappa = \frac{\pi}{\lambda}\sqrt{\frac{MI_{acoustic}}{2}} \qquad (2.21)$$

In practice, however, it is difficult to accurately predict the exact diffraction loss produced by an A-O modulator. Factors such as acoustic intensity, acoustic divergence, optical beam size and divergence, interaction length and even photoelastic constant can be difficult to measure and/or incorporate fully into any model. For example, given a typical situation used in our experiments, we had a lead molybdate Q-switch with the following parameters:

Acoustic Power (i.e. applied r.f. power) = 0.5 Watt

Acoustic Beam cross-section = 17 mm x 1 mm

$\therefore I_{acoustic} = 2.9 \times 10^4$ W m^{-2}

ℓ = path length in acoustic beam = 17 mm

n = 2.298

$\bar{p} = 0.28$

$\rho = 6.95 \times 10^3$ kg m^{-3}

$v = 3.75 \times 10^3$ ms^{-1}

$M = 31.5 \times 10^{-15}$ s^3/kg

$\kappa = 63.8$ m^{-1}

At $\lambda = 1.064\mu$m, this predicts a peak diffraction efficiency of 77.4%. When a measurement was made under these conditions with a beam width of around 0.6mm, we found that the diffraction loss was 42.7%. As the power to the modulator is varied, we found that the degree of difference from the predicted value changed and suggested that at low powers, agreement with equation (2.20) is better. Thus at 0.1W applied r.f. power the predicted loss is 21.7% compared to a measured value of 16.7%, whereas for 1W applied we predict 99.8% compared to 71.6% measured.

When we move away from the Bragg angle, say by $\Delta\theta$, the expression becomes more complex [Yariv, 1984]:

$$\frac{I_{diffracted}}{I_{incident}} = \frac{\kappa^2}{\kappa^2 + \left(\frac{1}{2}k_s\Delta\theta\right)^2} \sin^2\left(\kappa\ell\sqrt{1+\left(\frac{k_s\Delta\theta}{2\kappa}\right)^2}\right) \qquad \textbf{(2.22)}$$

with k_S being the acoustic wavenumber. This expression is important as it enables us to determine the diffraction loss at angles of incidence other than the Bragg angle. Tracing out the diffraction loss as a function of incidence angle gives us the *diffraction bandwidth* of the modulator, which as we shall see in the next section, is of considerable importance in determining the loss-difference in a ring laser. For angles away from the diffraction peak, Eq (2.22) can be rearranged to show that the shape of the diffraction bandwidth is simply a sinc-squared function:

$$\frac{I_{diffracted}}{I_{incident}} = (\kappa\ell)^2 \mathrm{sinc}^2\left(\kappa\ell\sqrt{1+\left(\frac{\pi\Delta\theta}{\kappa\lambda_s}\right)^2}\right) \qquad \textbf{(2.23)}$$

In view of the previously described difficulties in accurately predicting the diffraction loss, perhaps a more practical definition is given by:

$$L(\Delta\theta) = \frac{I_{diffracted}}{I_{incident}} = L_{max}\mathrm{sinc}^2\left(\sqrt{L_{max}+\left(\frac{\sqrt{L_{max}}\pi\Delta\theta}{\kappa\lambda_s}\right)^2}\right) \qquad \textbf{(2.24)}$$

where $L(\Delta\theta)$ is the diffraction loss as a function of the angle of incidence relative to the Bragg angle (θ_i-θ_B) and L_{max} is the measured peak diffraction loss for the experimental arrangement. In many practical situations of interest we find that $(\pi\Delta\theta)/(\kappa\lambda_S) \gg 1$, which means that

$$L(\Delta\theta) = L_{max}\mathrm{sinc}^2\left(\frac{\pi\ell\Delta\theta}{\lambda_s}\right) \qquad \textbf{(2.25)}$$

A typical case is shown below (Fig 2.10) for the diffraction bandwidth of a travelling-wave lead molybdate A-O modulator, comparing the theoretical shape of eq. (2.25) to experimental points obtained by passing a collimated Nd:YAG beam through a Q-switch that was rotated around the Bragg angle. The experimental details were the same as those described above for an applied r.f. power of 0.5 Watts.

The description of the A-O effect presented so far is the conventional one, and uses what seems to be quite justifiable assumptions. However, one assumption, that the speed of sound is so much smaller than the velocity of light that we can treat the refractive index grating as being stationary, whilst satisfactory for most situations, has very important consequences in ring lasers. In the next section we shall see how avoiding this assumption explains one of the mechanisms for acousto-optically induced unidirectional operation of ring lasers.

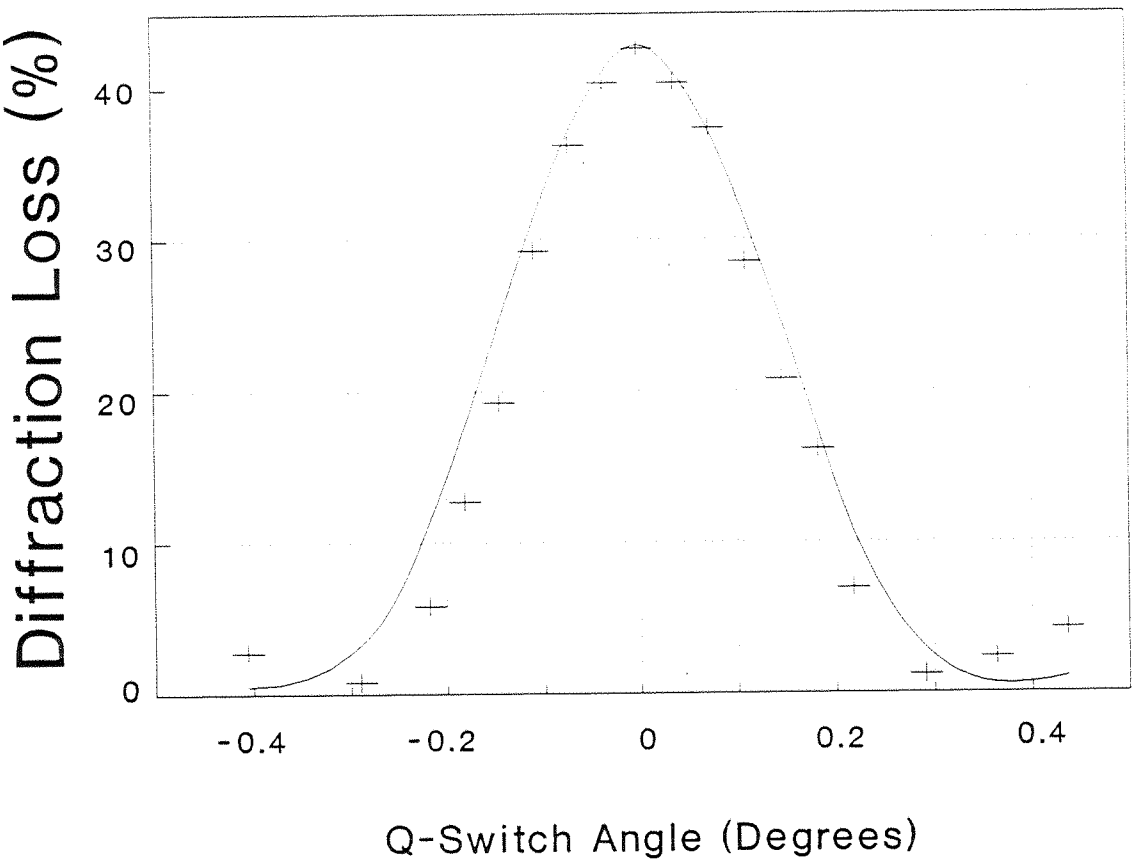

Fig 2.10 Experimental diffraction loss curve compared to the model described in equation (2.25). The points were measured at an applied r.f. power of 0.5W.

2.4 Intrinsic Mechanism for Unidirectional Ring Laser Operation

Acousto-optic modulators have been used in a number of ring laser cavities to successfully enforce unidirectional (and hence, single-frequency) operation. Early demonstrations in lamp-pumped Nd:YAG [Golyaev, 1987], Ti:Sapphire [Roy, 1987] and dye [Neev, 1988] ring lasers were followed by diode pumped Nd:YAG [Bromley, 1991], [Clarkson, 1991a] and Nd:YLF [Clarkson, 1991b] single frequency lasers. In all these cases, no adequate explanation of the mechanism responsible was offered, so there was no obvious strategy for optimizing the performance of these lasers. Observations of these ring laser systems indicated that two distinct mechanisms may be responsible for unidirectional operation. When the angle of tilt of the A-O modulator was altered it was observed that the direction of propagation could change sign, with an angular region where bi-directional operation occurred. This behaviour occurred around the Bragg angle (i.e. maximum diffraction loss) and suggested that an effect intrinsic to the modulator was present. We shall examine this effect in detail in this section. The other observation was that displacing the cavity mirrors by a small amount could reverse the direction of oscillation, and that placing apertures in the cavity suppressed this effect, with only the angle of the A-O modulator now being important. This suggested that the diffracted beam was re-entering the cavity, and interacting with the laser beam in the cavity in some way, and this is discussed in section 2.5.

2.4.1 Theory

The intrinsic 'non-reciprocity' of a travelling-wave acousto-optic Q-switch is a consequence of the fact that when light is reflected from a moving surface, the angles of incidence and reflection are no longer identical. Light which is incident on the Q-switch experiences partial reflection from moving refractive index variations caused by the acoustic waves propagating through the medium. When the angles of incidence and reflection are such that the reflected contributions are in phase then the Bragg condition is satisfied, and the amount of reflected light is at a maximum. However, a consequence of the travelling grating is that the Bragg condition is satisfied for the two counter-propagating beams at different angles of incidence, and as a result they generally experience different diffraction losses. At first sight it might be thought that

this angular difference is negligible. However we show here that under certain conditions a significant loss-difference results. It should be noted at this point that other authors offered similar explanations for the intrinsic mechanism at approximately the same time as our paper [Clarkson, 1992a], these being by Zinov'eva[1992] and Reed[1992]. Our work was independent of theirs, and the model and experimental verification presented here is more extensive than either of these papers.

In order to obtain an accurate estimate of the loss-difference it is necessary to know the difference in the incidence angles for the two counter-propagating beams which satisfy the Bragg condition. It is convenient to refer to these angles as the *Bragg incidence angles*, shown in Figs. 2.11(a) and 2.11(b) as θ_B^+ for the beam propagating in the forward (+) direction, which we define as a beam with a wavevector component in the same direction as the acoustic wave), and θ_B^- for the counter-propagating beam in the (−) direction. It is important to distinguish these angles from the *nominal Bragg angle* as defined in eq. (2.5), and a more general statement of the Bragg condition may be written as

$$\sin(\theta_B^{\pm}+\theta_d^{\pm})=\frac{\lambda}{n\lambda_s} \tag{2.26}$$

where θ_d^+ and θ_d^- are the diffraction angles for the two counter-propagating beams, λ is the wavelength of light in a vacuum, λ_S is the wavelength of sound in the acoustic medium and n is its refractive index. Thus, the Bragg incidence angles are related to the Bragg angle θ_B by

$$\theta_B^{\pm}+\theta_d^{\pm}=2\theta_B \tag{2.27}$$

The difference $\Delta\theta_B$ between the Bragg incidence angles for the two counter-propagating beams can be calculated quite simply from energy and momentum conservation considerations. Conservation of momentum requires that

$$\mathbf{k}_i^{\pm}\mp\mathbf{k}_s=\mathbf{k}_d^{\pm} \tag{2.28}$$

where $\mathbf{k}_S$ is the wavevector for the acoustic wave and $\mathbf{k}_i^{\pm}, \mathbf{k}_d^{\pm}$ are wavevectors for the incident and diffracted laser beams respectively. Resolving into components perpendicular to $\mathbf{k}_S$ we obtain, using equation (2.26)

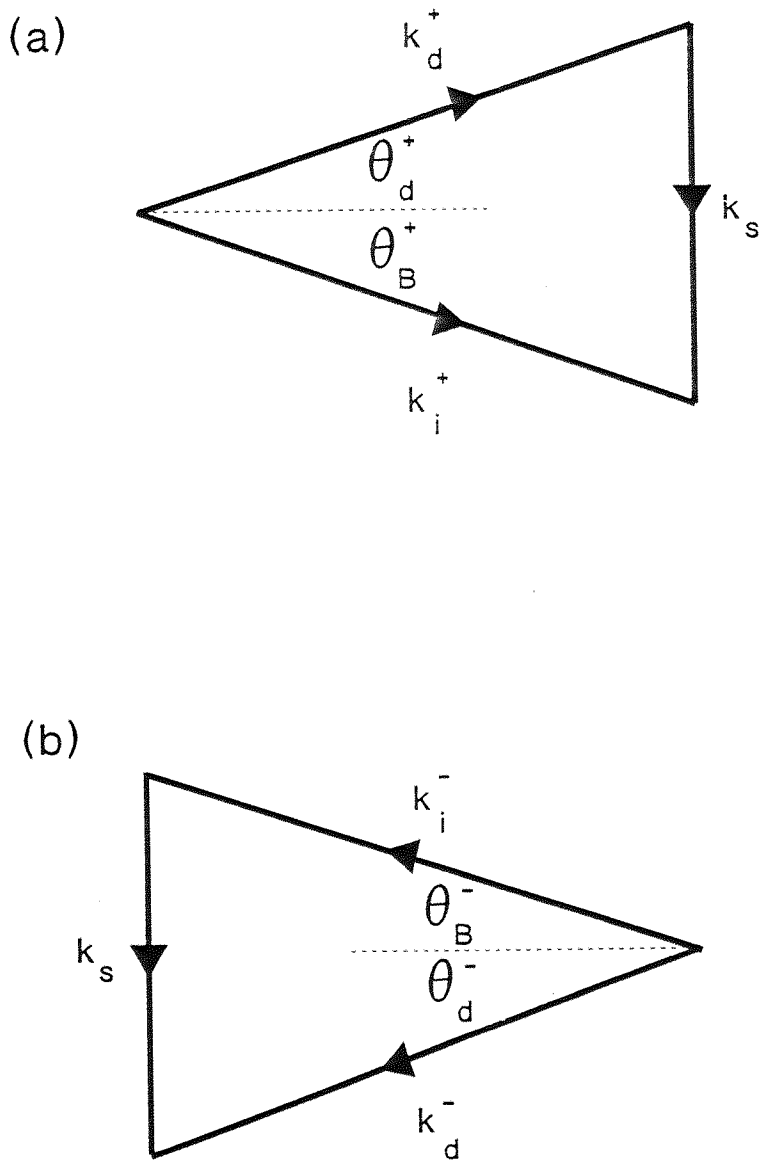

Fig 2.11 (a), (b) Wavevector diagrams showing the Bragg condition for the (+) and (-) counter-propagation directions, respectively.

$$k_i \cos(\theta_B^{\pm}) = k_d^{\pm} \cos(2\theta_B - \theta_B^{\pm}) \tag{2.29}$$

where k_i is a common symbol for k_i^+ and k_i^-, recognising that $k_i^+ \approx k_i^-$, . Since $|\Delta\theta_B| \ll 1$ and $|\theta_B^{\pm}| \ll 1$, then from equation (2.29) we obtain the following expression for $\Delta\theta_B$

$$\Delta\theta_B = \theta_B^+ - \theta_B^- \approx \frac{k_i(k_d^- - k_d^+)}{k_d^+ k_d^- \sin 2\theta_B} \tag{2.30}$$

In order to satisfy energy conservation

$$k_i - k_d^{\pm} = \pm \frac{2\pi n \nu_s}{c} \tag{2.31}$$

where ν_s is the acoustic frequency. By substituting equations (2.26) and (2.31) into (2.30) and using the approximation that $k_i^2 \approx (k_d^+)(k_d^-)$, we obtain a simplified expression for $\Delta\theta_B$, namely

$$\Delta\theta_B \approx \frac{2n\nu_s}{c} \tag{2.32}$$

where v_s is the velocity of sound in the acoustic medium. For most acousto-optic materials, values for v_s lie in the range $1 kms^{-1}$ to $10 kms^{-1}$ and values for n in the range 1.5 to 2.5. Thus we expect to find values for $\Delta\theta_B$ to be of the order of a few tens of microradians. At first sight this seems almost insignificant, and might be expected to produce almost no loss difference. However, it is not only $\Delta\theta_B$ but the diffraction bandwidth of the modulator which determines the loss. As we shall see later, it is the ratio of the Bragg angle shift to the diffraction bandwidth which determines the maximum available loss-difference.

We now define the loss-difference between counter-propagating beams to be

$$\Delta L = L_d^+ - L_d^- \tag{2.33}$$

where L_d^+ and L_d^- are the diffraction losses for the (+) and (-) propagation directions. This loss-difference can be calculated by simply considering two diffraction loss versus angle curves offset by angle $\Delta\theta_B$. From equation (2.25), we see that the diffraction

losses in the counter-propagating directions, L_d^+ and L_d^- for a beam incident at angle θ_i are given by

$$L_d^{\pm} \simeq L_{max} \mathrm{sinc}^2\left(\frac{\pi \ell \Delta\theta^{\pm}}{\lambda_s}\right) \tag{2.34}$$

where $\Delta\theta^{\pm} = \theta_i - \theta_B{}^{\pm}$.

We can express this in terms of the angular width (FWHM) of the diffraction loss curve ($\Delta\theta_{1/2}$), which along with L_{max} can be easily determined experimentally, to give the result that

$$L_d^{\pm} \simeq L_{max} \mathrm{sinc}^2\left(\frac{0.89\pi \Delta\theta^{\pm}}{\Delta\theta_{1/2}}\right) \tag{2.35}$$

where $\Delta\theta_{1/2}=0.89\lambda_s/\ell$. Since $\Delta\theta_{1/2}$ is typically ~ 1 mrad and hence $\Delta\theta_B \ll \Delta\theta_{1/2}$, the loss-difference can be expressed as:

$$\frac{\Delta L_d}{L_{max}} \propto 2\,\mathrm{sinc}\left(\frac{0.89\pi}{\Delta\theta_{1/2}}\Delta\theta\right)\left[\mathrm{sinc}\left(\frac{0.89\pi}{\Delta\theta_{1/2}}\Delta\theta\right) - \cos\left(\frac{0.89\pi}{\Delta\theta_{1/2}}\Delta\theta\right)\right]\frac{\Delta\theta_B}{\Delta\theta} \tag{2.36}$$

where $\Delta\theta = \theta_i - \theta_B$ is now the angular shift from the nominal Bragg angle. As with section 2.3 dealing with the acousto-optic effect, the above theory is only strictly valid for plane-wave conditions. In practice this will not be the case, however the model should be approximately valid providing the divergence of the laser and acoustic beams are small compared to $\Delta\theta_{1/2}$, which is the case in our experiments. From (2.36) we can show that the loss difference is a maximum when the angle of incidence with respect to the Bragg angle is

$$\Delta\theta_{max} \approx \pm\frac{0.415\lambda_s}{\ell} \tag{2.37}$$

at which angle the loss difference is

$$\frac{\Delta L_{max}}{L_{max}} = \frac{1.7\ell\Delta\theta_B}{\lambda_s} = 1.5\frac{\Delta\theta_B}{\Delta\theta_{1/2}} \qquad (2.38)$$

The results of this model for a typical experimental configuration at a lasing wavelength of 1.06μm are as follows. A lead molybdate A-O modulator, with transducer length 17mm, when operated at 80MHz has an acoustic wavelength (λ_S) of 47μm, and $\Delta\theta_B$ = 58μrad. The diffraction bandwidth is 2.5 mrad. The maximum loss difference obtainable, relative to the diffraction loss at the Bragg angle, as given by (2.38) is 3.6%, which is achieved by tilting the modulator away from the Bragg angle such that $\Delta\theta_{max} = \pm 1.1$ mrad. For the purpose of further discussion all of the angles quoted are those measured in air, since these can be compared directly with experimental results. In this case the values of $\Delta\theta$, $\Delta\theta_B$ and $\Delta\theta_{1/2}$ must be multiplied by an extra factor n. For the above example, this gives $\Delta\theta_B = 0.0076°$, $\Delta\theta_{max} = \pm 0.145°$ and $\Delta\theta_{1/2} = 0.33°$.

Theoretical plots of diffraction loss for counter-propagating beams and the resultant loss-difference for this example are shown in Fig 2.12. In Fig. 2.12(a) it can be seen that at any particular incidence angle θ_i the diffraction loss is generally different for opposite directions of propagation. For $\theta_i < \theta_B$ the diffraction loss is lowest for the (+) direction and lasing occurs preferentially in this direction for a ring laser. For the situation where $\theta_i = \theta_B$, the loss-difference is zero and lasing is likely to be bidirectional. However, when $\theta_i > \theta_B$ the loss is lowest for the (−) direction and this is now the preferred lasing direction. In Fig. 2.12(b) the predicted value for loss-difference as a fraction of the peak diffraction loss is plotted as a function of the angular deviation $(\theta_i - \theta_B)$ from the Bragg angle. In this particular case it can be seen that the loss-difference ΔL is a maximum around $\Delta\theta_{max} = |\theta_i - \theta_B| = 0.15°$ and has a value which is approximately 3.6% of the maximum diffraction loss (at $\theta_i \approx \theta_B$), and 5.0% of the actual diffraction loss at that angle. While this represents the maximum loss-difference which can be achieved for this particular Q-switch operating under the conditions described, it can be seen from Fig. 2.12(b) that a potentially better situation

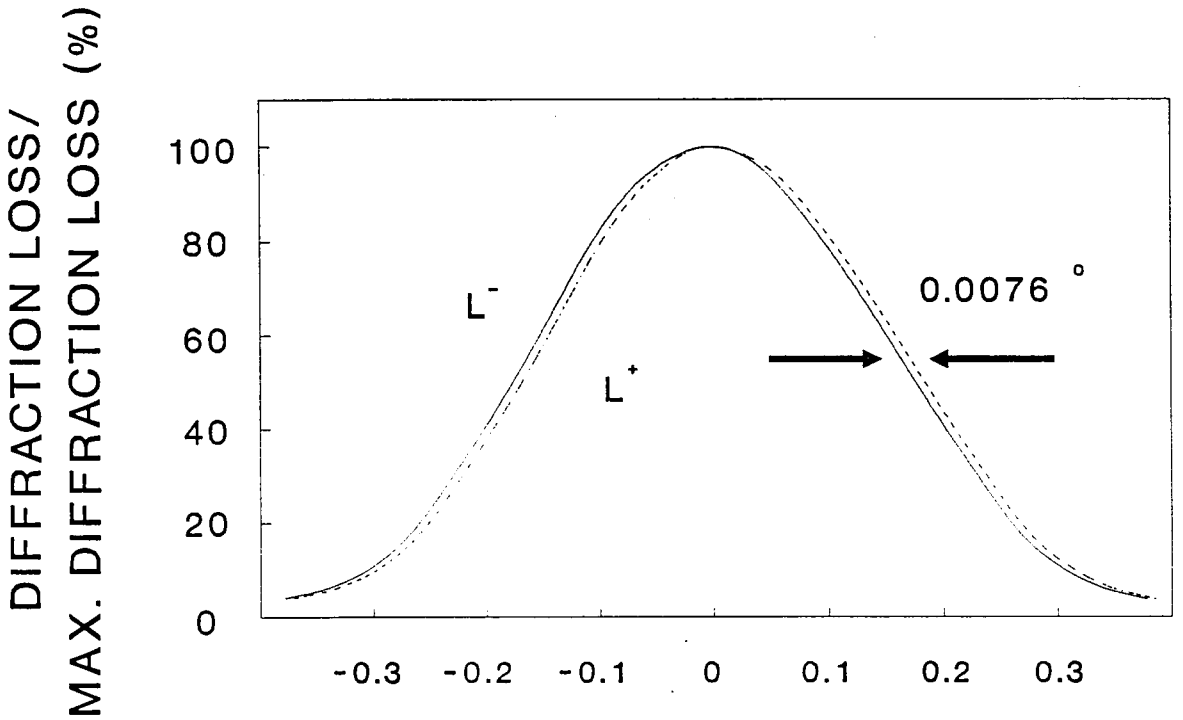

Fig 2.12 (a) Diffraction losses L^+ and L^- for the counter-propagating beams, as predicted by eq (2.35). The angles (in degrees) shown are as measured in air.

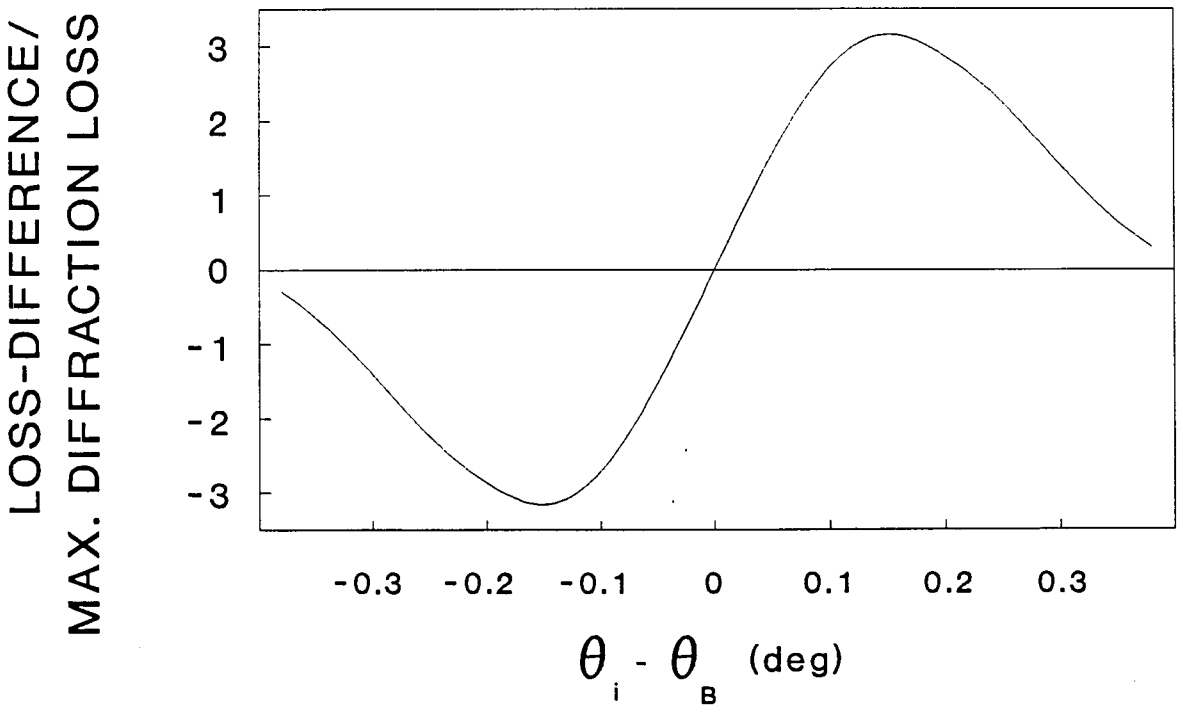

Fig 2.12 (b) Loss difference (scaled to maximum diffraction loss), $\Delta L = L^+ - L^-$ as a function of incidence angle, as predicted by eq (2.36)

for cw unidirectional operation is to tilt the Q-switch so that $|\theta_i - \theta_B| \approx 0.3°$. Here the loss-difference is decreased slightly, but is now approximately 14% of the diffraction loss at that angle. The net result is that for a particular value of loss-difference, the diffraction loss and hence the effective insertion loss for the Q-switch is now reduced. Clearly in any situation, for unidirectional operation to be realized, the loss-difference must be sufficiently large to overcome any coupling between the two lasing directions. Hence the value of the loss-difference required depends on the particular laser. For many miniature solid-state lasers this can be very small ($\sim 0.01\%$) [Clobes, 1972]. A net loss-difference of 0.01% would require in an increase in cavity loss of only 0.07% in this example, which can be considered negligible in most lasers. At any particular orientation of the Q-switch the ratio of the loss-difference to the diffraction loss should remain constant as the r.f. power is increased, as shown by eq. (2.34) since the shape of the diffraction loss versus angle curve does not vary with power. Hence loss-difference is expected to increase linearly with diffraction loss.

2.4.2 Experimental Verification

In order to verify that the Bragg condition is indeed satisfied at different incidence angles for counter-propagating beams, we made direct measurements of the Bragg incidence angles for a lead molybdate Q-switch. In order to ensure that the counter-propagating beams were exactly aligned, the measurements were made in a standing-wave laser. For this purpose a diode-pumped Nd:YAG laser utilising a folded-cavity design [Maker, 1989], with the A-O Q-switch placed in the collimated arm of the resonator (Fig 2.13) was used. In order to measure $\Delta\theta_B$, when a radio frequency (r.f.) signal at 80MHz was applied, the diffracted outputs in both the (+) and (−) directions were monitored independently, and an optical lever system employed to measure small angular tilts of the A-O Q-switch. It was found that the diffraction maxima did indeed occur for slightly different orientations of the A-O Q-switch resulting in a measured value for $\Delta\theta_B$ (in air) of $0.009° \pm 0.002°$. This is in good agreement with the theoretical value of 0.0076° predicted by equation (2.32).

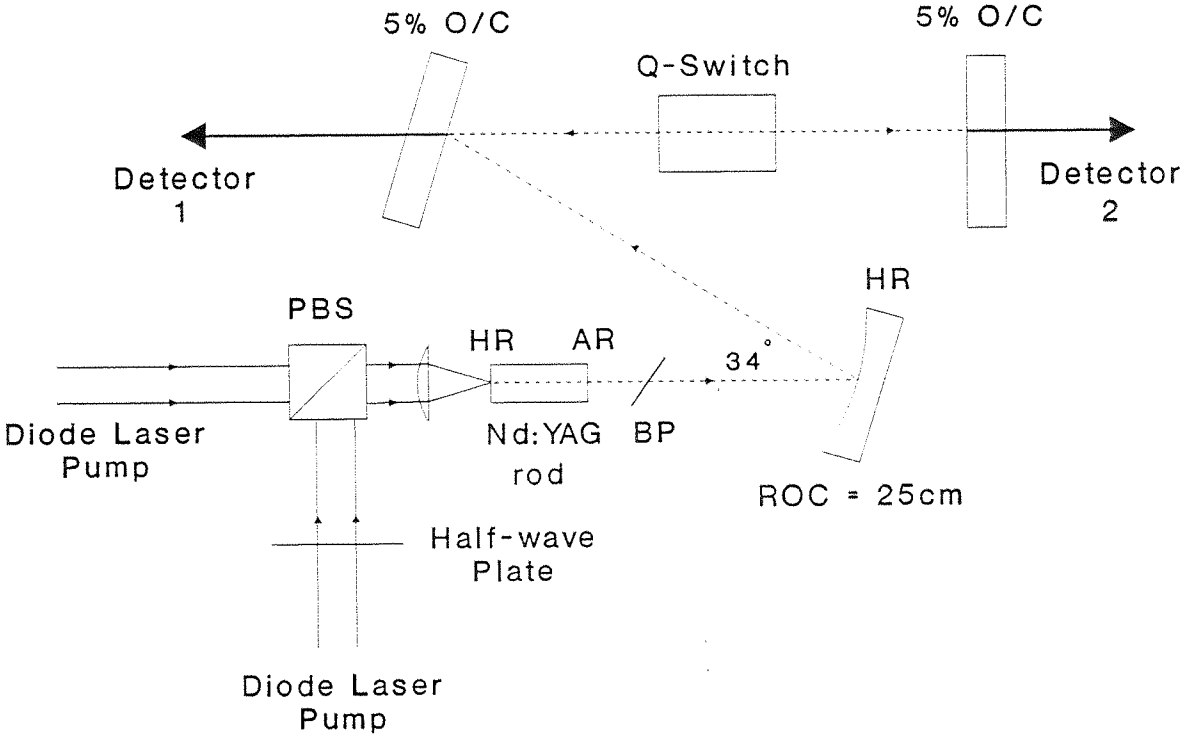

Fig 2.13 Laser cavity used to measure difference in Bragg incidence angles. PBS=Polarising Beam Splitter, BP=Brewster Plate.

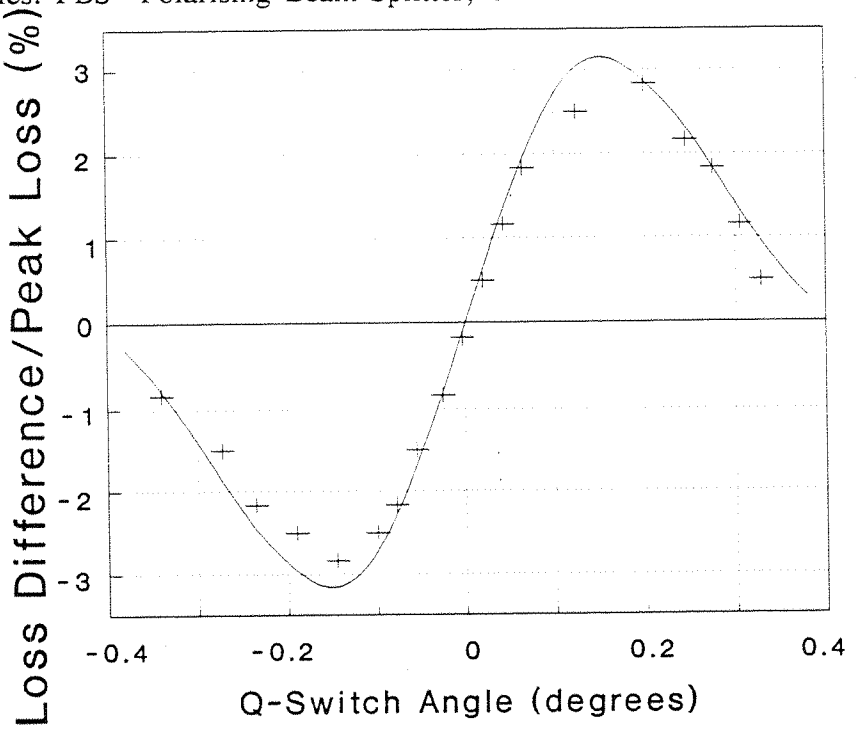

Fig 2.14 Loss-difference measured with the cavity shown above. The solid line is the theoretical loss-difference as given in (2.36)

Using this same arrangement it was also possible to directly measure the diffraction loss in each direction as the modulator was tilted, and from this the loss-difference could be calculated. The actual diffraction loss was measured by comparing the power of the transmitted laser beam with that of the diffracted beam emerging from the resonator. The results are shown in Fig 2.14, which demonstrates excellent agreement with the predicted loss-difference curve. This method of measurement of loss-difference is rather crude, however, as the signal levels detected were very small, and relied on very stable operation of the laser over the period of measurement.

An improvement to this standing-wave cavity is a ring laser incorporating the lead molybdate A-O Q-switch. A number of measurements were made on a diode pumped Nd:YAG ring laser, incorporating the lead molybdate acousto-optic Q-switch. Care was taken to use a resonator design such that the beam size in the Q-switch exactly matched that used previously in the determination of the diffraction loss versus angle curves. The resonator design used was a triangular ring configuration similar to that described in [Bromley, 1991], but with a much longer perimeter ($\sim$ 100cm) and with the Nd:YAG rod pumped by two polarization coupled one-watt diodes (Fig 2.15). The lead molybdate Q-switch was positioned mid-way between the two mirrors defining the longest arm of the ring resonator. This arrangement with the relatively long perimeter of the resonator ensured that any diffracted beams completely left the resonator and did not interfere with the operation of the Q-switch. When a low power ($\sim$0.01W) r.f. signal was applied to the Q-switch and it was orientated close to the Bragg condition, but with $\theta_i < \theta_B$, unidirectional lasing was observed in the (+) direction, as expected. When tilted slightly so that $\theta_i > \theta_B$, the direction of lasing reversed, also as predicted (see Fig. 2.12(b)).

To provide further confirmation of the proposed mechanism, the loss-difference was determined from observations of the transient behaviour of the ring laser. The procedure involves Q-switching the laser using a second A-O Q-switch, which was positioned quite close to the lasing mode waist. Since the loss-difference is generally quite small compared to the laser gain, it takes many round-trips of the resonator before lasing is suppressed in the higher loss direction. This does not usually occur on the time scale of build-up of a Q-switched pulse, hence Q-switched pulses are obtained for both

lasing directions. These pulses do however have different build-up times as a consequence of their different overall gains. If a measurement is made of the ratio γ of the output powers, near the beginning of the pulses (so that the inversion has not been depleted significantly and the gain is effectively constant), the loss-difference ΔL is

$$\Delta L = (1-L_r)(1-\gamma^{1/q}) \tag{2.39}$$

where q is the number of round-trips and L_r is the round-trip loss of the cavity. The results obtained are shown in Fig. 2.16. It can be seen that the values are in good agreement with those predicted by the model. When the r.f. power was increased, for a particular orientation of the Q-switch, we observed a linear increase in loss-difference with diffraction loss, and at $|\theta_i - \theta_B| \approx 0.3°$ we found the loss-difference to be approximately 11% of the diffraction loss. Accounting for experimental error, this is in good agreement with the predicted value of 14%.

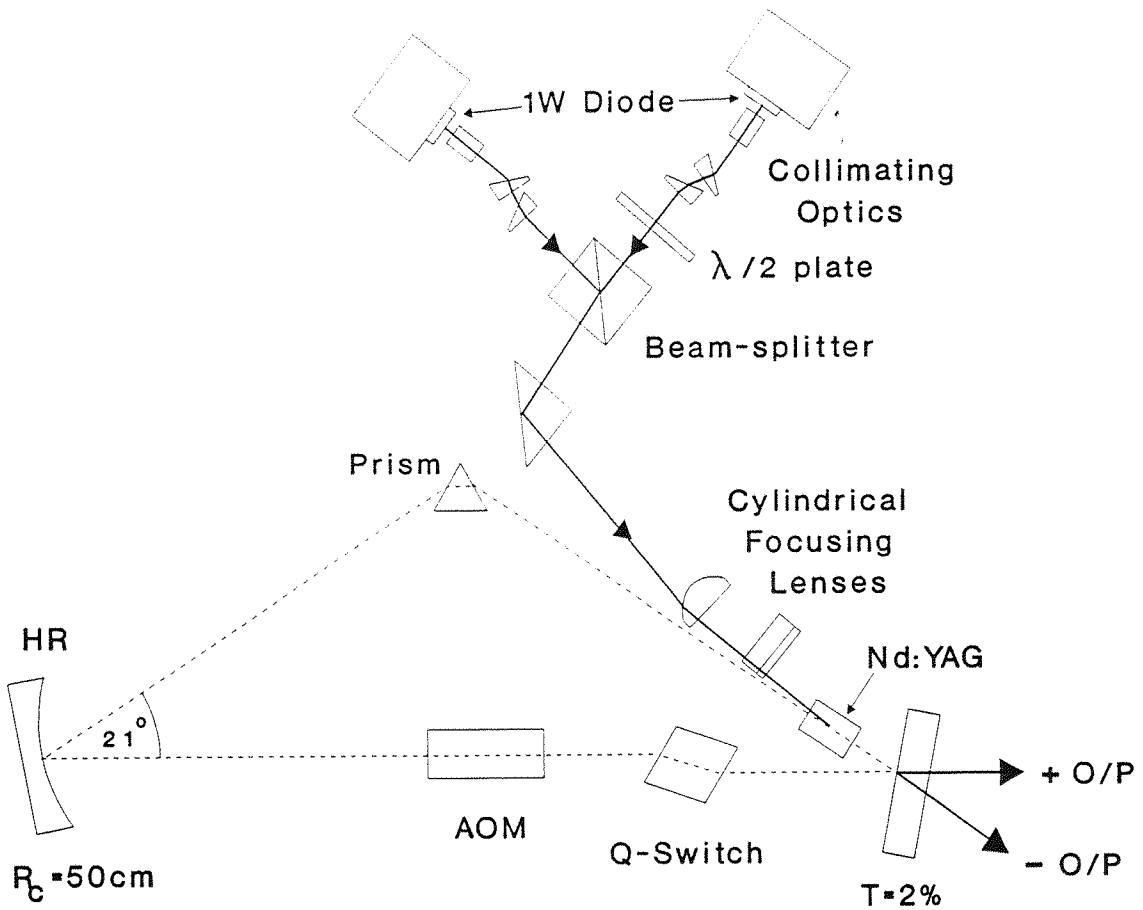

Fig 2.15 Ring resonator used to measure loss-difference.

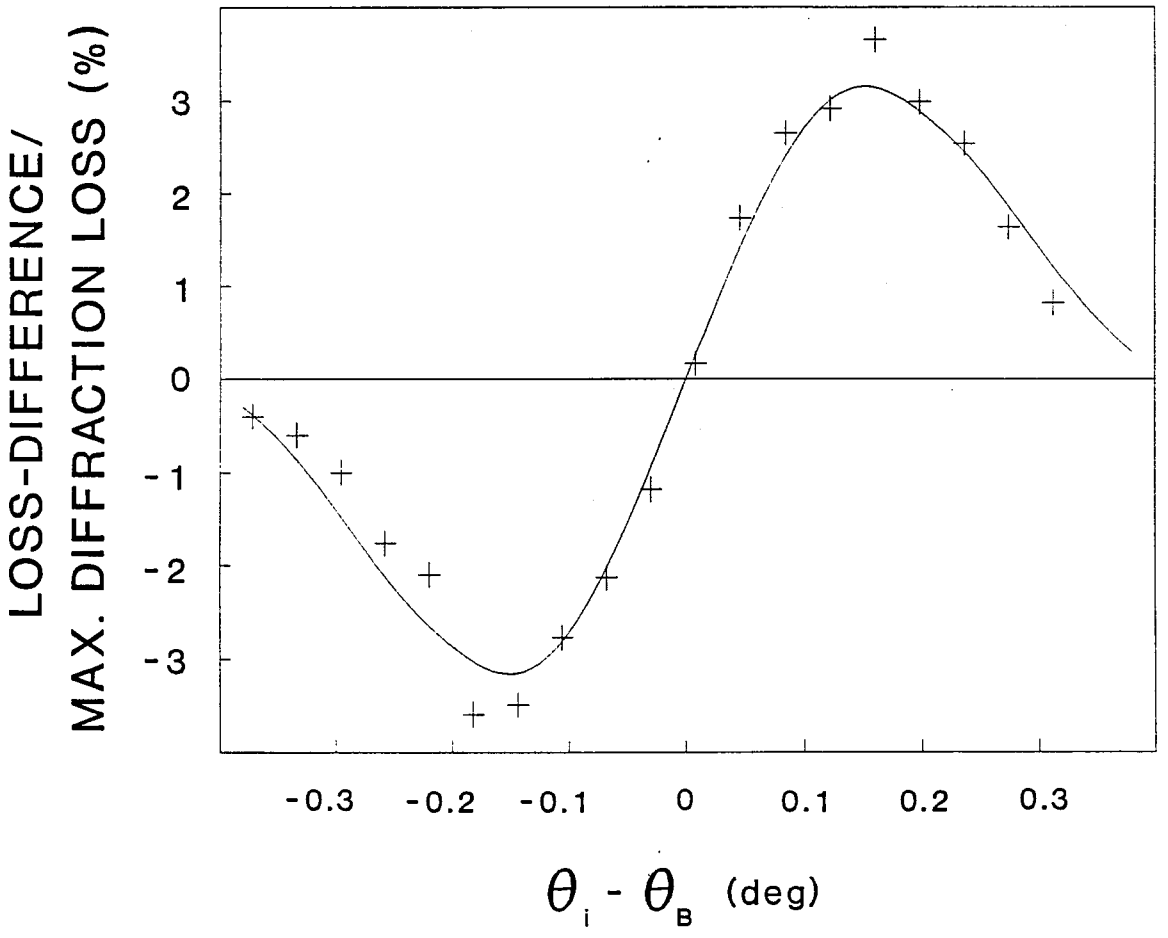

Fig 2.16 Experimentally determined loss difference in the ring cavity. The solid line shows the predicted value from eq (2.36).

2.4.3 Optimisation and Discussion

Further enhancement in the loss-difference with respect to the peak diffraction loss can be achieved by reducing the diffraction bandwidth ($\Delta\theta_{1/2}=0.89\lambda_s/\ell$) by, for example; using a longer Q-switch, operating at a higher acoustic frequency or using a larger laser beam with a smaller divergence. Alternatively, the ratio of loss-difference to applied diffraction loss at any angle can also be increased by using an acousto-optic medium in which the speed of sound is higher. One such material that is an excellent acousto-optic medium is tellurium dioxide (TeO_2). We had a TeO_2 modulator fabricated with the following parameters:

$n=2.35$

$v = 4.2\text{x}10^3\ ms^{-1}$

$\nu_s = 250MHz \qquad \therefore \lambda_s = 17\mu m$

This modulator has a Bragg angle of 1.8° (in air) at 1μm and a Bragg angle shift of 0.0089°. Using eq (2.38) we see that we should be able to obtain a loss-difference equal to 10% of the peak diffraction loss. This is approximately 3 times that possible with the lead molybdate modulator already described. As yet, this modulator has only been used in a 2μm ring laser (section 2.7), and appears to work very well as a unidirectional device, requiring only low r.f. power to enforce unidirectional operation.

It is worth noting that the requirements for efficient cw unidirectional operation are not necessarily the same as those for unidirectional Q-switched operation. This can be seen in Fig. 2.12(a) and (b). For cw operation it is desirable to have a high loss-difference but a low diffraction loss. For unidirectional Q-switched operation however, it is necessary to use the technique of prelase Q-switching and allow sufficient time between pulses to allow a unidirectional single frequency prelase to be established prior to opening the Q-switch. In this case it is desirable to have both a high loss-difference and a high diffraction loss. Clearly the choice of acoustic medium and orientation of the Q-switch will depend to a large extent on the desired mode of operation. However, since for many miniature solid-state ring lasers the loss-differences required are very small, it is often the case that a compromise can be made allowing either unidirectional cw or Q-switched operation to be achieved without adjusting the Q-switch.

2.5 Feedback Mechanism for Unidirectional Operation

When acousto-optic modulators were initially used as unidirectional devices in ring lasers, it was observed that two distinct mechanisms seemed to produce unidirectional operation. The first, described in the previous section, was an intrinsic property of the A-O effect, and only required the angle of the modulator to be altered. In some cavities, when resonator mirrors were moved, the oscillation direction repeatedly reversed, on a movement scale less than a millimetre. This occurred only when the diffracted beam was able to re-enter the modulator and then be diffracted back into the laser cavity. Thus, by using a sufficiently large cavity or using an aperture to block the diffracted beam, only the intrinsic mechanism could operate. When the diffracted beam could re-enter the modulator, the second mechanism could dominate the intrinsic mechanism.

This second mechanism, the "feedback" mechanism, is described in this section. It relies on the diffracted beam being resonated (either in an external cavity or in the main laser cavity) and fed back into the main beam, modifying the diffraction loss in a non-reciprocal manner. Although it is inherently more unstable than the intrinsic mechanism (this can be reduced, as discussed in section 2.5.2.3), it can provide loss differences of up to 100% for low insertion loss, and may be of use in a number of situations.

2.5.1 Theory

The basic principle of the feedback mechanism is shown in figure 2.17(a). The light wave in the laser resonator is of frequency ν. We shall consider only one axial mode of the laser resonator, for ease of discussion, although in principle there can be a number of frequencies oscillating in the laser. In the case shown, the light beam incident from the left on a travelling-wave A-O modulator is partially transmitted (at frequency ν) and partially diffracted, at frequency ν-ν_S, where ν_S is the frequency of the acoustic wave. The diffracted wave is then returned to the A-O modulator via a ring path involving three mirrors. The returning light wave is again partially diffracted by the acoustic wave, but now is frequency up-shifted so that the original frequency ν is

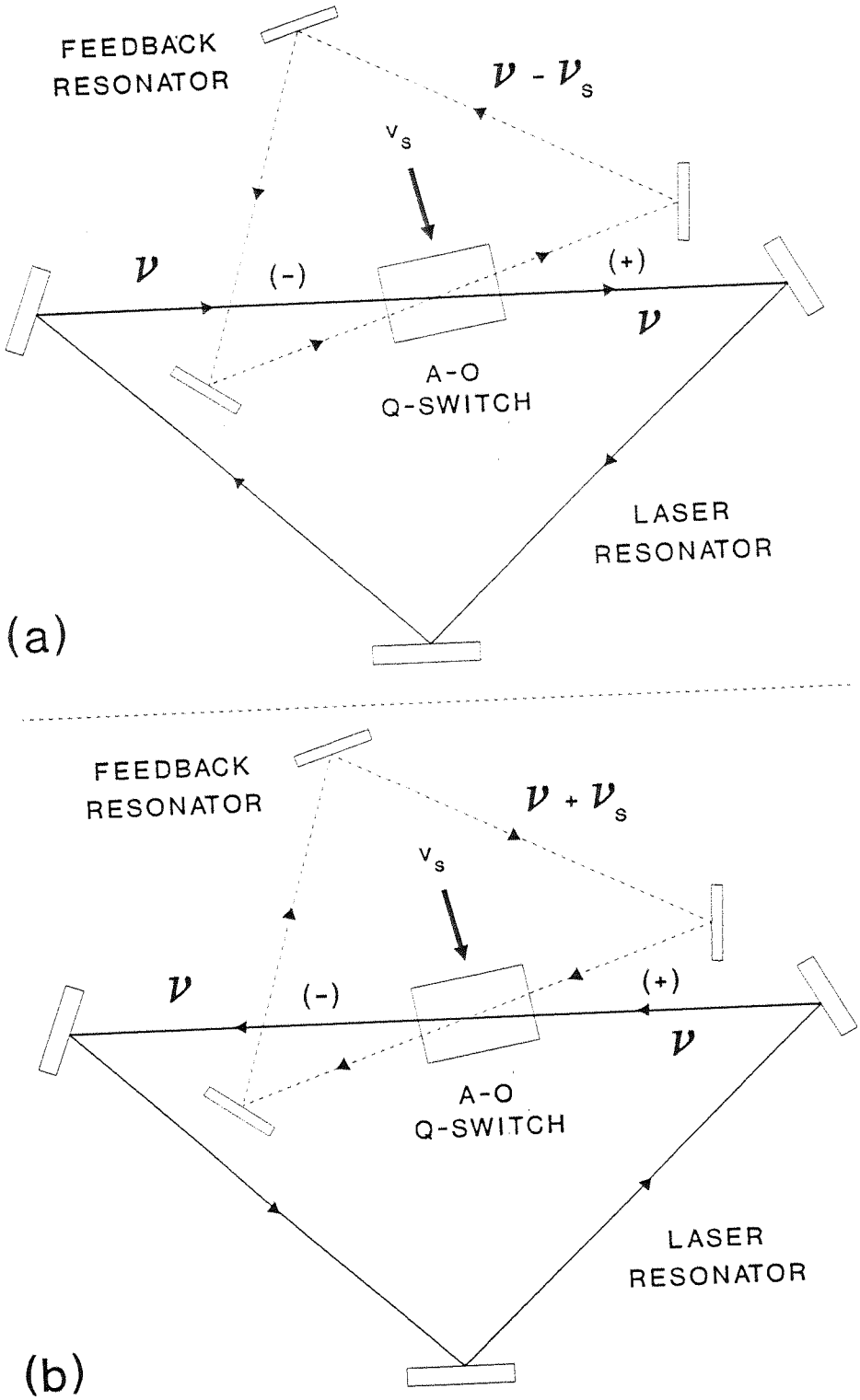

Fig 2.17 Basic principle of feedback mechanism. In **(a)** the laser beam propagating in the (+) direction produces a diffracted beam (shown as dashed line) which is frequency downshifted and returned to the main laser cavity, whilst in **(b)**, frequency upshifting occurs, producing a phase difference in the feedback cavity.

restored. If the feedback mirrors are correctly aligned, the original direction of propagation is also restored. The effective transmission of the incident light wave at the A-O modulator then depends on the round-trip phase shift of the resonated diffracted beam. A similar situation exists for the counter-propagating beam, shown in figure 2.17(b). Here the diffracted beam is initially frequency up-shifted to $\nu+\nu_s$, before being restored to its original frequency and direction on the second diffraction.

The two counter-propagating diffracted waves in figures 2.17a and 2.17b therefore have different frequencies (by twice the acoustic frequency) as they circulate around the feedback cavity, and must in general experience different phase shifts in this cavity. As a consequence the counter-propagating beams in the main laser cavity experience a different effective transmission at the A-O modulator. This attenuation at the modulator can be considered as an *effective diffraction loss* (e.d.l.), which can differ considerably from the diffraction loss in the absence of a feedback cavity. It can be shown, using a Fabry-Perot analysis (see Appendix A), that the effective diffraction losses, L^+_{eff} and L^-_{eff} for laser beams of frequency ν propagating in the (+) and (-) directions respectively are related to the single pass diffraction loss (in the absence of feedback) L_d and to the round-trip loss L_f of the feedback cavity (excluding diffraction loss), in the limit where $L_d \ll 1$ and $L_f \ll 1$, by the expression

$$L^{\pm}_{eff} \approx \frac{4L_dL_f}{(L_d+L_f)^2+16\sin^2\left(\frac{\delta^{\pm}}{2}\right)} \qquad \textbf{(2.40)}$$

where $\delta^{\pm}$ is the round-trip phase shift for the resonated diffracted beams produced in the counter-propagating directions. We have assumed here that the A-O modulator is operated close to the nominal Bragg angle so that $L_d^+ = L_d^-$. This phase shift is related to the optical path length ℓ_f of the feedback cavity and acoustic and optical frequencies by

$$\delta^{\pm} = \frac{2\pi\ell_f(\nu \mp \nu_s)}{c} \qquad \textbf{(2.41)}$$

We have also assumed that the counter-propagating beams have identical feedback paths, which is only strictly true if $\Delta\theta_B=0$, which will not be the case, as

shown in the previous section. However, the approximation is valid if $\Delta\theta_B$ is small compared to the laser beam divergence. From equation (2.40) it can be seen that the effective diffraction loss is at a maximum when $\delta^{\pm} = 2q\pi$ (q an integer), and is given by

$$L_{max} \approx \frac{4L_dL_f}{(L_d+L_f)^2} \tag{2.42}$$

whilst the e.d.l. is at a minimum when $\delta^{\pm} = (2q+1)\pi$ and is given by

$$L_{min} \approx \frac{L_dL_f}{4} \tag{2.43}$$

Eq. (2.42) shows that we expect the maximum e.d.l. to be much larger than L_d, and could approach 100% when the diffraction loss is matched to the feedback cavity loss (i.e. $L_d = L_f$). It is also apparent that for $L_f \ll 1$ the minimum e.d.l. is much smaller than L_d. The actual values of e.d.l. for counter-propagating beams will depend on the phase shifts for the (+) and (-) directions. Ideally all axial modes propagating in one direction (say +) would have phase shifts of $\delta^+ = 2q\pi$ and all counter-propagating modes to have $\delta^- = (2q+1)\pi$. In this situation the loss-difference between the two directions is

$$\Delta L = L_{max} - L_{min} \tag{2.44}$$

as all modes propagating in the (+) direction will have a net loss that is greater by this amount. Unidirectional lasing would then occur preferentially in the (-) direction. The effective insertion loss for the device is then simply given by L_{min}. As this is an interferometric technique, the phase-shift and hence lasing direction is very sensitive to relative changes in the length of the laser and feedback cavities. The lasing direction reverses with each half-wavelength change in difference between the lengths of the cavities. As we show in [Clarkson, 1992b], the loss-difference is large only close to the resonance condition, which at first suggests that unidirectional operation should only occur near resonance. However, since the loss-difference required for unidirectional operation can be very small (e.g. ~0.01% [Clobes, 1972]), it should be possible to operate the feedback cavity far from resonance and still obtain unidirectional operation.

2.5.2 Experimental Verification

The experiments described in this section were not necessarily performed in the order given here, but are described in this way to present a more logical sequence of verification of the theory described previously. First we look at the concept of effective diffraction loss (e.d.l.) and attempt to isolate this from the complex ring laser/feedback cavity system described in the theory section. Having established that e.d.l. operates as expected, we construct a ring laser with external feedback cavity and examine its behaviour. Finally the performance of self-feedback cavities is investigated.

2.5.2.1 Effective Diffraction Loss

To investigate e.d.l. the system shown in Figure 2.18 was used. The output from a single frequency rhomb ring laser (see, for example, Section 2.6 and Clarkson[1991a]) was fed into the triangular ring cavity which contained a lead molybdate A-O modulator. A single frequency source was used to simplify the comparison between theory and experiment as we do not need to consider adjacent axial modes. The input beam passes through a highly reflecting curved mirror and is incident on the A-O modulator at the nominal Bragg angle. After passing through the modulator, the input beam then reflects off the plane mirror and leaves the cavity (i.e. it is not resonated) where a detector connected to an oscilloscope monitors its amplitude.

The diffracted beam produced when the A-O modulator is operating is resonated around the cavity (out of the plane of the diagram) before being returned to the modulator at the same angle as it left at. Here it undergoes a second diffraction, and depending on its round-trip phase shift will modify the diffraction loss experienced by the input beam. The input HR mirror is mounted on a piezo-electric transducer (PZT) so that the cavity length can be rapidly scanned, thus altering the phase shift of the resonated beam. The oscilloscope trace (Fig 2.19) shows a typical example of the effect on the input beam. The large dips in the output correspond to a large e.d.l ($>90\%$) for an applied diffraction loss of only a few percent. This occurs only at the resonance condition for the diffracted beam, and off-resonance the e.d.l. is almost negligible (i.e. low insertion loss).

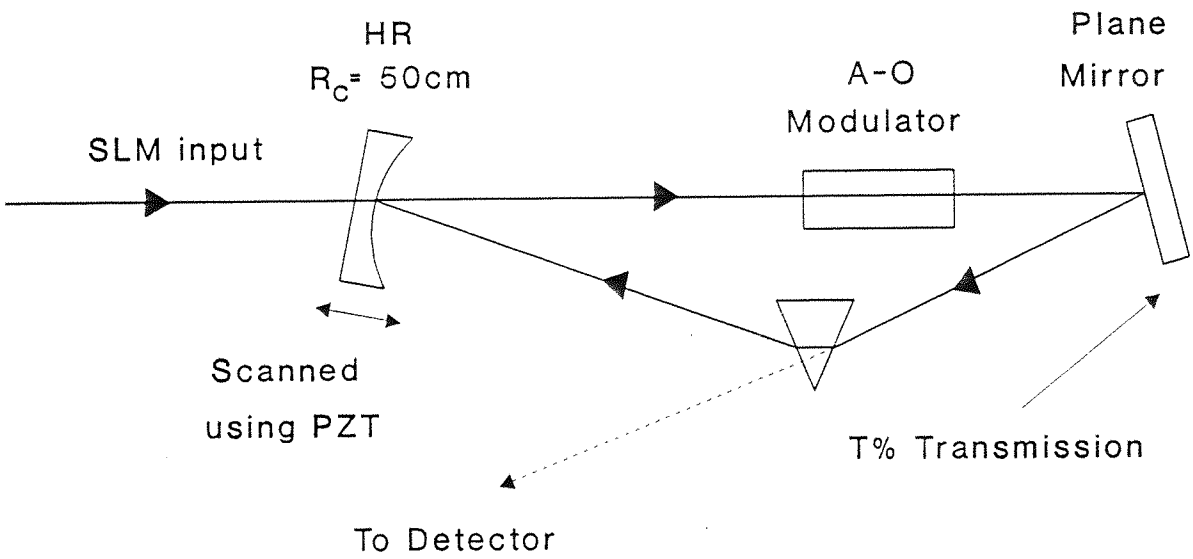

Fig 2.18 Experimental system used to measure effective diffraction loss. The dashed line shows the nondiffracted, unresonated beam that is detected, and from which the effective diffraction loss is determined. The diffracted beam is resonated in the ring cavity formed by the curved mirror, plane mirror and prism, and is inclined out of the plane of the page.

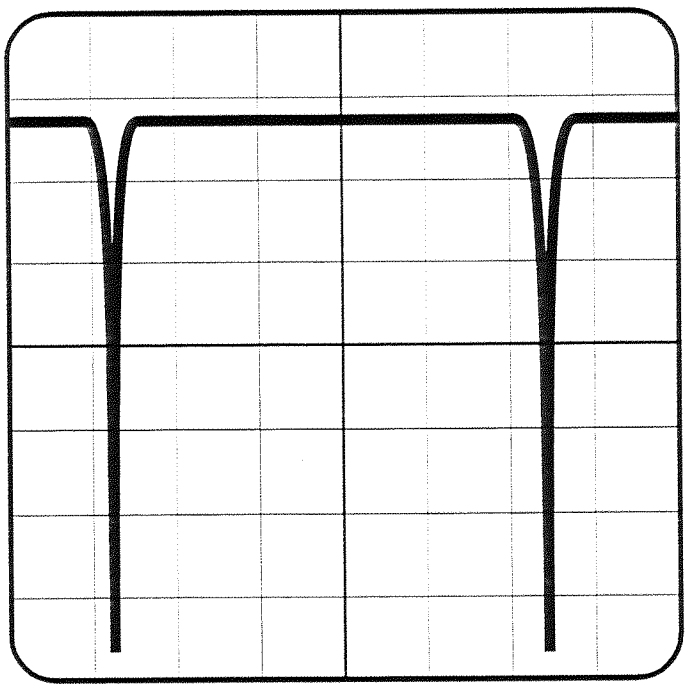

Fig 2.19 Oscilloscope trace showing effective diffraction loss as the feedback cavity length is scanned.

As shown in the theoretical development of this technique, the peak e.d.l. is obtained when the applied diffraction loss is matched to the loss in the feedback cavity. In the experiment here, the loss in the resonating cavity is mainly determined by the transmission (T) of the plane mirror. The cavity losses (excluding diffraction loss) were calculated to be approximately 1% when T=0 (i.e. HR mirror) was used. These losses are mainly due to imperfect AR coatings on the A-O modulator and losses in the prism.

We used a variety of plane mirrors with different transmissions and varied the diffraction loss to examine how the peak e.d.l. (on resonance) changed. The results for three mirrors are shown in Fig 2.20. It is clearly seen that the peak e.d.l. occurs when the applied diffraction loss is matched to the cavity loss (output transmission + 1%), and in each case was greater than 90%. This value is probably less than 100% due to factors such as the existence of some higher order diffracted beams which are not resonated, and the possibility that the diffracted beam does not have perfect Gaussian beam profile. Also of interest is the e.d.l. for very small diffraction losses, especially for low loss cavities. An e.d.l. of 46% was observed for an applied diffraction loss of ~0.2% and 16% for ~0.06% when the HR mirror was used. This shows that the feedback technique could be used to produce a large e.d.l. even for materials that are not normally considered to be good A-O media. These experiments successfully verified the concept of effective diffraction loss, and show that it could have applicability to situations other than unidirectional ring lasers, where a large effective diffraction loss is required for only a small available diffraction loss.

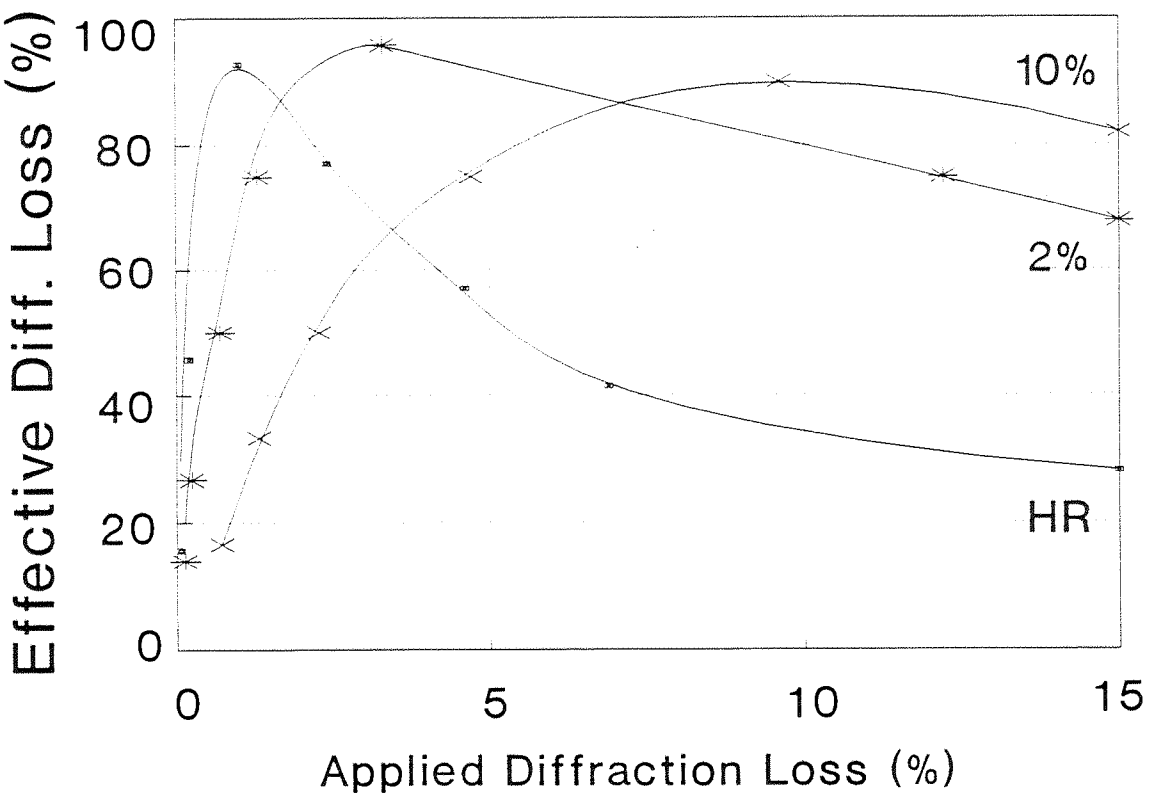

Fig 2.20 Peak effective diffraction loss for cavities with different losses. The output coupler used in each case is shown. E.d.l. is a maximum when the applied diffraction loss is equal to the cavity loss.

2.5.2.2 External Feedback Cavities

The next stage in verifying the feedback mechanism is to use an external feedback cavity to return the diffracted beam to an A-O modulator in a ring laser cavity. The experimental set-up shown in Fig 2.21 was used, consisting of a Nd:YAG triangular ring laser pumped by two polarisation coupled one-watt diode lasers and is similar to that described in section 2.4.2. The lead molybdate A-O modulator was positioned approximately at the mid-point of the longest arm of the ring cavity, which had a perimeter of 1 metre. The Nd:YAG rod, anti-reflection coated at 1.06μm at both ends, was positioned near the beam waist, and the pump light was incident at a small angle to the normal, as shown. The laser had a threshold of ~600mW incident pump power and an output of ~400mW for 1.8W of pump power. The A-O modulator produces a diffracted beam inclined at twice the Bragg angle with respect to the laser beam. This angle is small and determined the length of the ring resonator used, as we have to be able to access the diffracted beam without clipping the main laser beam. This was achieved using a prism and a high reflecting 50cm curved mirror placed, respectively, just above and just below the main beam (out of the plane of the diagram). The feedback cavity was completed using a high reflector mounted on a PZT so that the length of the feedback cavity (and hence the phase of the resonated beam) could be varied. This feedback cavity closely resembled the main cavity and was of approximately the same length.

The A-O modulator was operated at the nominal Bragg condition to eliminate any contribution from the intrinsic mechanism. This was achieved by blocking the feedback cavity and then adjusting the angle of the modulator around the Bragg condition until bidirectional operation resulted. The feedback cavity was then restored and its length adjusted until unidirectional operation resulted. This was confirmed to be single frequency with a scanning confocal Fabry-Perot interferometer with a free spectral range of 7.5GHz. The minimum r.f. power required to enforce unidirectional operation was less than 0.005W which corresponds to a single pass diffraction loss, L_d of less than 0.5%. From a comparison of the laser thresholds with and without the modulator operating and a knowledge of the laser round-trip loss (approximately 6.7% excluding diffraction) it was estimated that the effective insertion loss for the modulator

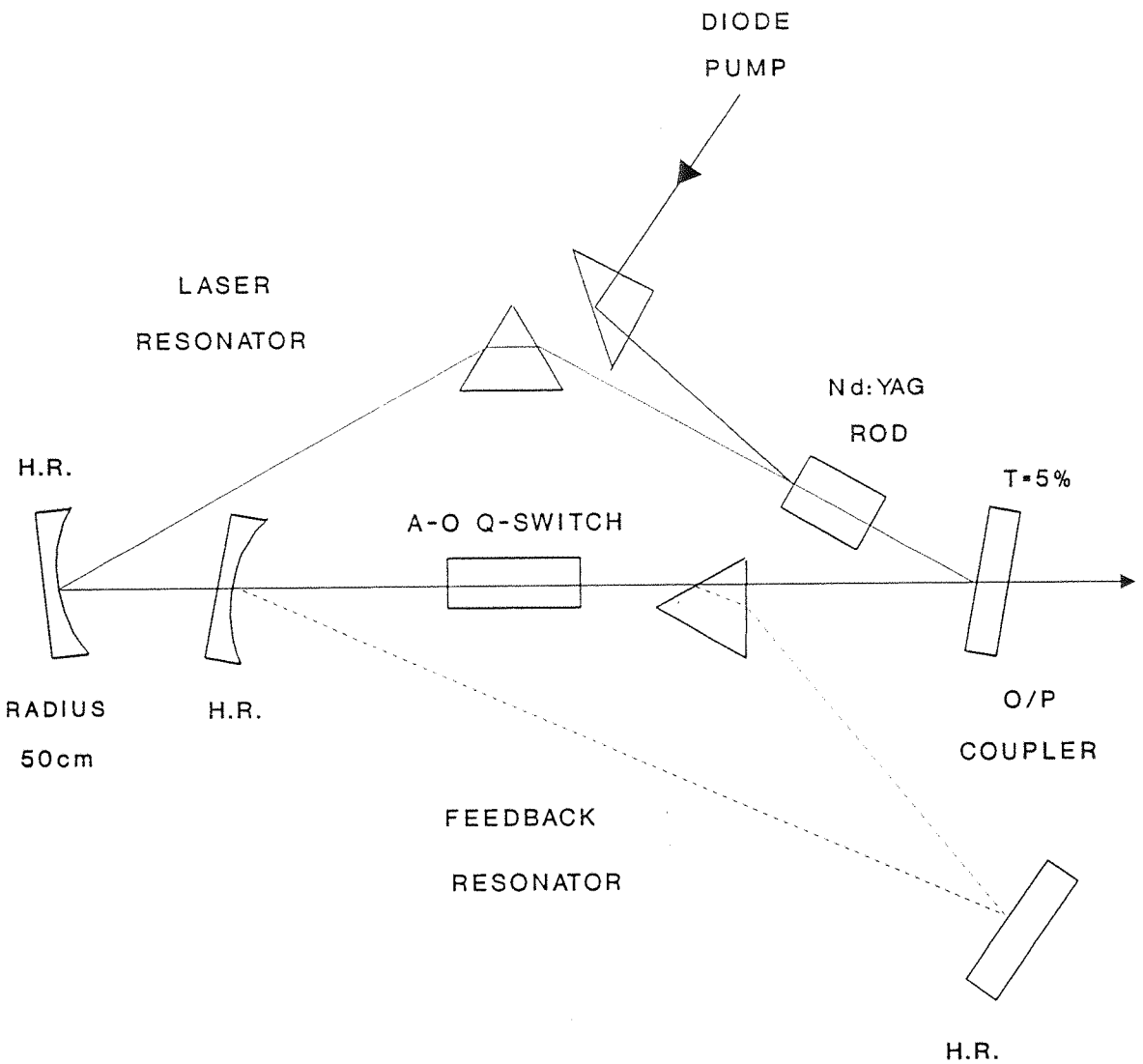

Fig 2.21 Schematic of ring laser with external feedback cavity to enforce unidirectional operation. The feedback cavity is shown with the dashed lines and is inclined out of the plane of the page. The curved HR mirror in the feedback cavity is below the main laser resonator and the prism is above the main cavity.

(excluding its imperfect antireflection coatings) is $<0.1\%$. This is negligible compared to other resonator losses.

For relatively low values of diffraction loss ($<10\%$, single pass), the insertion loss was found to increase linearly with diffraction loss as expected, but its value ($\sim 0.1L_d$) was significantly larger than the value $0.002L_d$ predicted by equation (2.43) and based on a known value for the round-trip loss of the feedback cavity of $\sim 1\%$. This discrepancy was thought to be due to a combination of imperfect mode matching, and the fact that a significant fraction of the light was also diffracted into other orders which were not resonated in the feedback cavity.

A direct measurement of loss difference predicted by equation (2.44) has not been made. Measurement techniques based on transient laser behaviour as earlier in section (2.4.2), would be complicated by the fact that for a high finesse feedback cavity it takes many round-trips for the loss difference to buildup. Instead, to gauge some idea of the magnitude for the loss difference, we have scanned the feedback cavity length over several microns using the piezo length adjustment whilst monitoring the laser outputs for both lasing directions. A typical oscilloscope trace (Fig. 2.22) shows the situation where $L_d \sim 1\%$. It can be seen that the lasing direction reverses as the feedback length is changed, as expected. In addition one also sees that unidirectional lasing is maintained over a range of feedback path lengths far from the resonance condition and that the change in lasing direction occurs rapidly over a very small cavity length change of $\sim \lambda/30$. This is consistent with our expectations that more than sufficient values of loss difference to provide robust unidirectional operation are indeed attainable via this technique.

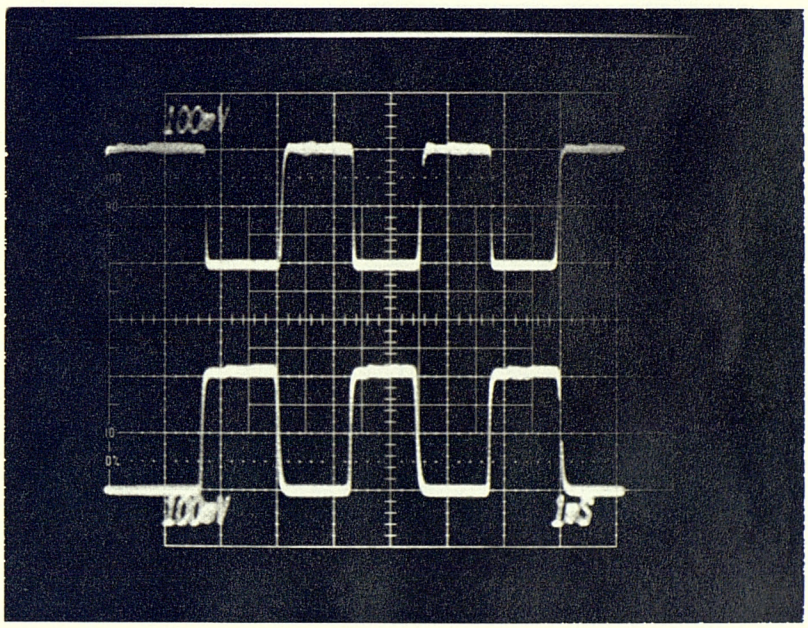

Fig 2.22 Oscilloscope trace showing change in lasing direction for every λ/2 change in feedback cavity length. Each trace shows lasing in one of the counter-propagating directions.

2.5.2.3 Self-feedback cavities

One obvious disadvantage of this feedback technique is the sensitivity of the direction of oscillation to relative changes in the length of the feedback and lasing cavities. As shown in Fig 2.22, every $\lambda/2$ change in relative length leads to a change in lasing direction, which is unsatisfactory for practical laser systems. One possible way of overcoming this problem is to use the laser resonator itself as the feedback cavity. In this way the laser and feedback cavities are coupled together and relative changes in length are greatly reduced.

Such a "self-feedback" cavity is readily achieved in a miniature ring laser, such as the rhomb-ring laser described in [Clarkson, 1991a and 1991b], and in the following sections in this chapter. Indeed, we believe that many of the early observations of acousto-optically induced unidirectional operation of ring lasers were as a result of the diffracted beam being resonated in the laser medium after re-entering the A-O modulator. When an aperture was inserted in the cavity to block the diffracted beam, the sensitivity of direction of lasing to cavity length disappeared, and only the angle of the A-O modulator was important. In the rhomb-ring laser which we have used, the direction of oscillation reverses for a 0.2mm change in length of the cavity, some 400 times greater length stability than for an external feedback cavity.

We also constructed a triangular ring resonator (Fig 2.23) where the diffracted beam is fed back into the A-O modulator by the main laser cavity, which in this case is defined by the dielectric mirror coating on the Nd:YAG rod, a curved mirror and a prism. This self-feedback cavity required only a very low applied diffraction loss to enforce unidirectional operation, with an insertion loss (neglecting imperfect AR coatings) of $<0.1\%$. The cavity was also relatively insensitive to length changes, with a change in lasing direction being produced by a 0.4mm change in cavity length.

These self-feedback cavities provide a practical means of using the feedback technique to enforce unidirectional operation, as no special stabilisation is required to maintain the direction of lasing. In lasers where the A-O modulator is also the laser medium, this may be the only way of achieving a high enough loss-difference to enforce

unidirectional and hence single-frequency operation, and will therefore become important in the development of monolithic single frequency lasers.

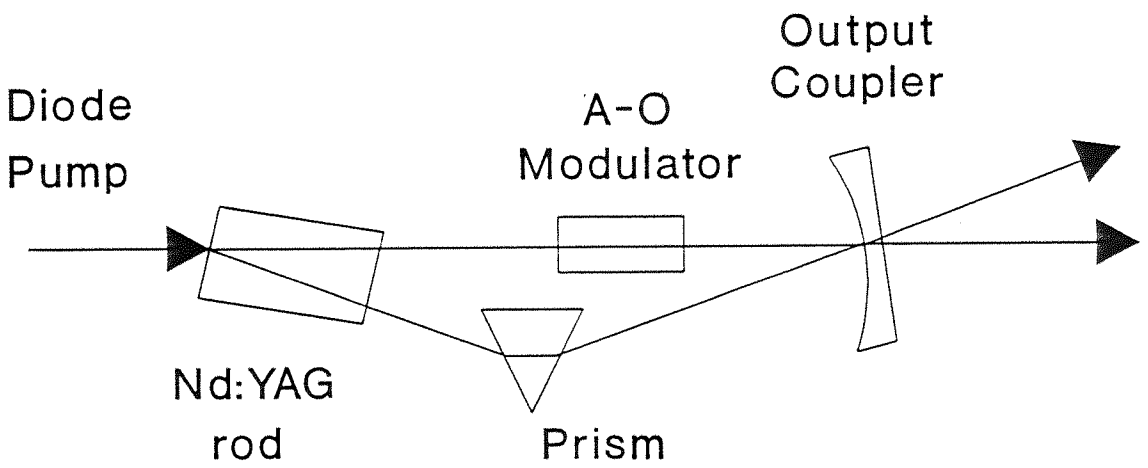

Fig 2.23 Triangular ring laser where the diffracted beam is fed back into the acousto-optic modulator by the cavity mirrors. In this diagram the main laser beam and resonated diffracted beam lie on top of each other, with the diffracted beam angled out of the plane of the page relative to the laser beam.

2.6 A 1.3μm Unidirectional Ring Laser

Having identified the mechanisms responsible for unidirectional ring laser operation, we extended the diode-pumped work at 1μm to the 1.3μm transition in Nd:YAG [Neilson, 1993]. This transition ($^4F_{3/2}$ - $^4I_{13/2}$), whilst weaker than the 1.064μm transition (cross-section ~5 times smaller [Singh, 1974]), can be made to oscillate by appropriate mirror coatings to suppress the 1μm line. The fact that the A-O effect can be a low-loss means of enforcing unidirectional operation suggests that it is ideal for use on a low-gain transition such as this. Initial expectations were that this experiment would demonstrate the applicability of this technique to a low-gain transition that is also of interest in a number of applications. However, behaviour we had not expected occurred. We were able to obtain stable, simultaneous single frequency operation on two closely spaced transitions around 1.3μm. Although other papers have observed this behaviour [Trutna, 1987], [Grossman, 1990], no explanation was offered to explain how two single axial mode frequencies could stably oscillate together. The explanation behind this effect is described in section 2.6.3 below, and demonstrates that very small amounts of spatial hole burning can result in gain being available for other frequencies to oscillate.

2.6.1 Experimental Details

The experimental arrangement is similar to that described in previous papers [Clarkson, 1991a and 1991b], and is also shown in figure 2.24. The laser cavity consists of only three elements; a Nd:YAG rod, a lead molybdate A-O Q-switch, and an output coupler. The Nd:YAG rod was coated at its input face to be highly reflecting (>99.8%) at 1.3μm and highly transmitting (>95%) at the pump wavelength (~800nm), with its other face antireflection coated at 1.3μm. The rhomb-shaped lead molybdate A-O Q-switch defines the ring path in the resonator, acts as a polarizer, and is used to enforce unidirectional operation. The output coupler had a radius of curvature of 50 mm, and reflectivity of 96% at the lasing wavelength. Output couplers with transmissions ranging from 0.7% to 10% were tested, with the 4% output coupler giving the maximum output power. Comparing laser threshold for each of these output couplers allowed the loss in the cavity (excluding the output coupling) to be determined

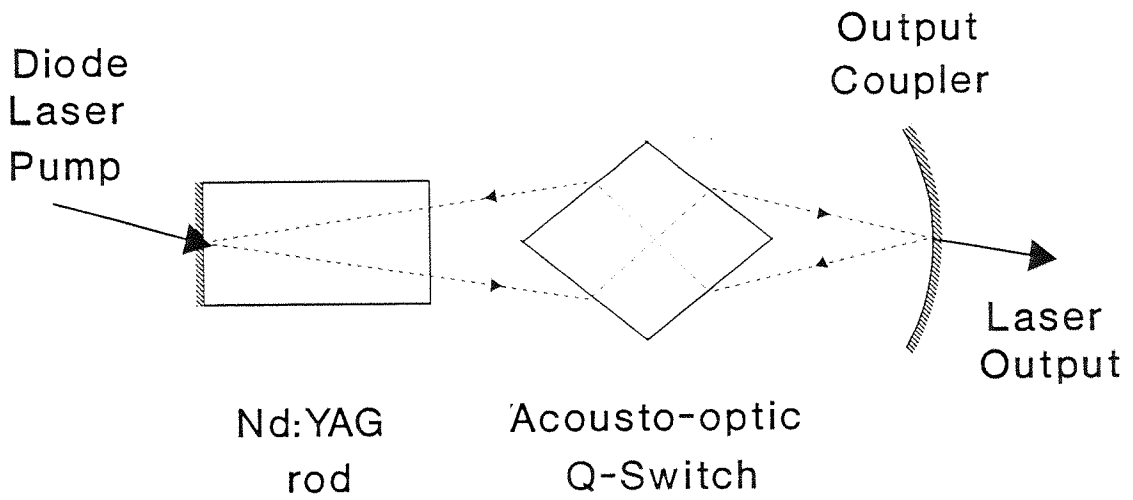

Fig 2.24 Schematic of rhomb-ring laser used in 1.3μm single frequency experiments.

as 1.4%. The short cavity length (physical length of 35 mm) is advantageous, since it increases the discrimination between adjacent axial modes (eq. (2.1)), thus facilitating single frequency operation, and also leads to shorter Q-switched pulses. The ring laser was pumped by two 0.5W laser diodes (SDL-2430), each collimated and compensated for astigmatism using anamorphic prisms and then polarization coupled and focused into one arm of the ring cavity with spot sizes matched to the lasing mode size. When combined, these diodes, temperature tuned to the peak of the Nd:YAG absorption, gave a maximum incident pump power of 850mW.

Unidirectional operation of the ring laser can be achieved using either the intrinsic or feedback mechanisms described in sections 2.4 and 2.5 respectively. The intrinsic method is implemented by placing an aperture in the cavity to prevent the diffracted beams from being fed back into the cavity, and then tilting the Q-switch to bias it slightly to one side of the Bragg condition, as explained in section 2.4. Alternatively, without the aperture, the diffracted beam can be fed back, via a second A-O diffraction, into the main resonator as described in section 2.5, thus introducing a large loss difference between the counter-propagating waves and thereby favouring one direction of propagation. The intrinsic method required more r.f. power to the A-O modulator than the feedback method for unidirectional operation, leading to an increase in loss in the cavity of $\sim 2\%$ under the conditions of this experiment. By comparison, the feedback mechanism only required sufficient r.f. power to produce $\sim 0.025\%$ diffraction loss, resulting in only a marginal increase in laser threshold and no observed change in maximum output power.

2.6.2 Results

Initially, when the laser was operated bi-directionally (i.e. with no applied r.f. field), it was noted that two wavelengths were lasing, corresponding to the 1.319μm and 1.338μm transitions of Nd:YAG. When the laser was made to operate unidirectionally by applying r.f. power to the A-O modulator, it continued to lase at these two wavelengths. Using a scanning Fabry-Perot plane-plane interferometer with a free spectral range of 37.5GHz, it was confirmed that for both of these lines lasing occurred on a single axial mode, i.e. just two lasing modes were being supported (Fig

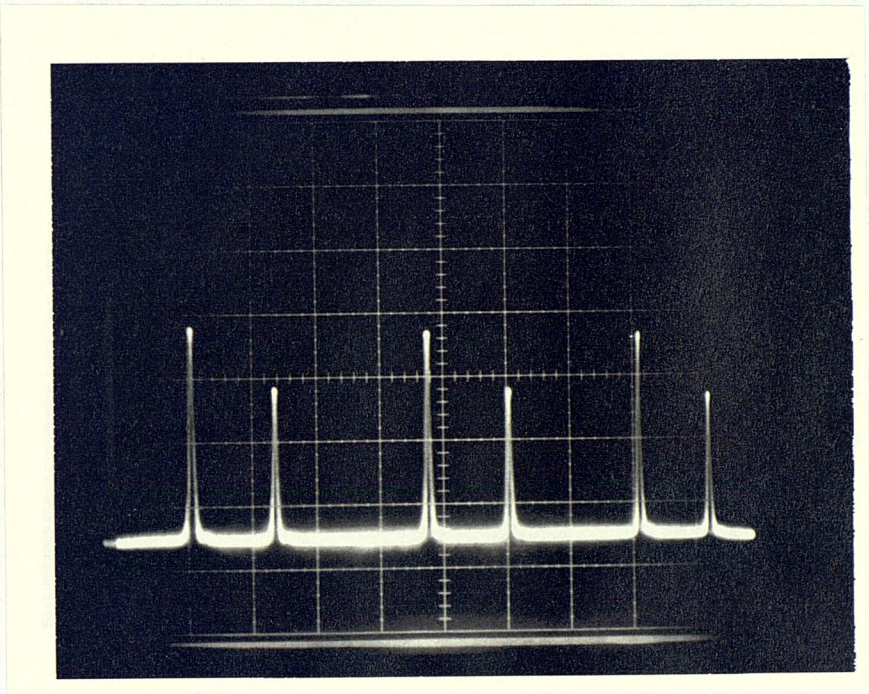

Fig 2.25 Output from the scanning Fabry-Perot interferometer. The two peaks correspond to the 1.319 and 1.338μm transitions, both oscillating single frequency.

2.25). It was observed that by applying a higher r.f. power, the 1.319μm line could be suppressed completely. This is consistent with the fact that the diffraction loss is inversely proportional to the square of the optical wavelength (for small diffraction losses), thus an increase of r.f. power leads to a greater increase (by $\sim 3\%$) in loss for the 1.319μm transition compared to the 1.338μm transition. This difference in diffraction loss for the two wavelengths means that the 1.319μm transition will be the first to be suppressed at higher r.f. powers. It was also noted that the 1.319μm transition had the lower lasing threshold of the two transitions for all the output couplers tried. Thus if the losses in the cavity could be increased uniformly for both wavelengths (which is not possible with just an A-O modulator), eventually only the 1.319μm transition would lase, as indeed observed by Trutna[1987], suggesting that this transition has the higher gain of the two.

The CW performance of the laser, as shown in figure 2.26, was as follows. With a 4% output coupler the threshold incident pump power was 285mW, and a slope efficiency of 28% (summing the output at the two frequencies) was achieved, with 155mW output for 850mW incident power. The output power at both frequencies was approximately equal under these conditions and their relative intensities (as well as the total output) remained stable. If the laser is Q-switched by building up from noise the output is observed to be multi-axial mode, as noted in [Clarkson, 1991a], since there is then insufficient time to establish unidirectional operation, and Q-switch pulses are then produced in both directions. To ensure single frequency Q-switched operation, we operate the laser with a low level unidirectional single-frequency prelase [Hanna, 1972]. At low prelase powers, i.e. 1-2mW output, operation on the 1.338μm line alone was observed, whereas for higher prelase powers simultaneous Q-switched pulses at both 1.319μm and 1.338μm were produced with single frequency operation on both of these lines. This is consistent with the earlier observation that the diffraction loss is higher at 1.319μm and hence with the higher r.f. power required to maintain a low prelase level, this transition can be suppressed. A scanning Fabry-Perot interferometer was used to confirm that the Q-switched pulses which build up from the prelase were single frequency. When the laser was operated Q-switched with only the 1.338μm transition operating single frequency, pulse energies of 30μJ were obtained at a 500 Hz repetition rate, with pulse widths of 40 nsec (Fig 2.27), corresponding to a peak power of 630 W.

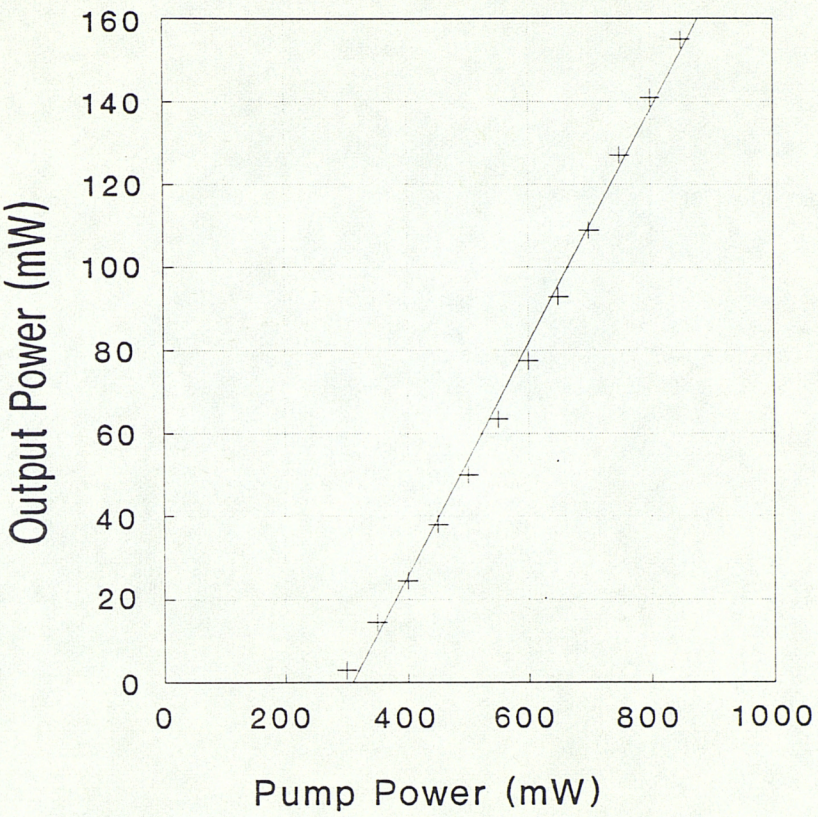

Fig 2.26 CW output power from unidirectional 1.3μm ring laser, summing the output at both lasing frequencies.

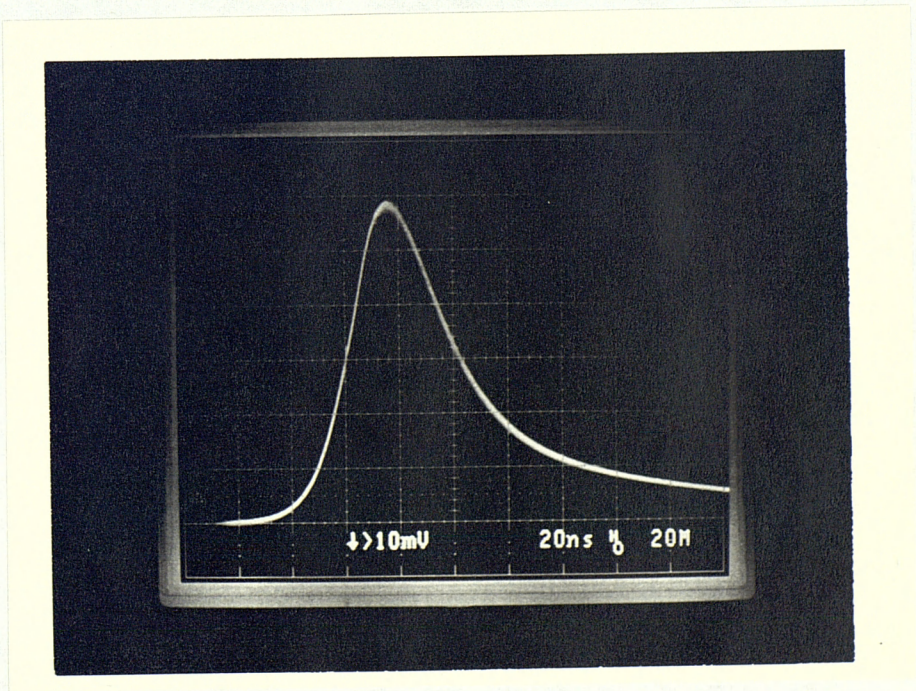

Fig 2.27 Oscilloscope trace showing Q-switched pulses at 1.338μm.

2.6.3 Explanation of Two-Frequency Operation

The stable simultaneous operation on two lines is at first sight surprising, since the two transitions share the same upper laser level ($^4F_{3/2}$) and hence compete for the same excited population. Single frequency operation is achieved in most unidirectional ring laser systems with adjacent mode frequencies of slightly lower gain suppressed once spatial hole burning is eliminated. On the same basis the expectation would be that one or other of the 1.3μm transitions would dominate since gain on the two transitions would be unlikely to be equalised to such a degree as to allow stable simultaneous operation. The mechanism that is responsible relies on the fact that spatial hole burning is not completely eliminated, there being a small degree of spatial hole burning at the high reflector of the laser rod, where there is an overlap between the incident and reflected beam. Thus, when the laser operates on a single frequency there is some gain available at the nodes of the standing wave pattern in the overlap region, as shown schematically in figure 2.28. For another frequency to access this gain it must be sufficiently well spaced from the oscillating frequency that its standing-wave pattern gets out of step with that of the oscillating frequency, within the overlap region, i.e. its antinodes fall on the nodes of the first frequency. Further, the gain of the second frequency must be close enough to that of the first frequency so that the extra gain it can access in the overlap region will allow it to reach threshold and oscillate simultaneously with the first. These requirements are both met under the conditions of our experiment for the 1.319μm and 1.338μm lines in Nd:YAG [Clarkson, 1993a]. Stable operation occurs because competition between the two frequencies is removed where the nodes of one standing-wave pattern overlap the antinodes of the other. All other frequencies are suppressed since near-neighbouring axial modes have antinodes closely coincident over the overlap region with antinodes at the already oscillating frequencies and thus find insufficient extra gain available to them. Stable, simultaneous two-mode operation is thereby achieved on these transitions.

The observation that a small degree of spatial hole burning can produce stable oscillation on more than one isolated frequency (i.e. with no neighbouring modes oscillating) has implications for many unidirectional ring laser systems [Clarkson, 1993b]. Complete elimination of spatial hole burning would require the gain medium

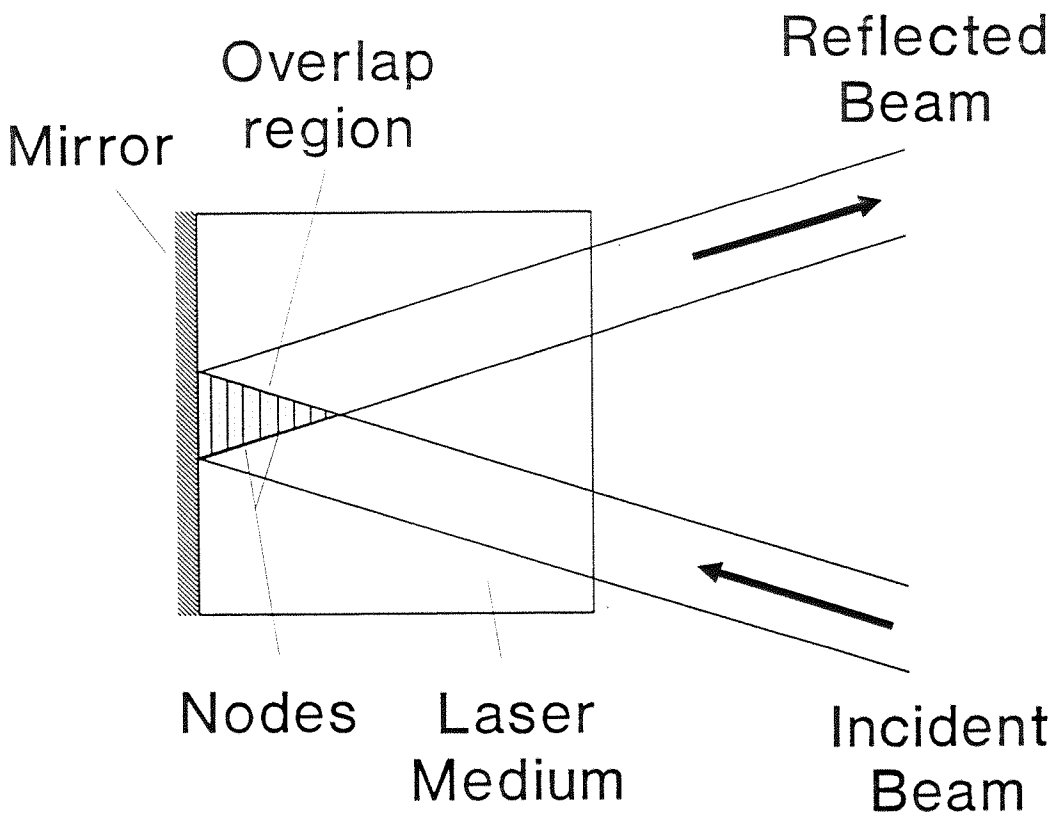

Fig 2.28 Schematic of spatial hole burning at the overlap region in the ring laser, and the resultant nodes that allow a second frequency to lase.

to be moved away from the high reflector. Attention may also have to be paid to residual reflections from antireflection coatings. Conversely the mechanism can be exploited for deliberate two (or more) frequency operation, and in this case control over the degree of spatial hole burning can be achieved by controlling the distance by which the high reflector is displaced from the gain medium, and by changing, for example, the mode size and beam angles in the gain medium.

2.6.4 Future Work

The measured losses in our cavity (1.4%) proved to be higher than expected, based on typical figures for 1μm lasers. The cause of this is not certain, however with an improved cavity design (i.e. lower resonator loss) we would expect to see a marked improvement over the powers reported here. A CW output of in excess of 200mW and Q-switched pulses of 40μJ should be readily realizable for 1W of pump power. With appropriate mirror reflectivities it would be easy to discriminate between the two lines and hence ensure operation on only one of the two lines. On the other hand the stable two mode operation that we have described is also of interest and may have a number of applications, including the generation of short wavelength microwave radiation, and the generation of high frequency phonons. The same principle can be extended to other lasers by deliberately equalising the (net) gain of two transitions, or inserting a Fabry-Perot etalon so as to give two equal (net) gain peaks within a single laser transition.

2.7 A 2μm Unidirectional Tm:YAG Ring Laser

2.7.1 Introduction

Lasers operating at wavelengths around 2μm are of interest in a number of fields, including medicine and laser radar (lidar). Because 2μm radiation is considered to be "eye-safe" compared to 1.06μm radiation it is suitable for atmospheric propagation in applications such as coherent Doppler velocimetry, DIAL measurements of CO_2 and H_2O, and as sources for upconversion to detect NO and CO molecules. Around 2μm there are also many atmospheric "windows" which allow long range lidar work, if the laser can be tuned to the appropriate wavelength. Two of the most common sources for 2μm radiation are the trivalent Holmium and Thulium ions, either in crystals on their own, e.g. Tm:YAG [Storm, 1989a], [Suni, 1991], [Pinto, 1992], in crystals using energy transfer between the two ions, e.g. Tm:Ho:YLF [Hemmati, 1989], Ho:Tm:YAG [Storm, 1989b] or intracavity pumping of Ho^{3+} in a Tm:YAG laser [Stoneman, 1992].

These lasers can be pumped at around 785nm, making them diode laser pumpable and hence suitable for making compact, efficient sources that can, for example, be flown on aircraft. We have used Tm:YAG to construct a unidirectional ring laser, as single frequency sources are needed as master oscillators for coherent Doppler applications such as windshear detection or global wind speed measurements from a satellite. Tm:YAG is a quasi-three level laser system, which is tunable over 200nm [Stoneman, 1990]. This tunability arises from the fact that the phonon broadening of the Stark transitions is much larger than in crystals such as Nd:YAG, and the multiplicity of transitions is much greater than in Nd:YAG. The upper laser level ($^3F_4$) is one of 9 Stark levels, and the lower ($^3H_6$) is one of 13, giving a large number of possible transitions. The ring laser described in this section, whilst only producing single frequency output for low powers, is potentially a diode-pumpable, high power, single mode laser, which should be easily tunable with the inclusion of an etalon or similar tuning device.

2.7.2 Experimental

The rhomb-ring laser used is of similar construction to that described in the previous section and for 1.06μm [Clarkson, 1991a] and 1.3μm [Neilson, 1993] lasers. Here the laser medium is a 4.3 at.% doped Tm:YAG rod, 4.2mm in diameter and 4mm long. The rod is HR coated at 2μm on its input face and AR coated on the opposite end. The Tm:YAG rod is wrapped in indium foil and cooled with a Peltier effect heat pump to reduce the lower level laser population of this quasi-three level laser and thus reduce the threshold and increase efficiency. When the Tm:YAG rod was cooled, condensation and icing up of the rod became a major problem. To prevent condensation, the entire laser cavity was sealed and purged with oxygen free nitrogen gas whenever the laser was operated below room temperature. Initially the lead molybdate rhomb modulator described earlier in this chapter was used in the laser, but a better optimised Q-switch became available during the course of these experiments. This A-O modulator was a Tellurium Dioxide (TeO_2) rhomb, with sides of length 15mm. This A-O modulator was operated at an acoustic frequency of 250MHz, which produces a larger Bragg angle shift $\Delta\theta_B$, as discussed in section 2.4.3. The output coupler used was a 50mm radius of curvature mirror with 2% transmission at 2μm. The physical length of the cavity was 47mm, producing lasing mode sizes of w_x=121μm and w_y=114μm at the plane mirror on the Nd:YAG rod. As no diode lasers were available to us that could pump at the peak Tm:YAG absorption of 785nm, we used an argon-ion pumped Ti:Sapphire laser tuned to this wavelength. As shown in Fig 2.29, the output from this laser was split into two beams, which could then be used to pump each arm of the ring laser cavity. This was done to reduce the reabsorption loss inherent in this quasi-three level laser. Without this measure, the unpumped arm of the laser rod would have produced a loss due to reabsorption of the laser beam, thus degrading the performance of the laser. The Ti:Sapphire laser produced up to 2.3W of power at 785nm, and after losses from the optics used to split, steer and focus the beam, we typically had around 2W incident on the Tm:YAG rod.

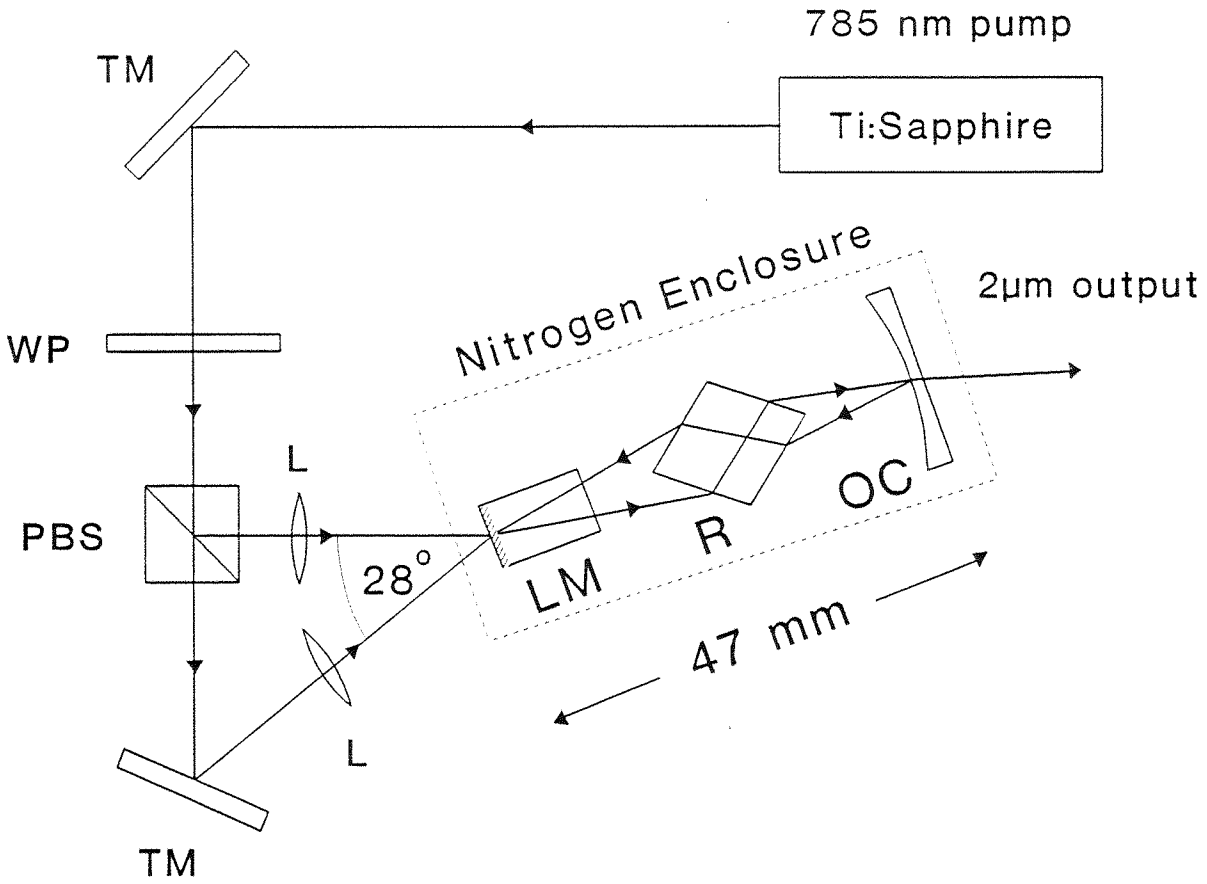

Fig 2.29 Schematic of 2μm rhomb-ring laser. The Ti:Sapphire pump laser is split using the half-wave plate (WP) and polarising beam splitter (PBS) and directed using the turning mirrors (TM). It is focused with lenses (L) into the laser medium (LM). The TeO_2 rhomb (R) enforces unidirectional operation, and a 2% output coupler (OC) is used.

2.7.3 Results

Initial results using a standing wave laser (i.e no rhomb element) demonstrated the importance of cooling the Tm:YAG rod to achieve good performance. At room temperature ($\sim 26°C$) the lasing threshold was around 300mW and the slope efficiency was 30%, whereas when cooled to -15°C, the threshold was 150mW and slope efficiency was again $\sim 30\%$, with a peak output of 250mW for 1W of input pump power (using one of the two pump beams). The lasing wavelength was measured using two different monochromators, and was found to be 2.013μm. No other wavelengths were observed to be lasing.

When the ring laser was constructed, the intrinsic mechanism was used to enforce unidirectional operation. At first, the modulator was operated 0.11° from the Bragg angle to maximise the total loss-difference, with 0.17W of r.f. power being required for unidirectional operation, corresponding to a diffraction loss of $\sim 0.9\%$. Later the modulator was tilted further from the Bragg angle to increase the loss-difference with respect to diffraction loss, resulting in a greater output power, as discussed in section 2.4.1. To achieve unidirectional operation, the Q-switch was tilted 0.24° from the Bragg angle and required 0.23W of r.f. power to be applied ($\sim 1\%$ diffraction loss). The Bragg angle for this modulator at 2μm is 3.6°, much larger than we had used in other ring laser systems. This may have led to increased losses in the cavity due to non-Brewster angles of incidence of the cavity beams and perhaps birefringence in the modulator. A possible solution to this problem is to cut and polish the modulator so that the transducer is angled at the Bragg angle when the modulator is at normal incidence to the laser beam at the desired wavelength. The advantage of operating away from the Bragg angle was demonstrated when the ring laser was operated at room temperature, where the threshold for bidirectional operation was ~ 550mW with no applied r.f. power. Near the Bragg angle, the threshold for unidirectional operation rose to 780mW, but when tilted by 0.24°, the threshold was only 620mW. When operated at this angle, the lasing threshold for the cooled rod rose from 300mW (no r.f. power) to 330mW. The cw performance of the laser when operated at both room temperature and at around -17°C, is shown in Fig 2.30, where we see that a peak unidirectional output of 380mW was obtained.

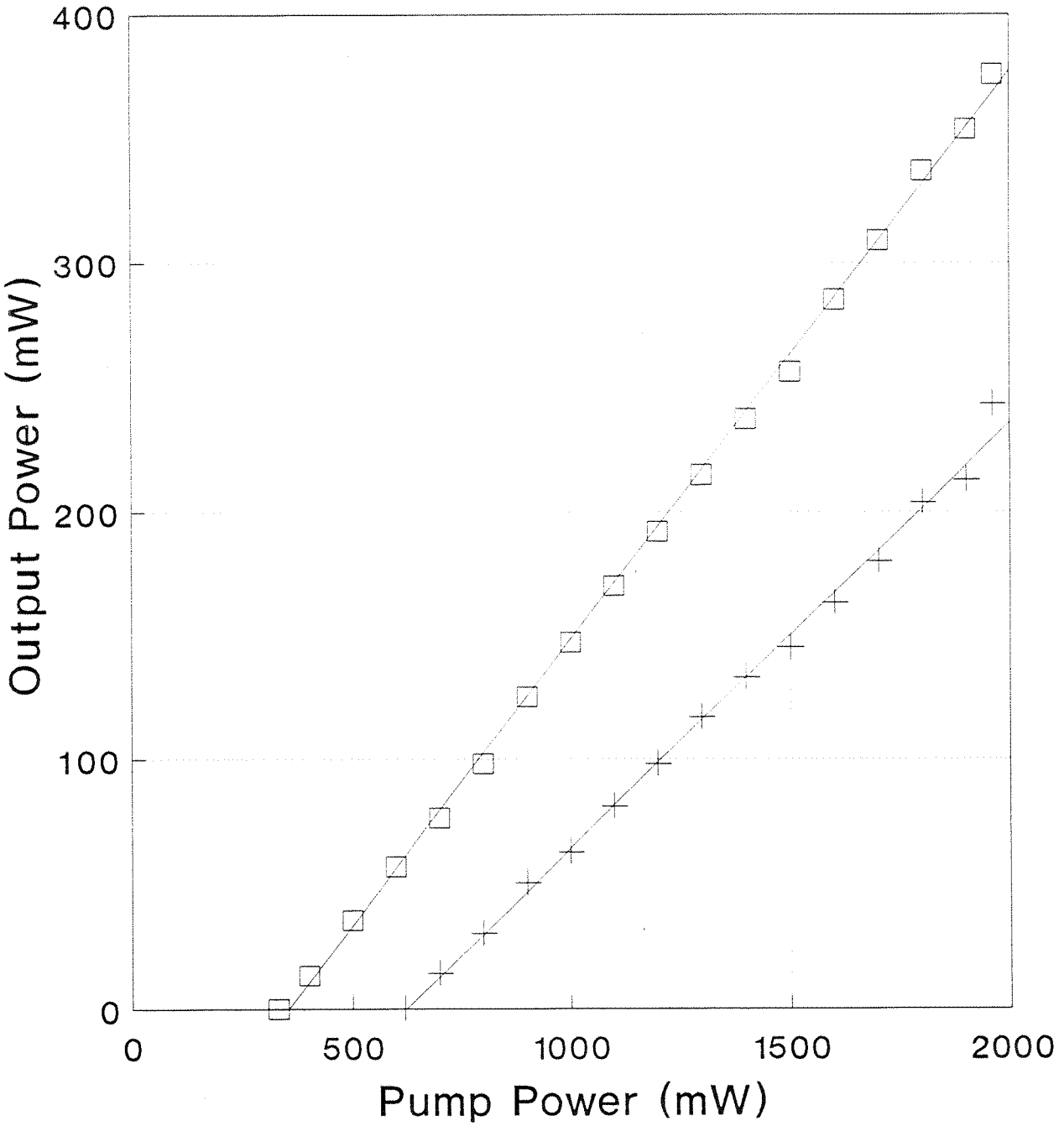

Fig 2.30 Unidirectional operation of 2μm Tm:YAG ring laser. Room temperature operation is indicated by (+), with cooled operation shown by (□).

Having achieved unidirectional operation, we next attempted to determine the axial mode properties of the output, to confirm single frequency operation. This was difficult to achieve, as no suitable high quality mirrors for constructing a Fabry-Perot interferometer were available. After experimenting with a number of mirrors we chose 2 mirrors that were 4% transmitting at 2.013μm. The finesse of the Fabry-Perot was very poor, probably due to a combination of reflections from uncoated, unwedged back mirror surfaces and poor quality coated surfaces. However, it seemed that at least three modes were oscillating when the ring laser was operating at peak power, although these modes were not adjacent, but appeared to be separated by ~ 20 axial mode spacings. When the pump power was reduced, the output appeared to be single frequency only up to 15mW of output. With the poor mode discrimination, this could not be absolutely determined, but the Fabry-Perot output appeared more stable when one mode only was oscillating. A priority for this experiment is acquisition of suitable Fabry-Perot mirrors to enable a proper study of the output of this ring laser. At present we can only say that more than one mode appears to be oscillating at higher output powers.

2.7.4 Discussion

With the lack of a suitable Fabry-Perot interferometer to evaluate the frequency performance of this ring laser, it was not possible to investigate the causes of the additional axial modes that appeared to be oscillating, and we have not eliminated them at this time. The development of a more detailed theory of residual spatial hole burning [Martin, 1993] may allow us to evaluate the source of this problem. To make this laser practical we would also need to pump it with a laser diode and achieve tunability over at least 0.5nm, as there are many sharp peaks in the atmospheric absorption separated by $<$ 1nm. Ideally we would like to tune the laser to around 2.022μm, where there is an excellent atmospheric window. The overall performance of this laser was not as good as might be expected when compared to other end-pumped Tm:YAG lasers, where slope efficiencies of around 50% are achieved [Stoneman, 1990], [Suni, 1991]. Possible explanations for this include: a mismatch between the pump and lasing mode sizes, which in addition to reducing the efficiency as explained in section 1.1.5, could also lead to increased reabsorption losses if the pump was too small or slightly misaligned, or poor Tm:YAG rod coatings.

2.8 Future Work

Now that the mechanisms responsible for acousto-optically induced unidirectional operation of ring lasers have been identified, there are a number of avenues of research that can be followed. We have already briefly discussed the optimisation of A-O modulator designs using the intrinsic mechanism (section 2.4.3) and this is an ongoing area of research. Although there are restrictions on the range of A-O parameters available (e.g. v_s, n), improvements can possibly be made in design areas such as interaction length and operating frequency. Differing requirements for cw and Q-switched operation may dictate the optimal modulator design for each of these modes of operation, but as already discussed, a design compromise should be possible that would allow satisfactory operation either cw or Q-switched, with no need to alter the modulator orientation.

In addition to optimising the design of A-O modulators, the results that we have obtained here suggest that materials that are not normally considered to be acousto-optic media can be used in laser cavities to produce unidirectional operation. In particular, using the laser medium itself as the acousto-optic modulator is an attractive option, as it reduces the system complexity and offers the potential of monolithic single frequency devices. We have had A-O modulators fabricated from Nd^{3+} doped phosphate glass and Nd:YAG, which do not have high A-O figures of merit, but nevertheless, using the feedback techniques, it is possible to produce single frequency output [Clarkson, 1993c] from a laser where the gain medium is also the unidirectional device.

A design for a monolithic Nd:YAG unidirectional ring laser has been developed, and it is anticipated that this device should be fabricated in the near future. This monolithic laser should be a compact, robust and efficient source of single frequency output, which can be used either on its own or as the master oscillator for an injection seeding system. Further work that is envisaged includes end-pumping with a diode bar to produce high power single frequency output, which could then be used as a pump for a non-linear system such as frequency doubling or an optical parametric oscillator.

References

Adler, R., IEEE spectrum, pg 42, May (1967).

Brillouin, L., Ann. Physique, **17**, 88 (1922)

Bromley, L.J. and Hanna, D.C., Opt. Lett. **16**, 378 (1991)

Carr, I.D., Hanna, D.C. and Wong, K.H., Opt. Commun., **55**, 179 (1985)

Clarkson, W.A. PhD Thesis, University of Southampton (1990)

Clarkson, W.A. and Hanna, D.C., Opt. Commun, **73**, 469 (1989)

Clarkson, W.A. and Hanna, D.C., Opt. Commun., **81**, 375 (1991a)

Clarkson, W.A. and Hanna, D.C., Opt. Commun., **84**, 51 (1991b)

Clarkson, W.A., Hanna, D.C., Kane, D.M., Martin, K.I. and Neilson, A.B., CLEO '93 (Baltimore, MA) Technical Digest, Paper CThS15, (1993a)

Clarkson, W.A., Hanna, D.C. and Neilson, A.B., A Stable Two Frequency Laser, United Kingdom Patent Application No. 9304076.4, (1993b).

Clarkson, W.A., Hanna, D.C., Lovering, D.S. and Jones, G.C.W., CLEO '93 (Baltimore, MA) Technical Digest, Paper CThR5, (1993c)

Clarkson, W.A., Neilson, A.B. and Hanna, D.C., Opt. Lett. **17**, 601 (1992a)

Clarkson, W.A., Neilson, A.B. and Hanna, D.C., Opt. Commun. **91**, 365 (1992b)

Clobes, A.R. and Brienza, M.J., Appl. Phys. Lett., **21**, 265 (1972)

Culshaw, W. and Kannelaud, IEEE J. Quantum Electron., **QE-7**, 381 (1971)

Danielmeyer, H.G., J. Appl. Phys, **42**, 3125 (1971)

Debye, P. and Sears, F.W., Proc. Nat. Acad. Sci. U.S., **18**, (1932)

Faxvog, F.R., Opt. Lett., **5**, 285 (1980)

Golyaev, Y.D., Zadernovskii, A.A and Livintsev, A.L., Sov. J. Quantum Electron. **17**, 583 (1987)

Grossmam, W.M., Gifford, M. and Wallace, R.W., Opt. Lett. **15**, 622 (1990)

Hanna, D.C., Luther-Davies, B. and Smith, R.C., Opto-Electron. **4**, 249 (1972)

Heatley, D.R., Dunlop, A.M. and Firth, W.J., Opt. Lett., **18**, 170 (1993)

Hemmati, H., Opt. Lett., **14**, 435 (1989)

Lucas, R. and Biquard, P., J. Phys. Rad., **3**, 464 (1932)

Kane, T.J. and Byer, R.L., Opt. Lett. **10**, 65 (1985)

Maker, G.T. and Ferguson, A.I., Opt. Lett. **14**, 788 (1989)

Martin, K.I., Clarkson, W.A., Neilson, A.B. and Hanna, D.C., *11th U.K. National Quantum Electronics Conference*, Belfast, Paper 73. (1993)

Neev, J. and Kowalski, F.V., Opt. Lett., **13**, 375 (1988)

Neilson, A.B., Clarkson, W.A. and Hanna, D.C., Opt. Lett., **18**, 1426 (1993)

Pinnow, D.A., Van Uitert, L.G., Warner, A.W. and Banner, W.A., Appl. Phys. Lett., **15**, 83 (1969)

Pinto, J.F., Esterowitz, L. and Rosenblat, G.H., Opt. Lett., **17**, 731 (1992)

Reed, M.K. and Bischel, W.K., Opt. Lett., **17**, 691 (1992)

Roy, R., Schulz, P.A. and Walther, A., Opt. Lett. **12**, 672 (1987)

Sabert, H. and Ulrich, R., Opt. Lett., **18**, 873 (1993)

Sapriel, J., *Acousto-Optics*, John Wiley and Sons Inc. (1979)

Scheps, R. and Myers, J., IEEE J. Quantum Electron., **26**, 413 (1990)

Singh, S., Smith, R.G. and Van Uitert, L.G., Phys. Rev. B., **10**, 2566 (1974)

Stoneman, R.C. and Esterowitz, L., Opt. Lett., **15**, 486 (1990)

Storm, M.E., Gettemy, D.J., Barnes, N.P., Cross, P.L. and Kokta, M.R., Appl. Opt., **28**, 408 (1989a)

Storm, M.E. and Rohrbach, W.W., Appl. Opt., **28**, 4965 (1989b)

Suni, P.J.M. and Henderson, S.W., Opt. Lett., **16**, 817 (1991)

Tang, C.L., Stays, H. and DeMars, G., J. Appl. Phys., **21**, 2289 (1963)

Trutna, W.R., Donald, D.K. and Nazarathy, M., Opt. Lett. **12**, 248 (1987)

Xu, J. and Stroud, R., *Acousto-Optic Devices*, John Wiley and Sons Inc. (1992)

Yariv, A. and Yeh, P., *Optical Waves in Crystals*, John Wiley and Sons Inc. (1984)

Zinov'eva, T.V., Igmetov, A.B., Kravtsoz, N.V., Nanii, N.V. and Nanii, O.E., Kvantovaya Elektron., **19**, 142 (1992)

Chapter 3
DIODE BAR PUMPED SOLID-STATE LASERS

3.1 Introduction

Semiconductor diode lasers have made dramatic advances in recent years in terms of efficiency and performance. As described in section 1.2 this has led to a renaissance in solid-state lasers. However, a serious shortcoming of diode lasers is the limitation on overall power that they can provide. The maximum output power is restricted either by thermal limitations or by catastrophic failure. Catastrophic failure occurs as a result of localised melting and damage at the facet of the laser and can be caused either by inadvertent optical feedback from external components, or ultimately by absorption of the laser light in unpumped regions of the active layer near the facet. This occurs at intensities of a few MW cm^{-2}. Thus for a typical double heterostructure quantum well laser with emitting dimensions 3μm x 1μm, the maximum output would be limited to around 30mW.

Two ways of increasing the output power are to increase the dimensions of the emitting region, or conversely by making an array of closely spaced lasers. As the dimensions of a single emitting area are increased, however, the lasing output may no longer be confined to a single transverse mode, and the operational lifetime can also be degraded. The output beam from such a device will be elliptical, and at present commercial devices of up to 4W with dimensions 500μm x 1μm are available. Diode arrays consist of a large number of emitters spaced on (say) 10μm centres, with the individual stripes being partially coherent due to evanescent coupling between adjacent stripes. Coupling between the stripes, while giving the benefit of increased coherence also places upper limits on output power, as the number of stripes must be restricted to prevent transverse lasing and other parasitic effects. Thermal effects also place limits on the maximum power that can be obtained. At present, the most powerful commercially available device is the SDL-2480, which produces 3W cw from an overall aperture of 500μm x 1μm.

The next step on the route to higher powers is the laser diode bar. In this structure a number of arrays are grown on a single substrate. A typical device (SDL-

3490-S) consists of twelve 200μm emitters on 800μm centres producing a total of 10W of cw output from a 1cm x 1μm device. The overall length of the bar is constrained by the growth process used. All the emitters are electrically connected in parallel, but there is little or no coupling between adjacent arrays, resulting in incoherent output. In addition there tends to be a wavelength spread across the bar of 2-3nm due to difficulties in precisely controlling the manufacturing process. Diode bars of 5W, 10W, 15W and 20W are commercially available for cw mode operation and up to 100W for quasi-cw operation. There are also available two-dimensional stacked arrays of bars (with dimensions up to 1cm x 2cm) which can emit up to 5000W in quasi-cw operation, but these are not discussed any further here, as it does not seem that they will become practical cw devices in the foreseeable future due to the massive thermal dissipation required, and we did not use any of them in our experiments.

On the other hand, cw diode bars potentially offer high power, compact, efficient, stable, cheap sources for solid-state laser systems. For example, a 10W diode bar (Heimann OPUS 3237) costs around £100 per watt of output. The operating lifetimes of diode bars are also very good ($\gg$5000 hours), orders of magnitude better than the main alternative pump source, flashlamps. One of the main problems to be solved with them is how best to couple their output into the lasing mode of a solid-state laser. At first sight the obvious answer might be to use them to side-pump the laser, which has been done in a number of systems, e.g. [Reed, 1988], [Burnham, 1989], [Ajer, 1992]. This allows simpler coupling of the light, but the mode matching is not as good, and overall efficiency is not as high as for longitudinal pumping for smaller diode devices. The main advantage of such systems is that scaling to higher powers is more easily achieved, as the output of more diodes can be coupled in, compared to end-pumped systems. At present, the highest average power system is a 1000W Nd:YAG slab laser pumped by two diode bar modules, each module incorporating 80 diode bars [Comaskey, 1993].

An attractive solution to the use of diode bars is the tightly folded resonator (TFR) design developed by Baer and his colleagues [Baer, 1989 and 1992]. The TFR is shown in Fig 3.1, and is pumped by a 10W diode bar with ten IW emitters. The output is roughly collimated by a fibre lens of 0.3mm diameter, and then close-coupled

into the lasing medium (either Nd:YAG or Nd:YLF). The lasing mode is defined by the external mirrors and dimensions of the laser slab such that the intracavity TEM_{00} mode bounces back and forth between the opposite sides of the slab, with vertices located at each 1W emitter location to extract maximum gain. This provides excellent overlap between the laser mode and the diode bar pump. Thus the advantages of a side-pumping type geometry are combined with the efficiency of an end-pumped laser resonator, giving good pump and laser mode overlap and high operating efficiencies. Output of over 3.5W from a Nd:YAG TFR has been reported [Baer, 1992], along with Q-switching and frequency doubling. The TFR is available as a commercial product, and appears to provide a reliable, compact source of either 1μm or blue-green output.

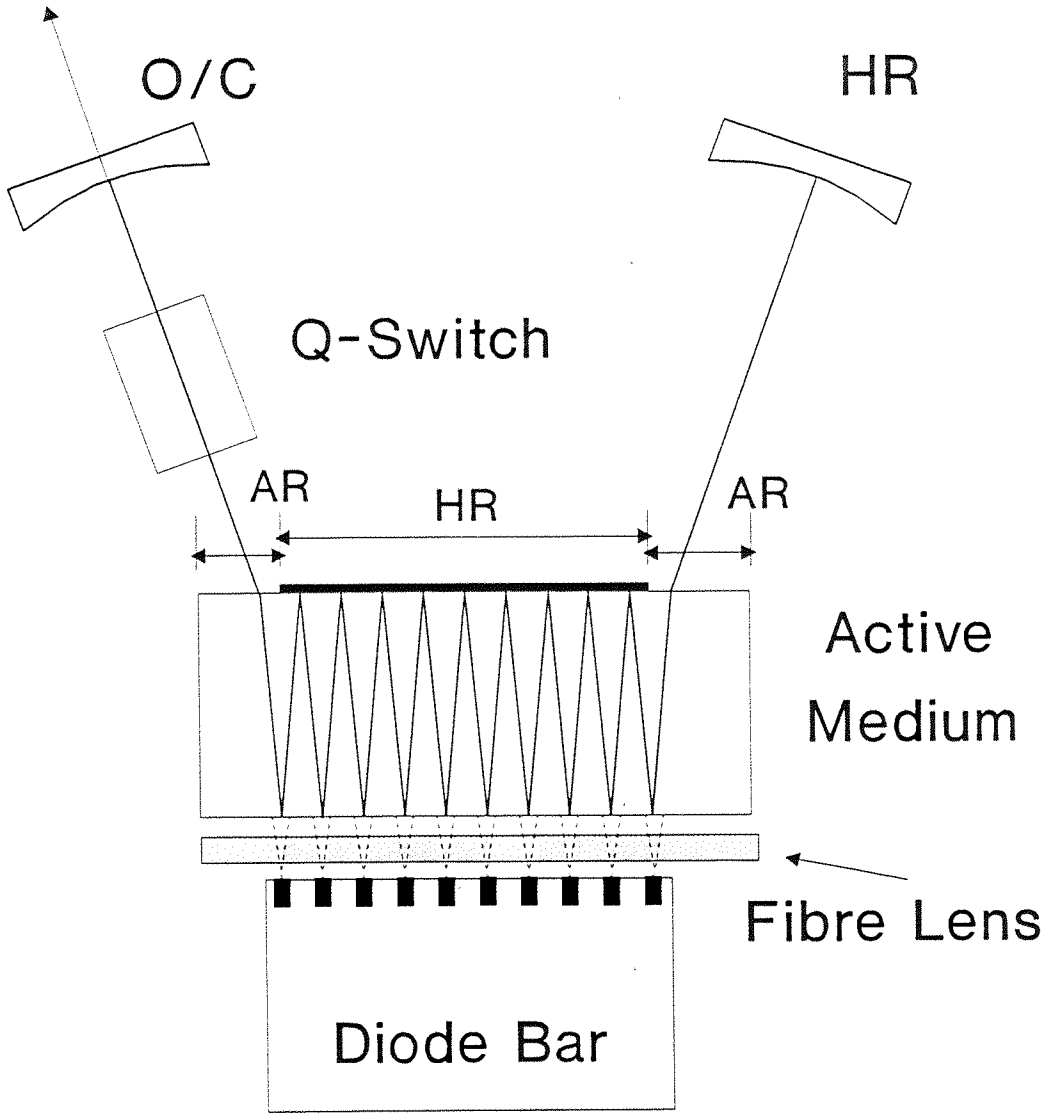

Fig 3.1 Schematic of tightly folded resonator (TFR) as described by Baer[1992].

In this work, however, our primary interest is in producing a beam from a laser diode bar that can be used to longitudinally pump a solid-state laser. As power requirements for various applications are continually being increased, it seems likely that for some time to come, the most economical and practical means for achieving watts of output from solid-state lasers will be diode bars. The ability to efficiently couple the diode bar output into the lasing mode will therefore become more important. End-pumping offers the advantage of being able to apply all the successful techniques employed in other end-pumped cavities, allowing a wide variety of different systems to be constructed. One would also expect a greater operating efficiency compared to side-pumped systems. While not being able to compete at present with side-pumped lasers in terms of total output power, end-pumped systems should offer advantages in terms of efficiency and cost at output power levels of the order of a few tens of watts, which is adequate for a wide variety of applications. The fundamental problem that must be addressed when trying to end-pump with diode bars is that in one plane there is a diffraction limited beam from a 1μm aperture, whilst the other plane is a >1000 times diffraction limited beam from a 10mm aperture. Treating this beam with conventional optics is difficult, and can result in asymmetric beams, spherical abberation, high divergence of focused beams, inefficient coupling, etc.

Some of the main approaches to producing a beam suitable for end-pumping are presented in the remainder of this section. The initial studies that we undertook with the diode bar involved side-pumping of laser slabs, and this work is discussed in section 3.2. In section 3.3 some resonator designs are described with which we attempted to produce end-pumped lasers, with varying degrees of success, before a novel and successful method was developed. This method is presented in the next chapter.

3.1.1 Fibre Bundles

A system that offers ease of use is a fibre-coupled diode bar where individual fibres collect the output of each emitting region, and are bundled together to form a circular cross-section array, which can then be focused. Thus the 1D diode array is converted to a 2D fibre array. A commercially available device (SDL-3490-P5)

produces a fibre bundle 400μm in diameter, with up to 10W output. A trade-off that has to be made with fibre coupled systems is between high collection efficiency (using large diameter fibres), and good spot sizes (using smaller fibres with better fill factor). Optimised systems [Graf, 1993] using a fibre lens to first collimate the output achieve a transmission of 67% with uncoated optics. Fibres with square cross-section, whilst more difficult to manufacture, offer a better fill factor, and have also been tried [Morris, 1993].

These fibre coupled systems are useful for remote delivery of the diode output in applications such as materials processing and medicine, and can also be used for end-pumping solid-state lasers [Berger, 1988], [Keirstead, 1993]. Similar schemes can also be used to couple the output of many separate laser diode arrays to increase the total available power for end-pumping [Kaneda, 1992].

3.1.2 Compound Lens Systems

As we have already noted, the dimensions of a diode bar make it difficult to manipulate the output with conventional optics. A number of lasers have been devised, however, which use multi-element lens systems to collect, collimate and focus the output from diode bars. A seven element system has been used to pump the quasi-three level Tm:YAG 2μm transition [Lynn, 1991]. A three lens system described by Shannon [1991] was used to end-pump a Nd:YAG laser with a 10W diode bar and produced 1.9W of cw output. This system is described in more detail in section 3.3, and was used in a number of our initial experiments. Marshall et al [1993] used a similar system to end-pump an astigmatic Nd:YLF cavity, giving up to 3.3W of TEM_{00} output using a 15W diode bar.

An approach somewhere between fibre bundles and multiple element lens systems is to use an array of Gradient Refractive Index (GRIN) lenses to collimate the output from each element of a diode bar, and then use a single focusing lens to produce the final spot. [Yamaguchi, 1992]. In this system, 20 GRIN lenses, each 500μm wide, were used to collimate the output from an individual diode array, with a total efficiency of 86%.

3.1.3 Cylindrical Microlenses

One attractive option for collimating the output of a diode bar in the "fast" (diffraction limited) plane is to use specially fabricated cylindrical microlenses [Snyder, 1991a, 1991b, 1993]. These lenses can effectively give a collimated, diffraction limited beam in one plane, which then leaves the problem of the non-diffraction limited plane to be solved separately. Our use of these microlenses is covered in detail in the next chapter, and here we introduce some of their main characteristics.

The lenses that we used are manufactured by Blue Sky Research, and are known as Single Axis Collimators (SAC) microlenses. One surface is polished to a hyperbolic cross-section (Fig 3.2) while the other side is flat. Thus one surface is made to perform all the collimation tasks. This hyperbolic surface, when properly designed, gives a collimated beam free from spherical aberration to all orders at the wavelength of interest. The shape of this hyperbola is given by

$$z=\frac{cy^2}{1+\sqrt{1-(1-e^2)c^2y^2}} \tag{3.1}$$

where c is the curvature of the surface and e the eccentricity of the conic section. The curvature is related to the index of refraction in the lens, n, and the working distance f between the source and the vertex of the hyperbolic curve by

$$c=\frac{1}{f(n-1)} \tag{3.2}$$

The eccentricity, e, in this situation is simply given by e=n.

These lenses are fabricated by first polishing a glass preform to the desired shape. The preform is then heated to the minimum drawing temperature and pulled out as a fibre to the appropriate cross-sectional dimensions. The fibre so drawn will have

an identical shape of cross section to that of the preform. In addition, the fibre surface will be fire polished in the drawing process, resulting in much higher surface quality than in the original preform. The fibre typically has dimensions of a few hundred microns, compared to the preform which is around 2cm on each side. Thus the fibre lens is easy to produce in quantity, making it relatively inexpensive. It is also possible to polish other shapes in the preform to perform different tasks, for example, circularising the output of visible laser diodes. As we shall see in the next chapter, the SAC microlenses can produce a high quality collimated output from a diode bar, but some effort is required to do so.

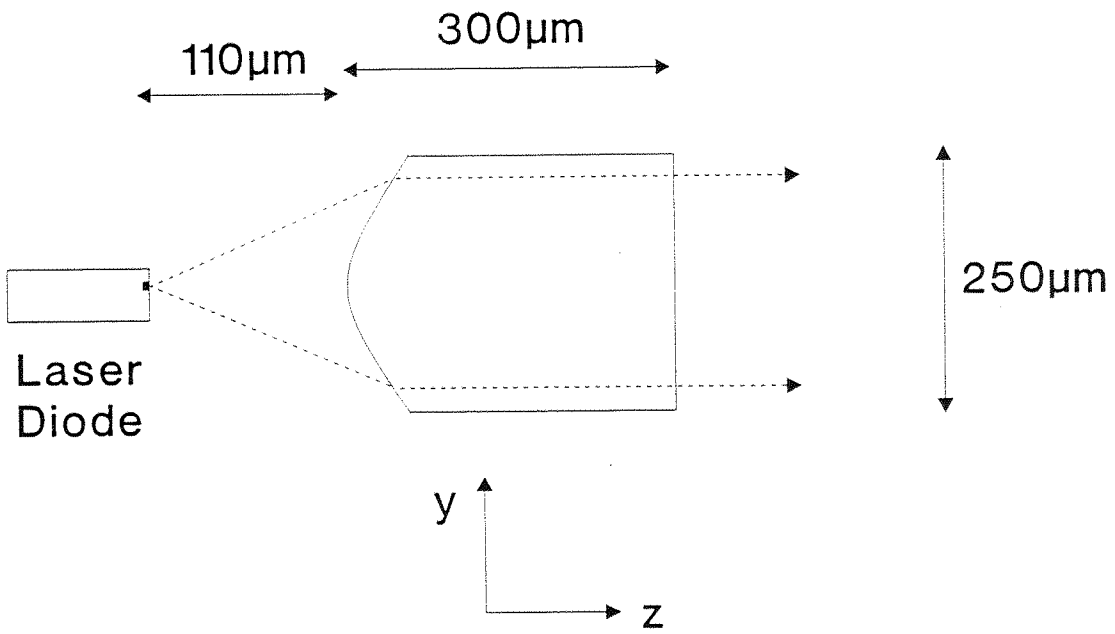

Fig 3.2 Cross-section of cylindrical microlens showing the action of the hyperbolic surface. The dimensions shown are for a SAC900 microlens. Here f=110μm, n=1.61.

3.1.4 Binary Optics Systems

A particularly sophisticated attempt to transform a diode bar output into a form suitable for end-pumping is the use of binary optics arrays to image the 1D diode bar to a 2D array [Leger, 1992]. The problem was addressed by considering the radiance theorem [Boyd, 1983] and the fundamental limits this places on how well the diode output can be focused. The radiance here is defined to be the power per unit area per unit solid angle. The main points are that the radiance of the image produced by the lens system cannot be greater than the original source radiance, and that the radiance of a collection of mutually incoherent sources (e.g. the discrete elements of a diode bar) cannot be greater than the radiance of the single brightest source.

Initially a system was devised that consisted of two planes of optical elements, one approximately 500μm from the diode and the other $\sim$26mm from the diode. In both planes, separate cylindrical lenses were used to expand and collimate the output from each element of the diode bar, and prisms were used to steer the output to form a 2D array from the 1D bar. This square, collimated array can then be mode-matched into a lasing mode with an appropriate focusing lens. This optical system involves a large number of components and would not be a practical means of producing an end-pumped system.

Instead, the action of each optical plane can be defined by an optical phase function, $\phi(x,y)$ that produces the equivalent result on each subarray of the diode bar. Evaluating $\phi(x,y)$ for each subarray means that the system of cylindrical lenses and prisms can be replaced by diffractive optical elements. These diffractive optical elements can be fabricated as binary optics arrays using microlithography and dry etching to create the phase function over a number of discrete steps. In the experiment described by Leger, the phase function was quantised into 8 discrete levels and fabricated in three etching stages. This approach has the advantage that having correctly specified the phase function, copies of the binary optics can be made relatively inexpensively and easily, under computer control.

The beam produced by this system, after focusing by a 38mm focal length lens,

produced a circular spot size of 57μm (radius), having an approximately Gaussian profile in both planes. The limit to the beam quality appeared to be that the diode bar facet is slightly bent by around 5-7μm over its 10mm length, resulting in a slight misalignment of the optical system. The major drawback to this technique is that the total transmission of the system is only around 20%, as each set of binary optics has a diffraction efficiency of only 50%. This can be improved by using more steps in the fabrication process to construct the phase function, but for (say) 5 phase levels, the efficiency for each plane is still only 90% at best. This method produces very good beams, but at the present efficiency levels, it may well be that conventional diode arrays would give better overall performance.

3.1.5 Multi-Diode Bar End-Pumped Lasers

In addition to schemes which couple the output from a single diode bar into a solid-state laser, much effort has been put into systems which are end-pumped by many diode bars, to achieve high output powers. Although the limit on total output power may be less than that possible with side-pumped systems, the efficiency of these end-pumped systems exceeds that of side-pumped lasers. At these high power levels, thermal effects in the laser medium have to be carefully considered, as thermal lensing [Koechner, 1973 and 1988] can considerably change the fundamental mode performance of the laser, and ultimately thermal fracture limits the pump power that can be used [Cousins, 1992]. Tidwell [1992] derives an expression for the thermal lens focal length of an edge-cooled, end-pumped Nd:YAG rod which has a radius r_0:

$$f = \frac{7.6\ r_0^2}{P_{abs}} \qquad (3.3)$$

where the focal length is in meters, r_0 in millimetres, and P_{abs} is the absorbed pump power in watts. Here the assumption is made that the pump spot size (r_p) is uniform over the length of the rod, and is chosen to be as large as possible with respect to the

rod to limit the temperature rise. In the derivation of eq (3.3), Tidwell has chosen $r_p = 0.57 \times r_0$. In addition, it is assumed that 30% of the absorbed pump power produces the heating of the laser rod.

Some of the main problems that have to be addressed with these systems are engineering ones: how to physically pack as many diodes as possible around the laser rod and how to cool the diodes and rods and reduce thermal distortions. Early work by Pfistner [1990] showed how 4 diode arrays could be arranged to efficiently end-pump a Nd:YAG slab. Tidwell [1991] arranged four 10W bars around a Nd:YAG rod to produce 15W of multimode cw output. A recent paper by Tidwell et al [1993], uses two Nd:YAG rods in the laser cavity, each rod being end-pumped by four angularly multiplexed 15W diode bars at each end. They achieved 92W of multimode power and 60W of TEM_{00} output for a total diode input power of 235W, with a TEM_{00} mode diameter of 2.4mm. They corrected for thermal distortions in the laser rods (thermal focal length = 25.7 cm) by using an aspherical lens located between the rods, while thermally induced birefringence is corrected by placing a quartz polarization rotator between the two rods. The beam produced was 1.3 times diffraction limited, which is acceptable for many applications.

3.2 Initial Experimental Investigations

The initial interest in diode bar pumped lasers in this work was to reproduce the results obtained by Baer with the TFR and to extend his work to produce a versatile high power laser. Our design for this laser called for a Brewster-angled Nd:YAG slab with very precise dimensions to define the TFR cavity. It was soon realised that the tolerances required for the design were impractical and expensive, with the result that simpler systems were investigated at first, to establish what difficulties one could expect with a TFR, and with using a diode bar. The diode bar that was initially available to us was a 5W cw device (SDL-3480-L), which consists of 20 ten-stripe phase-coupled arrays (the currently available version of this device has 12 arrays and is packaged differently). Whilst not having sufficient power to enable a proper study of TFRs to be carried out (due to the relatively high thresholds), it was expected that it would be adequate to demonstrate the principle of operation of diode-bar pumped solid-state lasers, later moving to higher power devices as they became more affordable.

The first systems that we studied were side-pumped Nd:YAG and Nd:GGG (Gadolinium Gallium Garnet) slabs, setting up standing wave cavities with the gain medium in the centre of the cavity. The idea was to collimate the diffraction limited output of the diode bar using a length of optical fibre and couple this collimated light into one side of the slab, while letting the beam in its non-diffraction limited direction expand at an angle of 10°, as this would not represent a significant change over the few millimetres length of the crystal slab. The slabs were cut at Brewster's angle at both ends to eliminate the need for antireflection coatings at the lasing wavelength. The laser cavity is then defined by the external cavity mirrors. The length of the cavity could be altered to allow the lasing mode in the crystal to be matched to the dimensions of the collimated output of the diode bar.

The first problem to be addressed, then, was how to best collimate the diode bar output in the "fast" direction, i.e. the 1μm diffraction limited plane. A 200μm diameter optical fibre was used at first, but this proved unsuccessful and also unsatisfactory from the point of view of potential damage to the diode. The working distance of the fibre was estimated to be $\sim 100\mu$m, at which distance from the diode facet the fibre was

hidden by the diode case (the facet is recessed in its case). As the fibre had a spherical cross-section, and was not optimised in any way for use as a lens, the spherical aberration was very large, which made the quality of collimation rather low. This then presented the possibility of accidentally moving the fibre into the diode facet while adjusting for a collimated output, with potentially fatal consequences for the diode. As will be seen in the next chapter, the positioning of an optimised fibre lens in front of a diode bar for collimation is a non-trivial task, and we now appreciate that the mounts and techniques used with this simple fibre lens would never have allowed a satisfactory beam to be produced.

In an effort to increase the working distance, a 4mm diameter glass rod was next used as a collimating lens. This gave a much safer working distance, but spherical aberration was still a major problem. When the collected light was focused, a spot size of only around 300μm could be achieved, with a significant amount of scattered light and very poor beam quality. As this rod was not designed to be of optical quality, such problems were not unexpected.

Higher quality cylindrical lenses were next used to collimate the output. The shortest plano-convex lens commercially available had a 6.4mm focal length, with a working distance of 2.9mm. Used in conjunction with an 18mm focal length aspherical lens to focus the light in both directions, a reasonable quality beam was produced, with dimensions of approximately 200μm x 4mm, which was too large to consider using for end-pumping. For side-pumping it was decided to just use a cylindrical lens to collect and focus the beam in the plane perpendicular to the diode junction, and allow the non-diffraction-limited beam to expand at 10°.

3.2.1 Nd:YAG Side-Pumped Laser

The Nd:YAG slab that we used was 13mm long, 0.9mm high and 1.6mm deep, and was doped with 1 at.% Nd^{3+} (Fig 3.3). The crystal was mounted on a Photon Control 5-axis micropositioner to allow full translation and rotation of the slab with respect to the pump beam. The end-mirrors used had a 10cm radius of curvature, with one being highly reflecting at 1.06μm, and the other transmitting 2.5% at that wavelength. The calculated lasing mode sizes in the centre of the Nd:YAG slab that resulted from this arrangement were $w_{Lx} \sim 180\mu m$ and $w_{Ly} \sim 100\mu m$. An analysis of slope efficiency and threshold for side-pumped lasers was made, based on the results obtained in Clarkson[1989] for end-pumped systems, which are outlined in section 1.2.5. The results of this analysis are very similar to that described for side-pumping Nd:YAG crystal waveguides [Hanna, 1992], where a detailed derivation is given, but were carried out independently, and show that the pump threshold for lasing is

$$P_{pth} = \frac{\sqrt{\pi} h \nu_p L}{\sqrt{2}\sigma \tau_f \eta_q \alpha_p} \left(w_{py}^2 + w_{Ly}^2\right)^{1/2} . \exp\left(\frac{t\alpha_p}{2} - \frac{w_{Lx}^2 \alpha_p^2}{8}\right) \qquad (3.4)$$

and the slope efficiency η is

$$\eta = \left(\frac{T\nu_L}{L\nu_p}\right)\left(\frac{w_{Ly}(2w_{py}^2 + w_{Ly}^2)^{1/2}}{w_{py}^2 + w_{Ly}^2}\right) . \alpha_p \sqrt{\pi} w_{Lx} \eta_q \exp\left(-\frac{t\alpha_p}{2}\right) \qquad (3.5)$$

where

ν_p, ν_L are the pump and lasing frequencies;

L = total round-trip loss;

σ = laser transition cross-section;

τ_f = fluorescence lifetime;

η_q = quantum efficiency of pump photons;

α_p = pump wavelength absorption coefficient in crystal;

t = thickness of the crystal;

T = output coupling;

w_{Lx}, w_{Ly}, w_{py} are the lasing and pump mode sizes respectively. The pump "size" in the x direction is determined by the pump absorption in that direction.

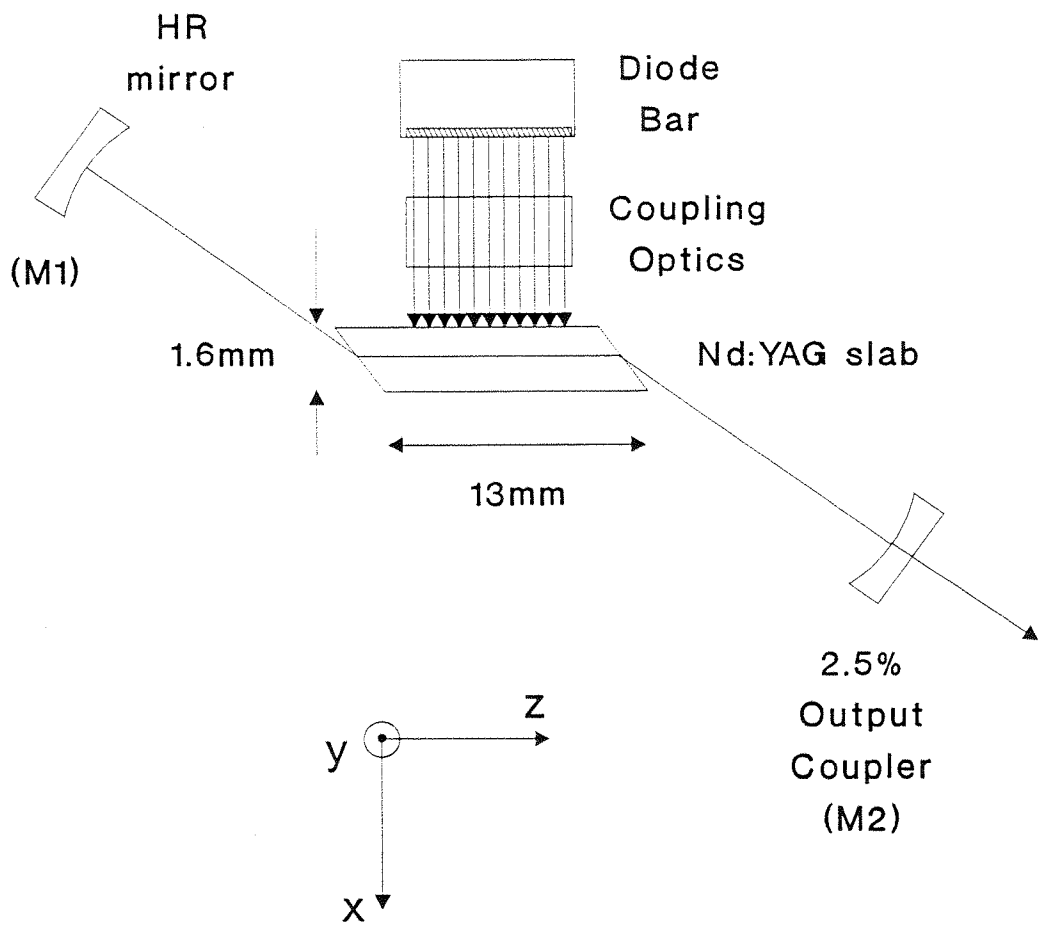

Fig 3.3 Schematic of cavity used for side-pumped Nd:YAG laser.

For the Nd:YAG slab used, α_p^{-1} = 3mm, t = 1.6mm, σ = 3.5x10^{-19} cm^2, τ_f = 230μsec. For a pump diameter of ~200μm and output coupling of 2.5%, with an assumed cavity round-trip loss (excluding output coupling) of ~0.5%, which was based on previous experience with end-pumped lasers, a threshold of around 630mW and slope efficiency of 4.4% would be expected. On these figures, the total output would be approximately 200mW for 5W of input pump power.

In fact, the laser could not be made to lase using conventional alignment techniques, and a rigorous alignment procedure was necessary to establish any lasing. This involved using a beam from a diode end-pumped Nd:YAG alignment laser, passing it through the Nd:YAG slab along the path of the lasing mode, and maximising its throughput. If the input beam is correctly aligned at Brewster's angle, then the transmission should be 100%. Next the diode bar is turned on and used to pump the Nd:YAG slab as an amplifier. The transmitted beam from the alignment laser is monitored to maximise the gain produced by the Nd:YAG slab as the diode bar focus and slab orientation are adjusted. In this way the diode should be optimised for pumping a lasing mode set up along the same path as the alignment beam. The cavity mirror (M1) on the opposite side of the Nd:YAG slab to the alignment laser is then put into place, and used to direct the beam back through the Nd:YAG slab. To ensure that the beam was aligned back on itself, apertures were used to define the laser path, and a portion of the beam was extracted from a slightly misaligned Brewster plate located between the alignment laser and the Nd:YAG slab, as shown in Fig 3.4. When mirror M1 was aligned, the second cavity mirror (M2) was put in place and the transmitted output from M1 was monitored. What we now have is a regenerative amplifier, where a Fabry-Perot cavity (defined by the cavity mirrors) with a circulating signal (supplied by the alignment laser), has a gain element (the Nd:YAG slab). As the Fabry-Perot is better aligned, and the gain is increased, the magnitude of the Fabry-Perot transmission peaks will increase rapidly. As the magnitude of the round-trip gain in the cavity is increased to a limiting value of unity, the transmission gain through the regenerative amplifier will suddenly shoot up towards infinity, as a result of regeneration in the laser cavity. At this point the side-pumped laser will lase of its own accord, and the alignment laser can be removed.

When this procedure was adopted, the Nd:YAG slab laser did lase, although with a poor performance. The threshold (power actually emitted by the diode) was ~3.7W, and only 6mW (TEM_{00}) output was produced, which explained why such an involved procedure had to be adopted to observe any lasing. Comparing the thresholds for a cavity with two HR mirrors to that comprised of one HR mirror and one 2.5% output coupler, revealed that the round-trip cavity loss (excluding output coupling) was around 6.5%, which was significantly higher than expected. This may have been due to imperfect Brewster-angled ends of the slab, or intrinsic losses in the Nd:YAG slab, which was polished from offcuts. In addition, if the diode collection system was not operating as efficiently as expected, again the performance of the laser would be degraded. With a measured intra-cavity loss of 6.5%, the performance predicted by equations (3.4) and (3.5) would give $P_{pth}=1.9W$ and $\eta=1.5\%$. With the uncoated optics used, and allowing for Fresnel reflections at the input face of the Nd:YAG, the collection efficiency would be ~74%, which would correspond to a total laser output of only 27mW, corresponding more closely to what was actually observed. This poor performance led us to consider using materials that might be more suitable for side-pumping. In the next section, one such material, Nd:GGG was used, with an improvement in performance resulting.

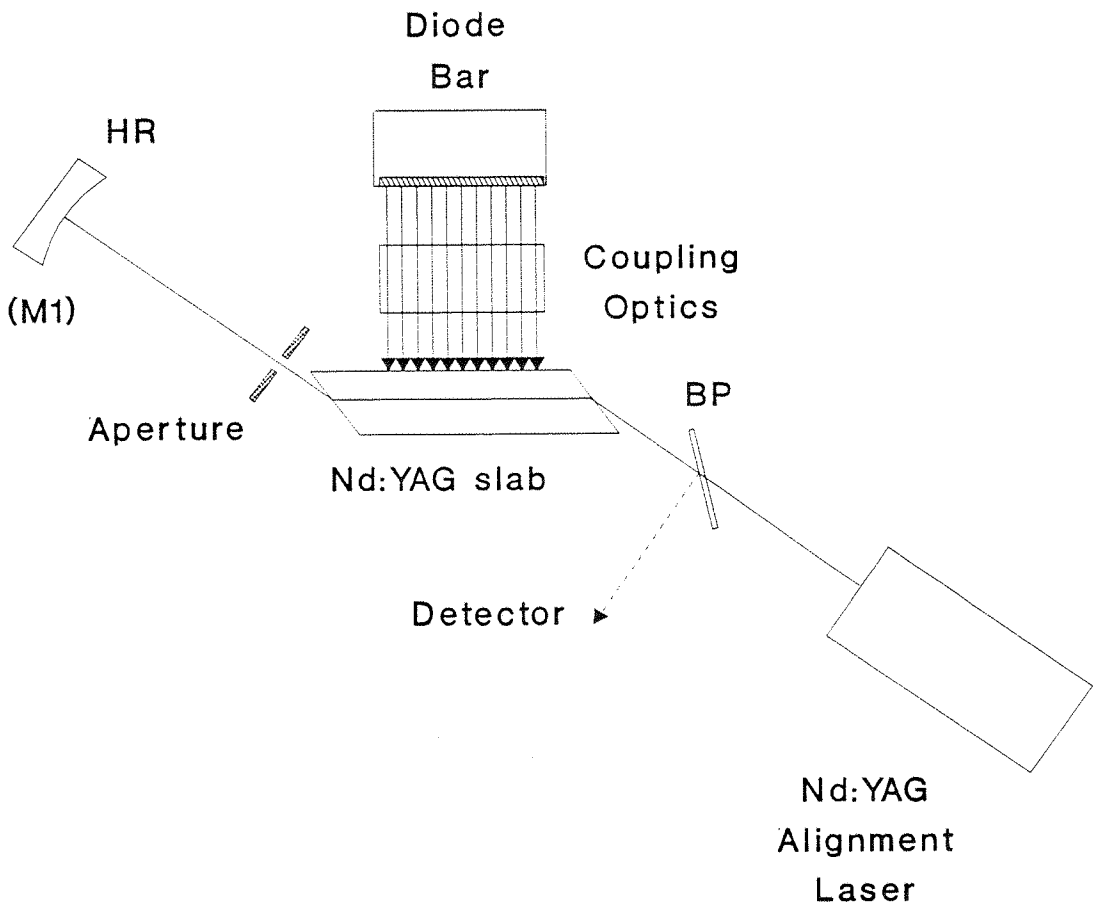

Fig 3.4 Setting up regenerative amplifier to allow alignment of laser cavity. The signal light, after passing through the gain medium twice, is aligned by monitoring the reflection off the Brewster plate (BP).

3.2.2 Nd:GGG Side-Pumped Laser

Whilst YAG (Yttrium Aluminium Garnet, $Y_3Al_5O_{12}$) is the most widely used host for Nd^{3+} lasers, other materials can be used in a variety of applications such as material processing, medicine, dentistry, military range-finding and target acquisition. Common alternatives to YAG are YLF (Yttrium Lithium Fluoride, $YLiF_4$), GSGG (Gadolinium Scandium Gallium Garnet, $Gd_3Sc_2Ga_3O_{12}$), YAP (Yttrium Aluminate, $YAlO_3$) and silicate or phosphate glasses. Another option is Nd:GGG (Gadolinium Gallium Garnet, $Gd_3Ga_5O_{12}$), which was first used in a laser almost 30 years ago [Geusic, 1964] and has been extensively studied, e.g. [Bagdasarov, 1974], [Kaminskii, 1978], [Maeda, 1984]. Some of the main advantages of Nd:GGG over Nd:YAG are that it can be grown as a crystal at greater rates and to larger sizes, and is capable of being doped to higher Nd^{3+} concentrations with less concentration quenching problems. It is perhaps best suited to high power lasers [Yoshida, 1988] because of this higher doping concentration, but has also been used in waveguide lasers [Field, 1991 & 1992] and frequency stabilised ring lasers [Day, 1990]. In our case, the higher Nd^{3+} concentration and consequent shorter pump absorption length should allow better matching of the pump beam distribution to the lasing mode, and hopefully better performance.

The Nd:GGG slab used was 12mm long, 2mm thick and 7mm high, with Brewster surfaces polished at each end (Fig 3.5) and was 2.7 at.% doped with Nd^{3+}. The crystal was slightly green in appearance, in contrast to the pink/purple colour normally associated with Nd:YAG, and also with a 3.35 at.% Nd:GGG crystal that we had available for comparison. The absorption spectrum of the 2.7% doped crystal showed a very strong UV absorption compared to the 3.35% doped sample, suggesting that there were significant differences in the composition of the crystals. It also had noticeable striations in the laser propagation direction. These factors may have been significant in the later performance of this laser. The relevant material properties of this Nd:GGG slab are:

n = 1.9

τ_f = 200μsec (measured, and also [Maeda, 1984])

σ = $2x10^{-23}$ m^2

λ_L = 1.062μm (transition from $^4F_{3/2} \rightarrow {}^4I_{11/2}$)

$(\alpha_p)^{-1}$ = 0.7mm

λ_p = 805nm

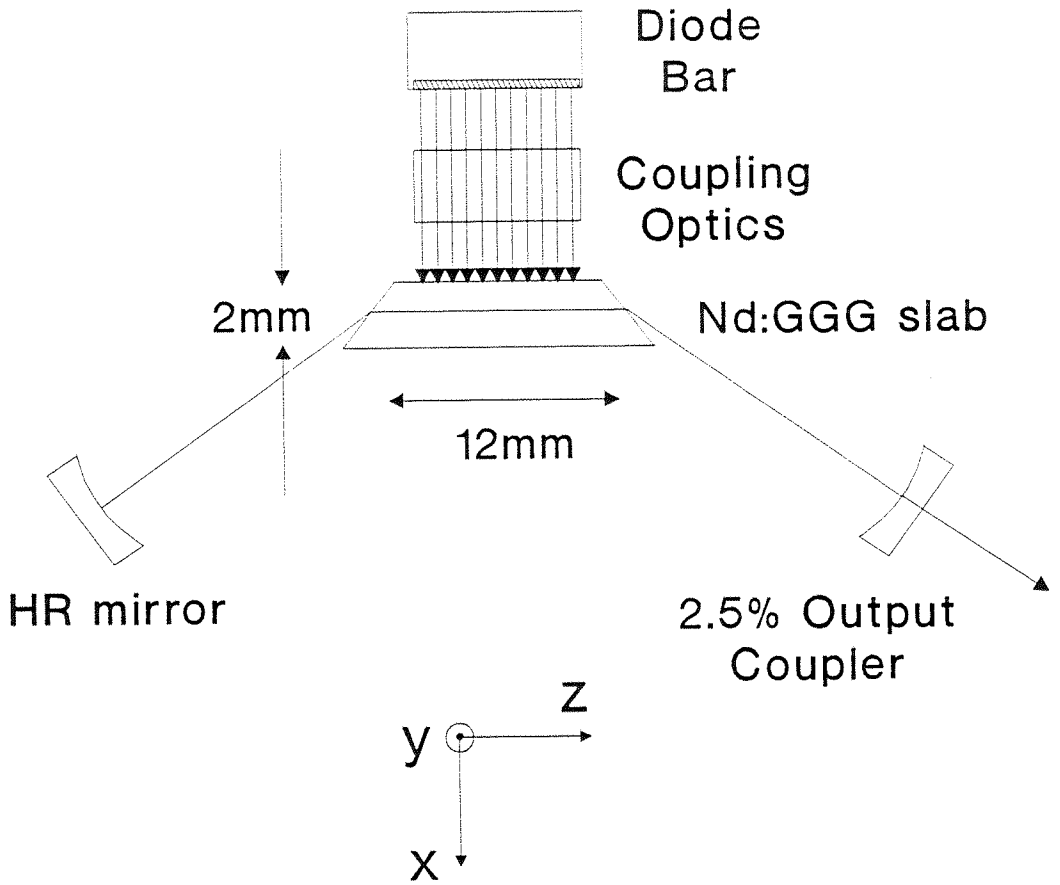

Fig 3.5 Schematic of side-pumped Nd:GGG laser.

For the laser cavity shown in Fig 3.5, the mode sizes at the centre of the Nd:GGG crystal were w_{Lx} = 190μm, w_{Ly} = 100μm. The output coupling used was 2.5%, and an additional intracavity loss of 0.5% was assumed. From equations (3.4) and (3.5), the calculated values for pump threshold and slope efficiency are: P_{pth} = 700mW, η = 6%, which implies a total output of ~260mW. The same alignment procedure described in the previous section for Nd:YAG was used to set up the Nd:GGG laser. As the lasing wavelengths of Nd:YAG (1.064μm) and Nd:GGG (1.062μm) are sufficiently different to not allow a Nd:YAG laser to be used as the signal for a regenerative amplifier, a Nd:GGG alignment laser had to be constructed. This was made from a 2mm thick piece of 2.7 at.% doped Nd:GGG, oriented at Brewster's angle (to eliminate the need for coatings) in a plano-concave cavity (Fig 3.6). When the alignment procedure described in the previous section was followed, the side-pumped laser did not lase, until we observed that blocking and unblocking the pump beam allowed lasing to occur. The laser power dropped exponentially to half of its peak value after 15 sec, indicating that thermal problems were a major consideration.

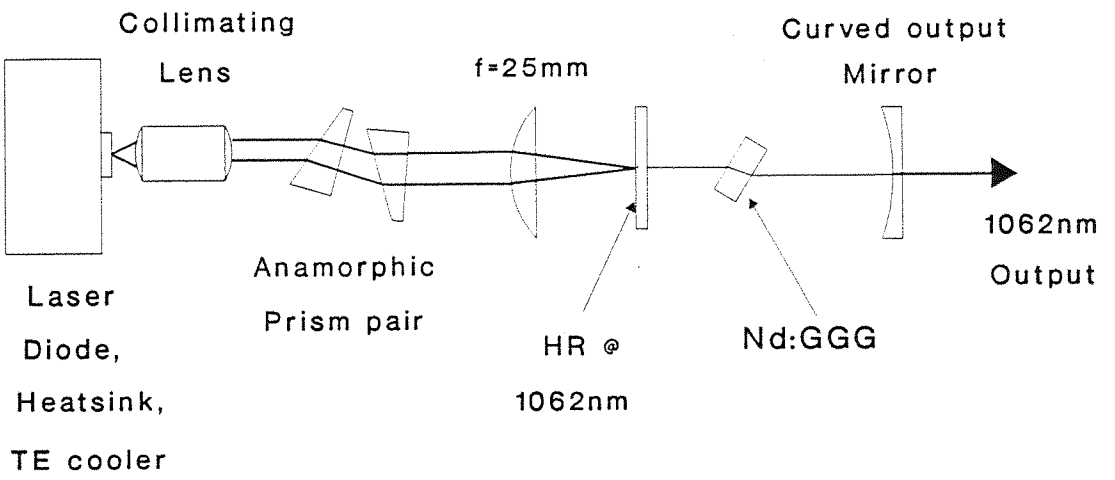

Fig 3.6 Mini-GGG laser used to produce the signal injected into the Nd:GGG regenerative amplifier.

An optical chopper with a 50% duty cycle was used to allow a measurement of peak power. The performance is shown in Fig 3.7, where the pump power transmitted into the Nd:GGG slab is corrected for losses in the focusing lenses and Fresnel losses at the input face of the slab (10%). The threshold for lasing was 1.4W, and slope efficiency was 3.9%. The cavity loss was calculated to be ~ 1.2% by comparing the thresholds for three different output couplers. This would suggest that the threshold should be 880mW and slope efficiency 5%. Again we see that the performance achieved is less than might be expected from theory, but that the main discrepancy is in terms of lasing threshold. We have already noted the unusual colour and striations in the crystal, and the thermal problems experienced must also play some part in the poor performance of the laser. With a better quality piece of Nd:GGG, the performance may be expected to improve. The thermal effects may have been associated with the striations in the crystal, as these problems should not have occurred at these power levels for a normal crystal of Nd:GGG.

What these side-pumped systems do show, however, is the low efficiency of side-pumping, even in the theoretical limit. While the system is, in theory, easier to pump as we only have to worry about the pump dimensions in one direction, the difficulties of mode matching will mean that poorer performance than an end-pumped system is likely to result. In our situation, where only a 5W diode bar was available, we had insufficient pump power to satisfactorily explore the high power possibilities of side-pumping. Generally, a lot of power is required for side-pumping, and most experiments have tended to use a number of 10 or 15W devices to give a high overall output. These high powers were not available to us and we therefore decided to concentrate on end-pumping schemes for which much lower pump powers can be used. Our aim, then, was to achieve moderately high powers from pumping with one or two diode bars, where low thresholds and high efficiencies are possible.

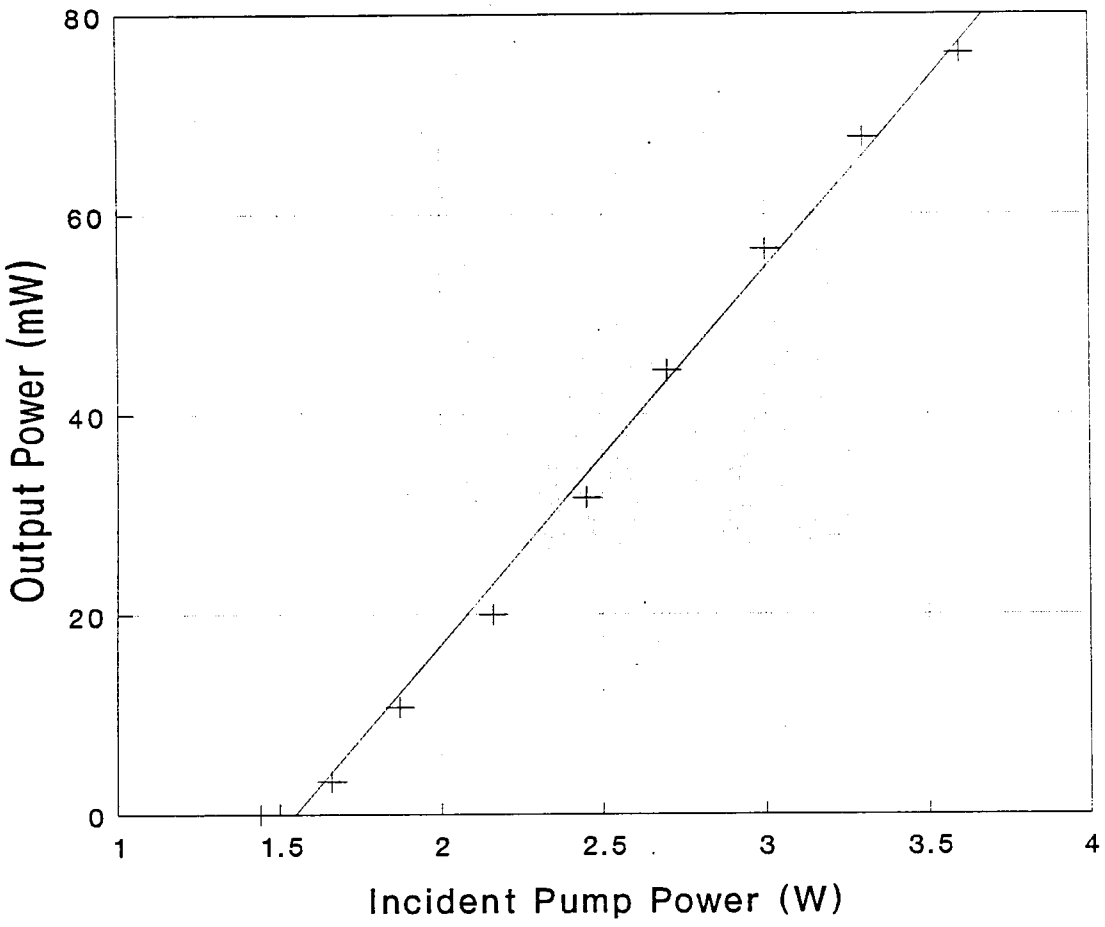

Fig 3.7 Performance of side-pumped Nd:GGG laser, using a chopper to measure peak output power.

3.3 Diode Bar End-Pumping

The method used to collect and focus the diode bar output for the end-pumped laser systems described in the remainder of this chapter is that described by Shannon & Wallace [1991], and is shown in Fig 3.8 below. The rod and cylindrical lenses collect and roughly collimate the output in the plane of the diode junction. The aspherical lens is used to focus the beam in both directions. This system produces an asymmetric focused beam of around 1.1mm x 150μm (diameter), which still presents mode matching problems for end-pumping for which a variety of solutions can be tried. This method has the advantage of using readily available optics, simplicity of design, and compatibility with any diode bar (unlike many approaches which are specific to the diode bar geometry such as the TFR and fibre-coupled schemes). Shannon and Wallace used intracavity beam expanders to produce an elliptical laser mode to match the pump focus, and in the rest of this chapter a number of alternative methods for doing so are examined.

The system that we constructed used cylindrical and aspherical lenses that were antireflection coated at 800nm, with an uncoated rod lens, giving a total throughput of around 85%. The focused spot size depended on the particular separation of the three lenses and the diode, but a typical case for the 5W diode bar used, produced a focused spot in the non-diffraction limited plane of around 1.5mm in diameter (Fig 3.9). Some evidence of a two-lobed structure is seen, which was much more pronounced with a 10W bar used later. The focused spot in the other plane was typically around 200μm. This arrangement is very compact, with the overall length of the lens system being only 14mm, with the focused spot being produced $\sim$4mm from the final lens element.

Using this spot, two end-pumped resonators were designed to attempt to match up the cavity mode size to the diode pump beam and hence achieve good efficiency. These approaches are described in sections 3.3.1 and 3.3.2, and whilst not proving to be totally successful, are interesting alternatives to end-pumped systems described elsewhere [Shannon, 1991], [Marshall, 1993].

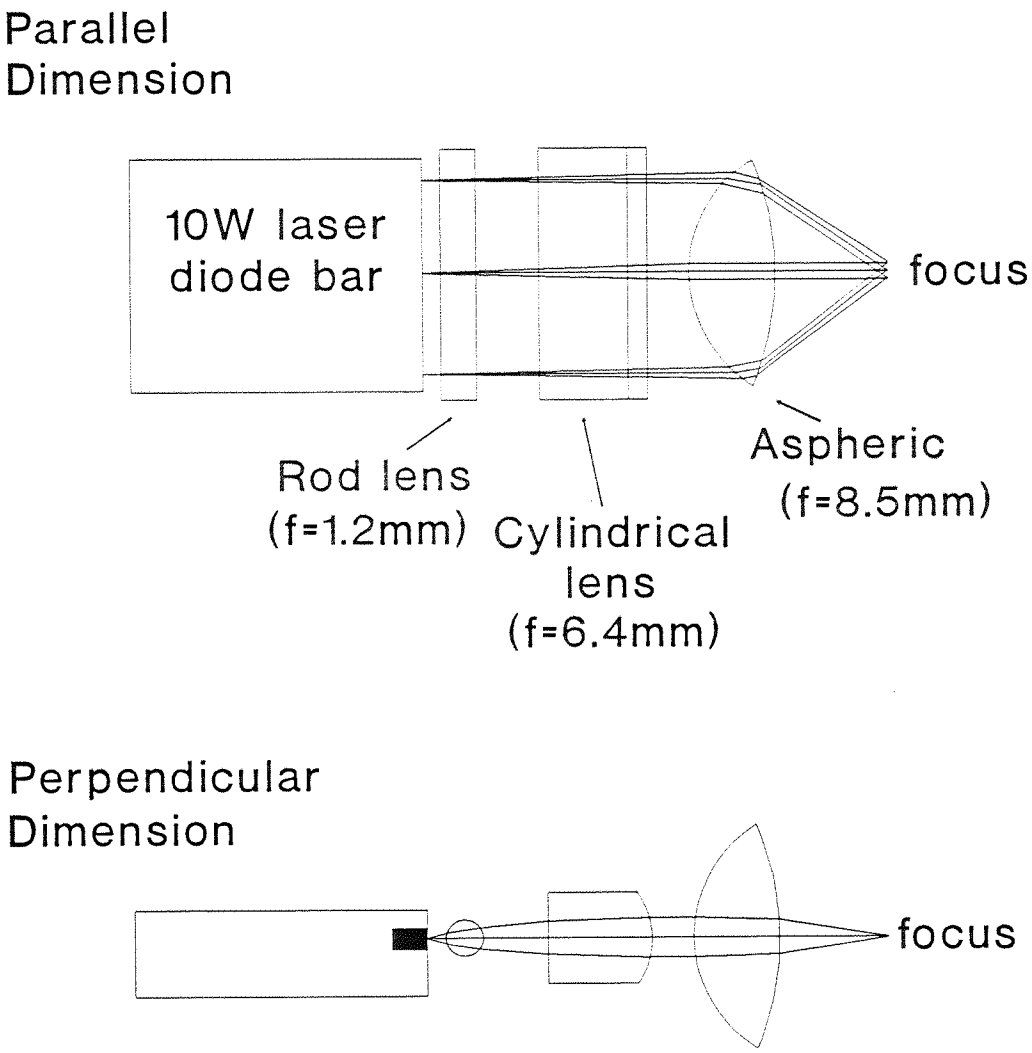

Fig 3.8 Diode bar focusing scheme. The 1.2mm focal length rod lens and 6.4mm focal length cylindrical lens collect and collimate the output in the diffraction limited plane. The 8.5mm focal length aspheric lens focuses in both planes. The lenses are separated from each other by ~1mm, with the rod lens ~1mm from the front facet of the diode.

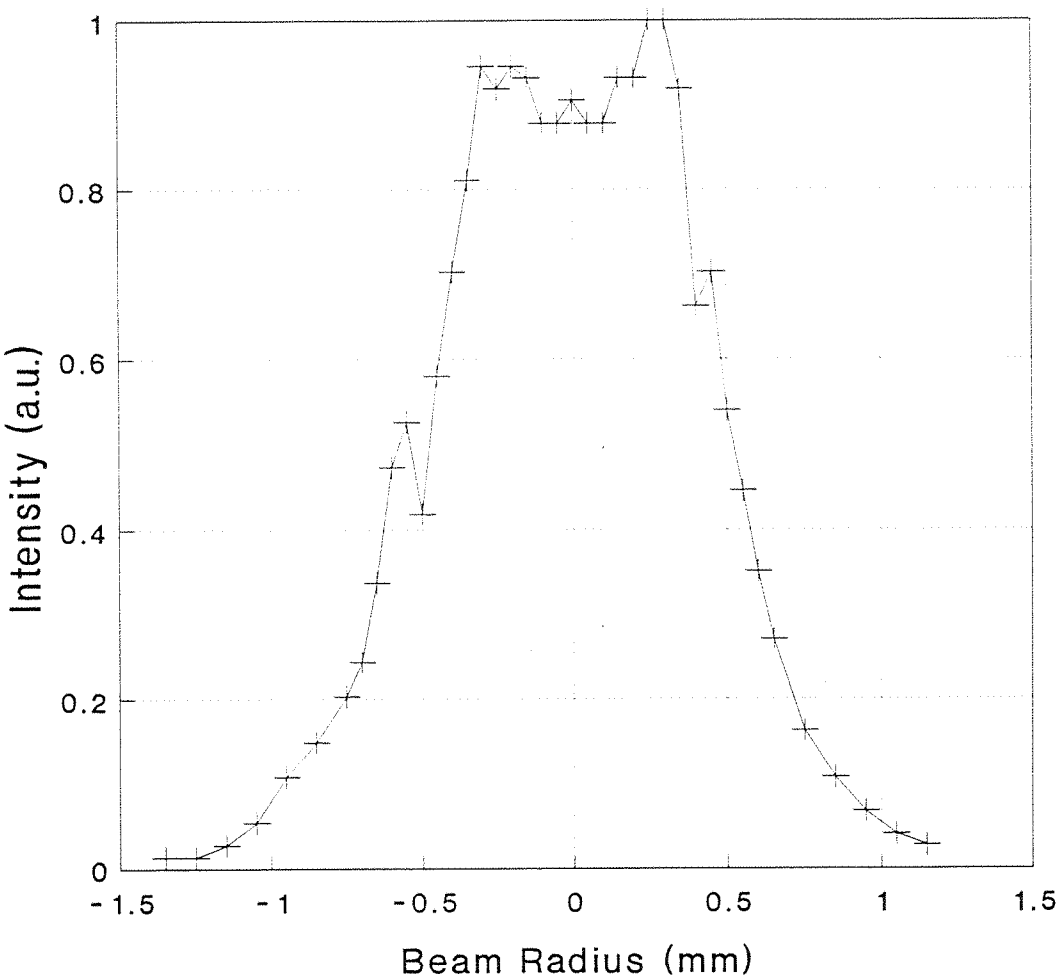

Fig 3.9 Focused spot profile in the non-diffraction limited plane.

3.3.1 Cylindrical Mirror End-Pumped Resonator

An initial attempt at a design for an end-pumped Nd:YAG laser was made using a cylindrical mirror as the output coupler in a standing wave cavity (Fig 3.10). Here the cylindrical surface is used to determine the mode size in the plane of the diode junction, and in the other plane the cavity is plane-plane, where the intention was that the cavity would select a lasing mode size that matched the pump dimensions and so minimise threshold. The mirrors were fabricated from high-quality concave cylindrical lenses (with as good a surface finish as possible, to minimise cavity losses), which were coated to be either 2% or 5% transmissive at 1.06μm, with the rear plane surface antireflection coated. Mirrors with different radii of curvature (R_c) were obtained to evaluate what was most suitable for our pumping arrangement. These radii were 37mm, 75mm and 125mm.

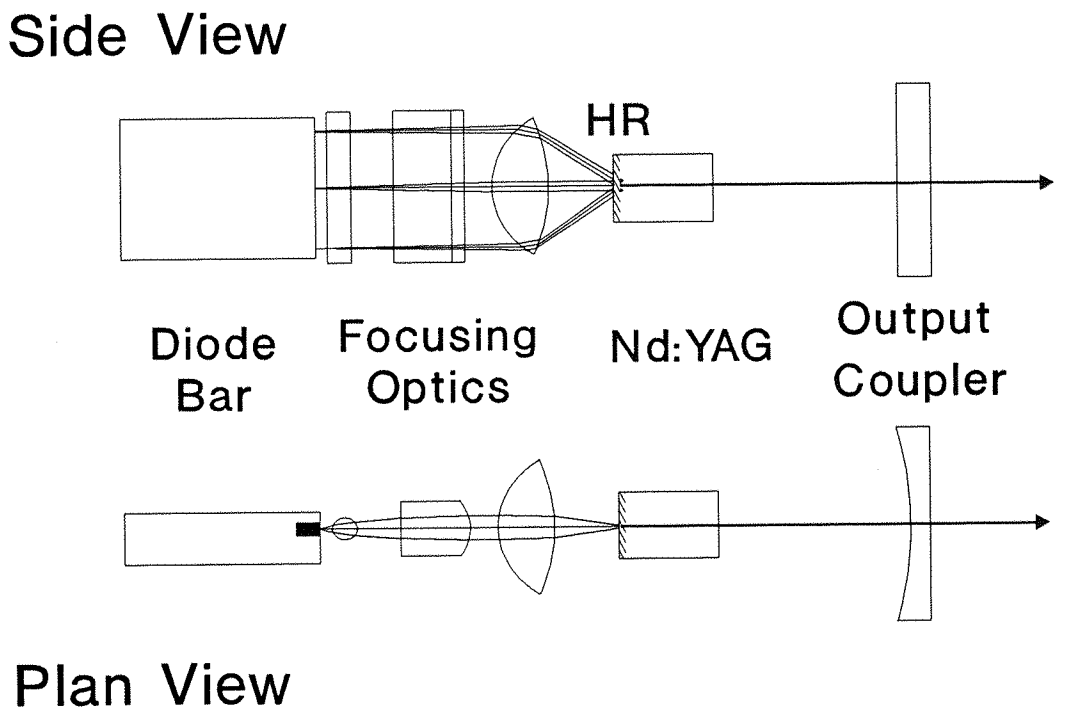

Fig 3.10 End-pumped laser cavity using cylindrical mirror as the output coupler. In the plane of the non-diffraction limited pump beam, the cavity is plane-plane.

The initial performance of lasers using these mirrors was encouraging, with pumping thresholds as low as 200mW (measured after the lens system) being observed. The different reflectivities and radii mirrors were tested in the cavity, with typical values of threshold being under 500mW, and the output from the Nd:YAG laser being in excess of 400mW for 3.7W of input pump power. The performance of the best cavity is shown in Fig 3.11, which used R_c=125mm, T=2%, with cavity length of 6cm. The threshold was 0.6W, with total output of 600mW for 4.3W of incident pump power (here the diode was operating at 11.2 Amps, a current exceeding manufacturers specifications), giving a slope efficiency of around 18%. Thus, for a 10W diode bar we would expect that over one watt of output from the Nd:YAG laser could be achieved.

The mode quality of this laser was not very good, however, with many transverse modes being observed in the vertical (i.e. plane-plane cavity) direction. The output in the other plane appeared to be single transverse mode. At output powers of up to 200mW, the laser output seemed to be TEM_{00}, with more modes being excited as the power was increased. When operating on a single mode, the mode-size in the vertical direction appeared to be only around 200μm, much smaller than the pump dimensions. This mismatch in laser and pump spot sizes led to the additional transverse modes lasing. Thus this simple approach to end-pumping was shown to be not adequate for producing TEM_{00} mode beams, with some means of actively increasing the mode size to match the pump dimensions being required.

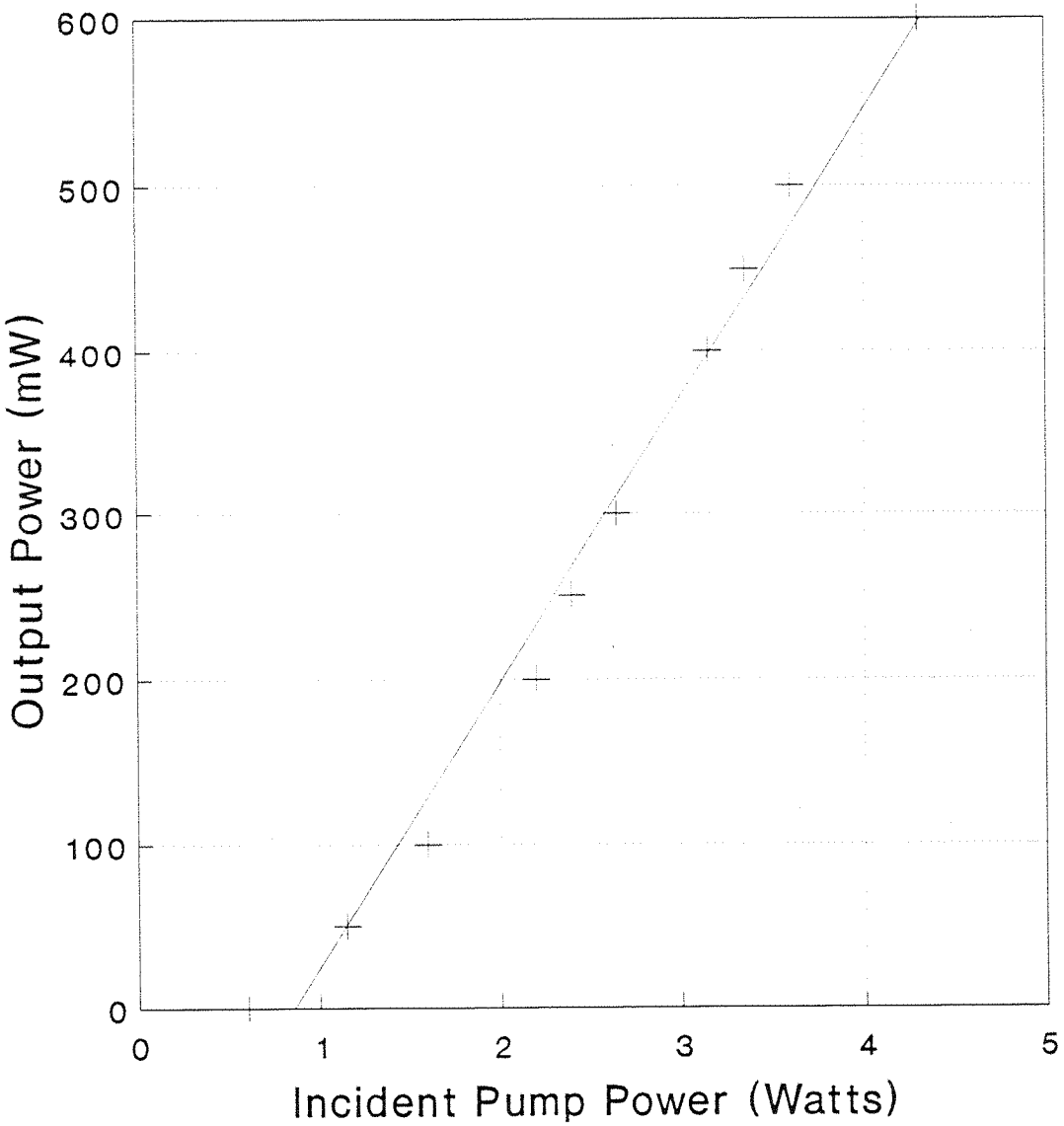

Fig 3.11 Output from end-pumped laser with $R_c = 125$mm.

3.3.2 Variable Curvature Mirror End-Pumped Resonator

One approach to the problem of increasing the lasing mode size to match the diode bar output is to deliberately bend a plane output coupler to make the laser cavity approach the geometric stability limit in the plane of the large non diffraction-limited pump beam. This is shown in exaggerated fashion in Fig 3.12, where the variable curvature mirror (VCM) is bent by applying a force at one edge, while being held at the opposite edge. The mirror is bent until the output is made to oscillate on a single transverse mode in the plane of bending. In effect, we are attempting to increase the lasing mode until it expands to match the pumped volume of the gain medium, by compensating for the thermal lensing in the laser medium. In the diffraction limited plane, the mode size is selected by Fresnel diffraction losses in the plane-plane cavity.

It is unclear whether the resonator we describe here is geometrically unstable, or if it is just close to the limit for stable operation. The concept of "resonator g parameters" (e.g. [Siegman, 1986]) is a standard way of describing the stability of a two mirror resonator. These parameters are given by

$$g_1 \equiv 1 - \frac{L}{R_1} \quad , \quad g_2 \equiv 1 - \frac{L}{R_2} \tag{3.6}$$

where R_1 and R_2 are the radii of curvature of the resonator mirrors and L is their spacing. The spot sizes at the two mirrors are then given by

$$w_1^2 = \frac{L\lambda}{\pi}\sqrt{\frac{g_2}{g_1(1-g_1g_2)}} \quad , \quad w_2^2 = \frac{L\lambda}{\pi}\sqrt{\frac{g_1}{g_2(1-g_1g_2)}} \tag{3.7}$$

Finite solutions for spot sizes are only obtained if the g_1 and g_2 parameters are confined to a stability range defined by

$$0 \le g_1g_2 \le 1 \tag{3.8}$$

Thus, for example, a plane-plane cavity would have a g_1g_2 product of 1 and be precisely on the border of being stable.

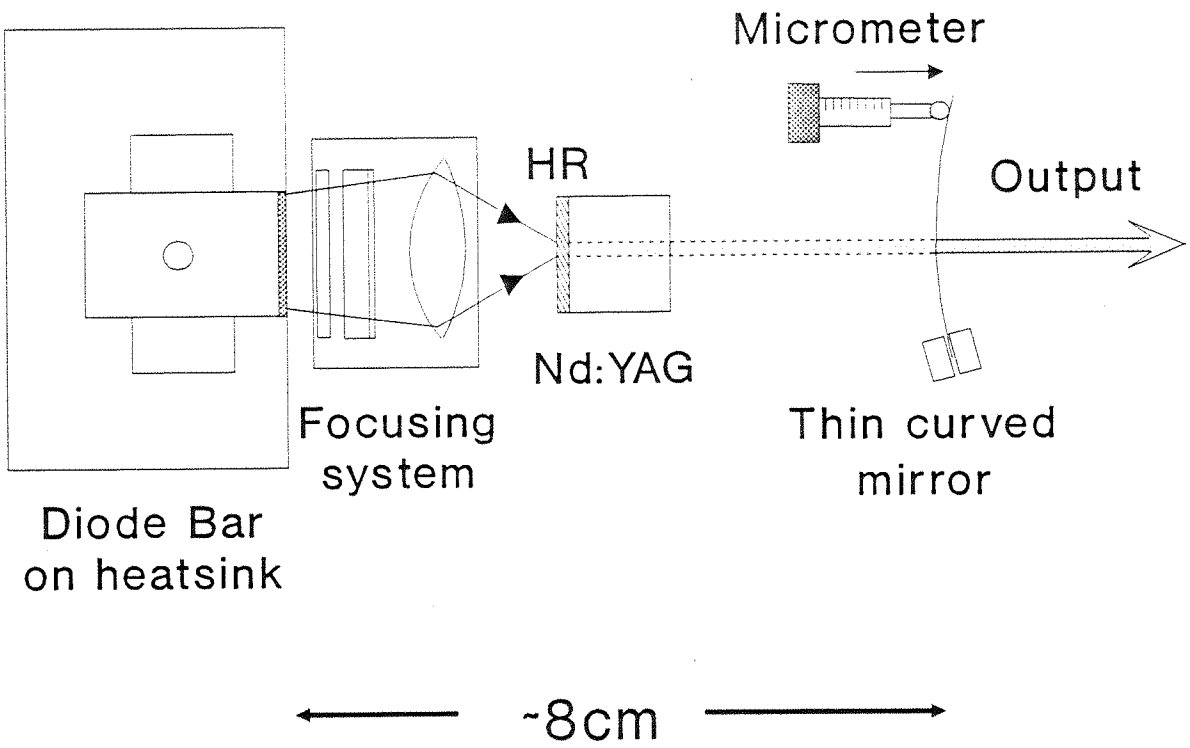

Fig 3.12 Schematic of diode-bar end-pumped resonator with variable radius of curvature output coupler.

In the laser described in this section, we initially began with a plane-plane cavity defined by the HR dielectric mirror coating on the laser rod, and a plane output coupler. However, when end-pumped by the diode bar, the rod experiences thermal lensing (eq. 3.3), which results in the resonator mode size decreasing, leading to the multi-transverse mode operation observed. Bending the output coupler in the opposite direction can compensate for this thermal lensing to some extent, and can place the resonator very close to the stability limit. It may even be the case that the resonator is marginally unstable, in the sense that $g_1 g_2 > 1$ and the mode size is increasing on successive round trips.

If this resonator is unstable, then it differs from the usual types employed for flashlamp pumped lasers [Siegman, 1965 and 1974], [Anan'ev, 1972]. There the beam is either extracted from around the edges of the mirrors [Herbst, 1977], [Latham, 1982], or from cavities with variable reflectivity mirrors (VRM) with a Gaussian or supergaussian reflectivity profile [Zucker, 1970], [Chester, 1972], [Casperson, 1974]. The first approach suffers from problems with diffraction "ringing" of the output beam from the hard edges of the mirrors, and is usually annular in cross-section. The difficulty in mounting the mirror so that the beam can pass around it without being attenuated by the mirror mounts is also a problem. Unstable resonators with VRMs have much better output beam properties, with well defined modes. Our resonator perhaps resembles VRM unstable resonators as it has a "soft-edged" aperture defined by the gain distribution in the laser medium which is in some way analogous to the varying reflectivity of the VRM output mirror. The gain distribution in the laser rod will only amplify the expanding laser mode until it reaches the same size as the gain profile, hence contributing some beam shaping on the resonator mode. If the resonator is marginally unstable, the gain profile will act as an aperture to restrict the size of the largest mode that experiences net gain. Thus, is some sense, the gain distribution acts as a soft aperture that assists in the mode selection in an analogous manner to a VRM unstable resonator. However, the output beam in our resonator is not extracted through this soft aperture, as is the case with VRMs, but at the opposite end of the cavity, through a plane mirror with variable curvature. This system is less complex than those using VRMs, as no special techniques are required to fabricate the mirrors.

Initial investigations with non-optimised mirrors (ordinary 1mm thick glass microscope slides coated to be 99.5% reflective at 1.088μm) were promising. The laser rod used was a Nd:YAG rod 6mm in diameter, 10mm long, coated to be HR at 1.06μm and highly transmitting at 810nm on the input face, and antireflection coated at 1.06μm at the other end. The length of the laser cavity was around 40mm. Bending the mirror slightly made the output change from very multimode to a few modes and then to one distinct mode in the plane of the large pump dimension. The mode size in the two planes was measured to be 270μm x 580μm, which corresponded well to the dimensions of the pump beam. The threshold was around 0.6W and 200mw of output was produced for 3.6W of incident pump power.

In an attempt to improve on these initial results, laser quality 0.5mm thick mirrors with 3% output coupling were obtained, and an improved mount for bending the mirror was constructed. Again it was found that bending the mirror could enforce single transverse mode operation for all pump powers. The radius of curvature of this mirror in the vertical plane was calculated to be 2.4 metres, which was obtained by displacing the upper edge of the 1" diameter mirror by 0.085mm. The performance of this laser is shown in Fig 3.13, which indicates that thermal effects do not seem to produce any deterioration in performance. The lasing threshold for a 5W diode bar was 2.03W, with a maximum output of 480mw for 4W of incident pump, with a slope efficiency of around 30%. After performing these experiments, we were later to receive a 10W bar, with which a peak single transverse mode output of 1.6W was obtained for 8.2W of incident power, which agreed with an extrapolation of the output power from the 5W diode. This result compares favourably with that of Shannon [1991], using the same pumping arrangement, where 1.9W of TEM_{00} output was obtained, with a cavity that used intracavity prisms to expand the lasing mode to an elliptical shape. Direct comparison is not possible, as they used a higher value output coupler (8%), giving a higher lasing threshold (3.23W). The stability of this laser was not as good as from similar length stable cavities pumped by diodes, but still respectable. Over a 15 minute period, the output power dropped by less than 2%, and had a typical amplitude jitter of $\sim$1%, although occasionally a large fluctuation of the order of 20% was observed as a second transverse mode oscillated briefly. As we are operating near the stability limit, any small changes in cavity parameters such as bend on the mirror, degree of

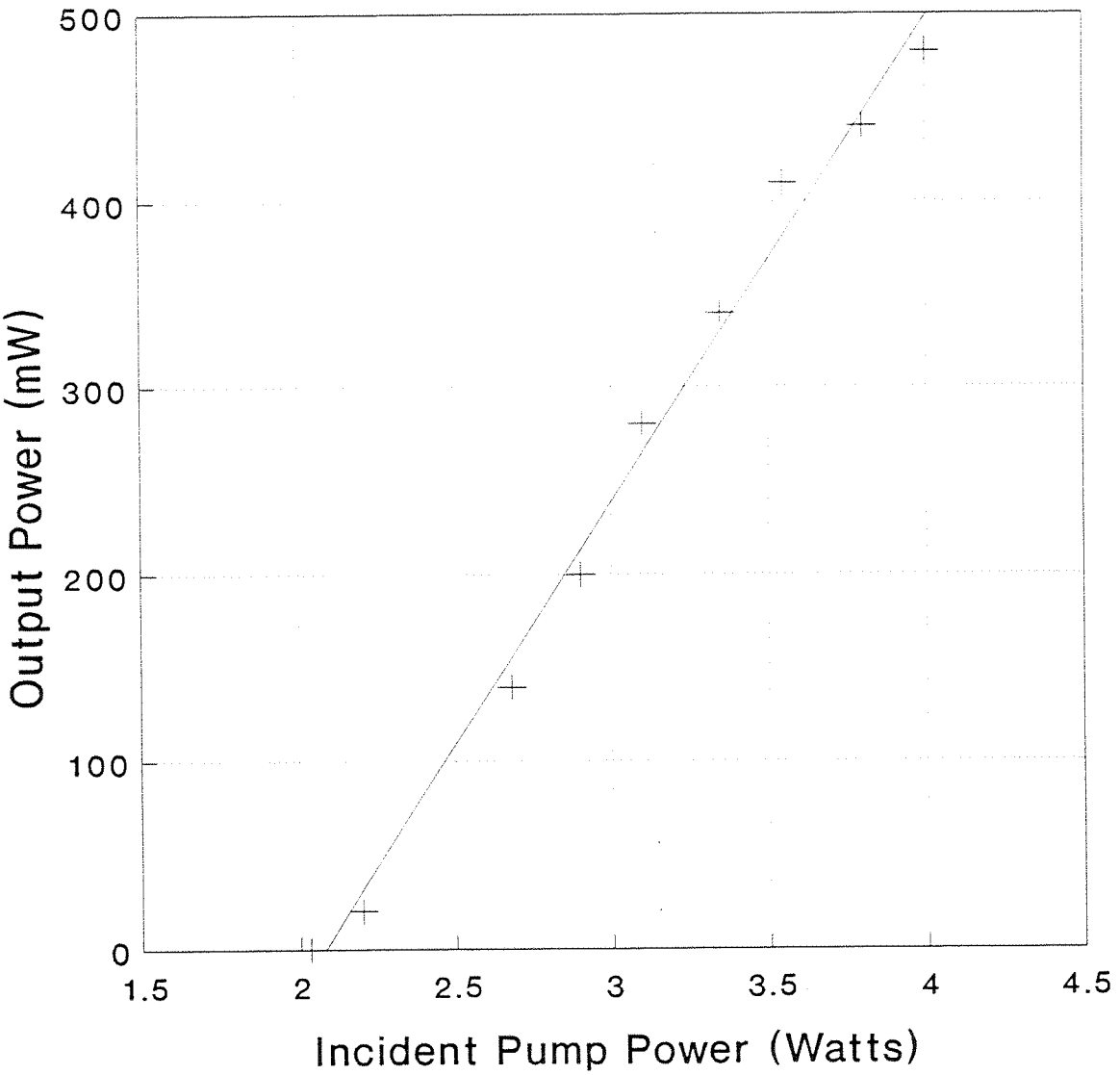

Fig 3.13 Performance of VCM resonator end-pumped by 5W diode bar.

thermal lensing, length of cavity, etc, will have a pronounced effect on the mode quality and size. In turn, this may lead to instabilities in the output power from the laser.

An important parameter of this system is the beam quality in the vertical direction (i.e. in the plane of the diode junction). Increasingly the concept of "M^2" is used to define the quality of a laser beam [Sasnett, 1989], [Johnston, 1990], [Siegman, 1992] rather than the usual notion of "times diffraction limited" [e.g. Siegman, 1986], although the two concepts are similar. A beam which "looks" Gaussian and to have a TEM_{00} transverse mode can in fact have a number of other higher-order modes oscillating, which degrades the spatial quality of the beam and changes the way it propagates through an optical system. M^2 can be defined by the propagation equation:

$$W(z) = W_0\left[1+\left[\frac{M^2\lambda(z-z_0)}{\pi W_0^2}\right]^2\right]^{1/2} \qquad (3.9)$$

where $W(z)$ and W_0 are the measurable ("real") beam sizes and beam waists respectively, and z_0 is the location of the beam waist. The M^2 concept is highly versatile, as it is a single number that expresses the laser beam quality of any arbitrary beam. Knowing M^2, and measuring W_0 and z_0, everything is known about how the beam propagates. One way of visualising how M^2 can be used is to imagine an "imbedded Gaussian" beam in the real beam, that propagates as in eq (1.2), but with $w_0=W_0/M$. The real beam will propagate in exactly the same way as the imbedded Gaussian, but will be M times larger at every point. It will have the same focal point and complex radius of curvature, and also the same Rayleigh range. A "perfect" laser beam would have an M^2 value of 1, but in practice this can be difficult to achieve.

A difficulty in determining the quality of a laser beam is actually knowing what the beam diameter is at any given point. If a beam is not truly Gaussian, then the usual definition of the beam width being defined by the $1/e^2$ intensity points may not be meaningful, and we find that there are a number of ways of defining and measuring the

beam size, of which the main ones are:

(i) Finding the radius at which the intensity drops to $1/e^2$ of the peak intensity, as we would with a true Gaussian beam;

(ii) Finding the radius of a circular aperture that passes all but $1/e^2$ of the total power in the beam;

(iii) Finding the radius at which the intensity drops to $1/e^2$ of the outermost peak in the beam profile;

(iv) Computing the radius from the second moment of the intensity distribution.

This fourth method, which is used in a commercially available "M^2-meter" (Coherent Modemaster™), uses the following definition of the second moment of the intensity distribution:

$$\overline{r^2} = \int_0^\infty r^2 I(r) dA \qquad (3.10)$$

where I(r) is the normalised intensity distribution, and the area of integration, A, is centred on the beam axis. Thus for modes with circular symmetry:

$$\overline{r^2} = 2\pi \int_{r=0}^\infty r^3 I(r) dr \qquad (3.11)$$

and the beam radius W is defined as:

$$W = \sqrt{2\overline{r^2}} \qquad (3.12)$$

which gives the same result for a pure TEM_{00} mode in that the radius is the distance at which the intensity falls to $1/e^2$ of the peak value.

Each of the four methods described above can give a different value of M^2 for the same beam, depending on the particular beam parameters, and it is suggested by Sasnett[1989] that the method using the beam second moments may be the best one, as it at least produces a value somewhere between that of the other methods. When measuring M^2, it is important to use the same method of measuring beam dimensions

throughout. M^2 is then determined by measuring W_0 at a focus and W at at least two other positions, and then finding the best fit of M^2 to eq. (3.9)

The profile of the laser beam in the vertical plane at a number of (z-) positions was measured using a thin slit, and some of these shown in Fig 3.14, where it can be seen that they appear to have a Gaussian profile. Using method (i) to measure the beam radius, we calculated that $W_0 = 530\mu m$, and from (3.9) the best fit M^2 value was 1.17, which suggests that the beam is very close to being a pure TEM_{00} Gaussian. Johnston [1990], suggests that an M^2 of less than 1.2 is a practical definition for an effectively fundamental-mode beam.

These results were very encouraging, as they showed that a relatively simple system could be used to produce good quality laser beams. Problems with stability need to be addressed, however, and mechanical and thermal stabilisation should improve the overall stability of the system. Improved thermal handling of the laser rod, such as reducing the dimensions of the rod and better heat sinking of it should reduce thermal lensing, while more robust mounts for the thin mirror will reduce mechanical instabilities. The output powers produced, whilst not spectacular, are perhaps sufficient to warrant further work using this approach, but at present the system described in the next chapter looks to have the greatest potential for realising a convenient means for end-pumping solid-state lasers.

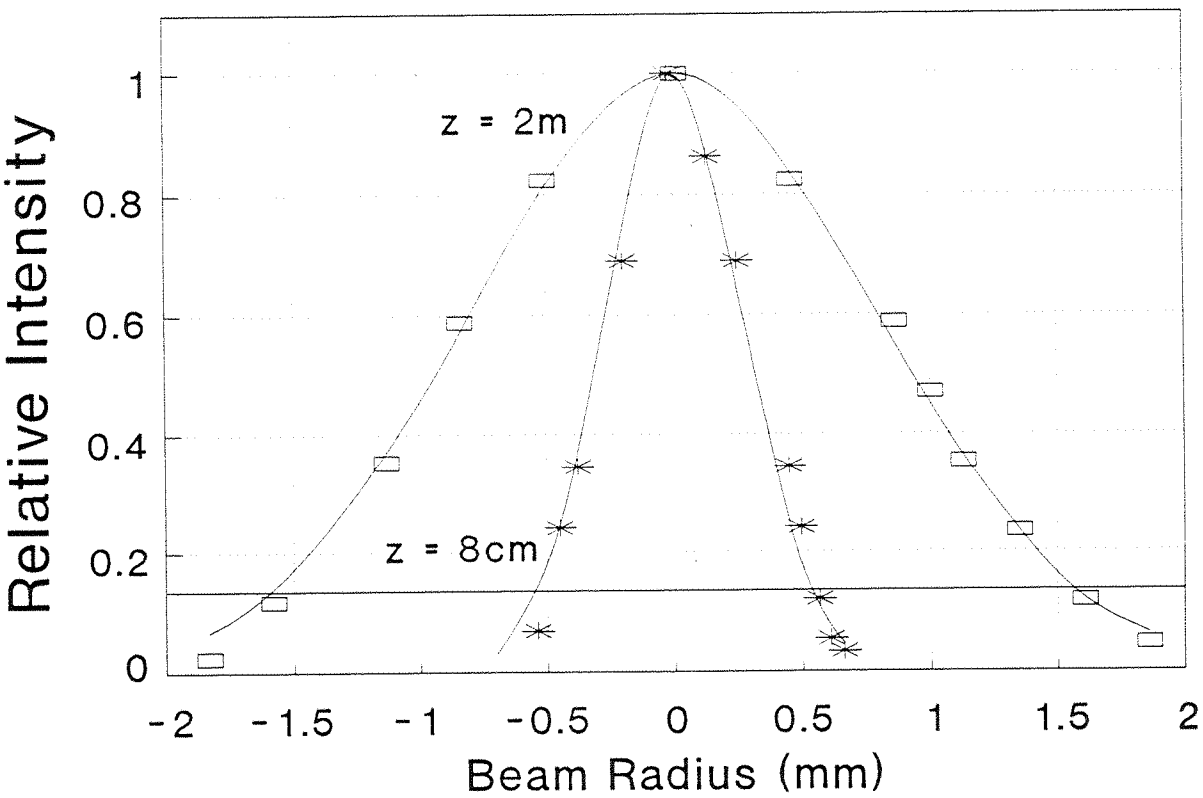

Fig 3.14 Beam profiles of output of variable radius of curvature resonator in the plane of the large mode size at 8cm and 2m from the output coupler. The horizontal line shows the $1/e^2$ intensity level. The fitted curves are gaussian profiles using w=533μm and w=1.58mm respectively.

References

Ajer, H., Landrø, S., Rustad, G. and Stenersen, K., Opt. Lett., **17**, 1785 (1992)

Anan'ev, A., Sov J. Quantum Electron., **1**, 565 (1972)

Baer, T.M., Head, D.F. and Sakamoto, M., CLEO '89 Technical Digest, Paper FJ5 Baltimore, MA (1989)

Baer, T.M., Head, D.F., Gooding, P., Kintz, G.J. and Hutchison, S., IEEE J. Quantum Electron., **28**, 1131 (1992)

Bagdasarov, Kh., S., Bogomolova, G.A., Gritsenko, M.M., Kaminskii, A.A. and Kevorkov, A.M., Sov. Phys. Doki., **19**, 353 (1974)

Basu, S. and Byer, R.L., Appl. Opt., **29**, 1765 (1990)

Berger, J., Harnagel, G., Welch, D.F., Scifres, D.R. and Streifer, W., Appl. Phys. Lett., **53**(4), 268 (1988a)

Berger, J., Welch, D.F., Strieffer, W., Scifres, D.R., Hoffman, N.J., Smith, J.J., and Radecki, D., Opt. Lett., **13**, 306 (1988b)

Boyd, R.W., *Radiometry and the Detection of Optical Radiation*, New York, Wiley (1983)

Burnham, R. and Hays, A.D., Opt. Lett., **14**, 27 (1989)

Carts, Y.A., Laser Focus World, **28**(2), 87, (1992)

Casperson, L.W., IEEE. J. Quantum Electron. **QE-10**, 692 (1974)

Chester, A.N., Appl. Opt., **11**, 2584 (1972)

Clarkson, W.A. and Hanna, D.C., J. Mod. Opt., **36**, 483 (1989)

Comaskey, B., Albrecht, G., Beach, R., Sutton, S., Mitchell, S., CLEO '93 Technical Digest, paper CWI5, Baltimore, MA (1993)

Cousins, A.K., IEEE J. Quantum Electron., **28**, 1057 (1992)

Day, T., Gustafson, E.K. and Byer, R.L., Opt. Lett., **15**, 221 (1990)

Fan, T.Y. and Byer, R.L., IEEE J. Quantum Electron., **24**, 895 (1988)

Field, S.J., Hanna, D.C., Large, A.C., Shepherd, D.P., Tropper, A.C., Chandler, P.J., Townsend, P.D. and Zhang, L., Opt. Comm., **86**, 161 (1991)

Field, S.J., Hanna, D.C., Large, A.C., Shepherd, D.P., Tropper, A.C., Chandler, P.J., Townsend, P.D. and Zhang, L., Opt. Lett., **17**, 52 (1992)

Geusic, J.E., Marcos, H.M. and Van Uitert, L.G., Appl. Phys. Lett., **4**, 182 (1964)

Graf, Th. and Balmer, J.E., Opt. Lett., **18**, 1317 (1993)

Hanna, D.C., Large, A.C., Shepherd, D.P., Tropper, A.C., Opt. Comm., **91**, 229 (1992)

Herbst, R.L., Komine, H. and Byer, R.L., Opt. Comm., **21**, 5 (1977)

Johnston, T.F., Jr., Laser Focus World, **26**(5), 173 (1990).

Kaneda, Y., Oka, M., Masuda, H. and Kubota, S., Opt. Lett., **17**, 1003 (1992)

Keirstead, M.S., Baer, T.M., Hutchison, S.H. and Hobbs, J., CLEO '93 Technical Digest, paper CFM4, Baltimore, MA (1993)

Koechner, W., J. Appl. Phys, **44**, 3162 (1973)

Koechner, W., *Solid-State Laser Engineering*, 2nd ed. New York, Springer Verlag (1988)

Latham, W.P., Jr. and Smithers, M.E., J. Opt. Soc. Am., **72**, 1321 (1982)

Leger, J.R. and Goltsos, W.C., IEEE J. Quantum Electron., **28**, 1088 (1992)

Lynn, J.G., Stoneman, R.C. and Esterowitz, L., OSA Proceedings on Advanced Solid-State Lasers Topical Meeting 1991, Hilton Head, SC, pg 286 (1991)

Maeda, K., Wada, N., Umino, M., Abe, M., Takadam Y., Nakano, N. and Kuroda, H., Japanese J. Appl. Phys., **23**, L759 (1984)

Marshall, L.R., Kaz, A. and Verdún, H.R, CLEO '93 Technical Digest, paper CMF5, Baltimore, MA (1993)

Morris, P.J., Lüthi, W. and Weber, H.P., Appl. Opt., **32**, 5274 (1993)

Pfistner, C., Albers, P. and Weber, H.P., IEEE J. Quantum Electron., **26**, 827 (1990)

Reed, M.K., Kozlovsky, W.J., Byer, R.L., Harnagel, G.L. and Cross, P.S., Opt. Lett., **13**, 204 (1988)

Sasnett, M.W., *The Physics and Technology of Laser Resonators*, D.R. Hall and P.E. Jackson, eds., Adam Hilger, N.Y., Chapter 9. (1989)

Shannon, D.C. and Wallace, R.W., Opt. Lett., **16**, 318 (1992)

Siegman, A.E., Proc. IEEE., **53**, 277 (1965)

Siegman, A.E., Appl. Opt., **13**, 353 (1975)

Siegman, A.E., *Lasers*, University Science Books, Mill Valley, CA (1986)

Siegman, A.E., Sasnett, M.W. and Johnston, T.F., Jr., *Defining and Measuring Laser Beam Quality: The M^2 factor*, NATO Advanced Study Institute, Elba, Italy (1992)

Snyder, J.J. and Reichert, P., Proceedings of the Advanced Solid-State Lasers 1991

Topical Meeting, Paper WC5-1 (1991a)

Snyder, J.J., Reichert, P. and Baer, T.M., Appl. Opt., **30**, 2743 (1991b)

Snyder, J.J. and Cable, A.E., Laser Focus World, **29**(2), 97, (1993).

Streifer, W., Scifres, D.R., Harnagel, G.L., Welch, D.F., Berger, J. and Sakamoto, M., IEEE J. Quantum Electron., **24**, 883 (1988)

Tidwell, S.C., Seamans, J.F., Hamilton, C.E., Muller, C.H. and Lowenthal, D.D., Opt. Lett., **16**, 584 (1991)

Tidwell, S.C., Seamans, J.F., Bowers, M.S. and Cousins, A.K., IEEE J. Quantum Electron., **28**, 997 (1992)

Tidwell, S.C., Seamans, J.F. and Bowers, M.S., Opt. Lett., **18**, 116 (1993)

Verdún, H.R. and Chuang, T., Opt. Lett., **17**, 1000 (1992)

Yamaguchi, S. and Imai, H., IEEE J. Quantum Electron., **28**, 1101, (1992)

Yoshida, K., Yoshida, H. and Kato, Y., IEEE J. Quantum Electron., **24**, 1188 (1988)

Zucker, H., Bell Sys. Tech. J., **49**, 2349 (1970)

Chapter 4
DIODE BAR BEAM SHAPING TECHNIQUE

4.1 Introduction

In the previous chapter we reviewed various attempts that have been made to produce a beam from a diode bar suitable for end-pumping solid-state lasers. These systems all use conventional optics (lenses, prisms, etc) to manipulate the diode beam, and typically produce focused beams that are too large to be effective in end-pumping applications. In this chapter we describe a beam-shaping technique that reconfigures the transverse intensity profile of the diode bar beam so that a more circularly symmetric pump beam with its orthogonal divergences approximately equalised can be produced. This reduces the restrictions on the laser cavity design that is required to mode-match with the pump beam, allowing simple cavities to be constructed. In addition, we are able to produce much smaller spot sizes than are usually achieved with diode bars, producing a much higher gain, thus allowing transitions with low gain to be accessed. This system should prove important in the development of efficient diode bar end-pumped laser systems.

In the remainder of this introduction, the M^2 concept will be examined in more detail than in Chapter 3, showing some of the fundamental limitations for end-pumping with diode bars using conventional optics, and how it would be advantageous to alter the divergence properties of the diode bar output in its orthogonal emission planes. In section 4.2 we describe a novel system for re-shaping a diode bar beam that allows much more symmetric beams to be produced, and present results from a particular implementation of this technique in section 4.3. The method that we describe is highly versatile, and some further applications of this technique to other laser systems are discussed in section 4.4, as are some additional benefits of this system.

In section 3.2.3 we introduced the concept of M^2 as a way of characterising the spatial quality of a laser beam. A fundamental result from this is that a beam with a particular M^2 value will have a far field divergence M^2 times greater than a diffraction limited beam with the same waist dimension. For end-pumping, an important

consideration is how well the pump beam is matched to the TEM_{00} lasing mode size over the length of the laser medium, or over approximately one absorption length, whichever is the shorter. If the pump beam diverges much more rapidly than the lasing mode over an absorption length, then the extra gain produced in the wings of the fundamental laser mode may excite additional transverse lasing modes, and in any case, will result in a lower operating efficiency than a pump beam which is properly matched to the lasing mode size. A parameter that indicates the suitability of a pump beam for end-pumping is the minimum average beam size that can be maintained over a given length (e.g. an absorption length). Referring to eq (3.9), which describes the propagation of a beam M^2 times diffraction limited, we can calculate that for a given focused spot size, w_0, the average beam size over a length ℓ, centred around the focal plane is:

$$\overline{w}_{av}(w_0,M)=\frac{w_0}{\ell}\int_{-\frac{\ell}{2}}^{\frac{\ell}{2}}\left(1+\left(\frac{M^2\lambda z}{\pi w_0^2}\right)^2\right)^{\frac{1}{2}}dz \qquad (4.1)$$

and the minimum average spot size over length ℓ is then given by the condition that

$$\frac{d}{dw_0}\overline{w}_{av}(w_0,M)=0 \qquad (4.2)$$

When this expression is evaluated numerically, it can be shown that the minimum average spot size a beam can be focused to is proportional to M, and is given by

$$\overline{w}_{min}=\frac{M\sqrt{\lambda\ell}}{2.398} \qquad (4.3)$$

For a pump wavelength of 807nm, the minimum average spot sizes maintained over a length ℓ (in air) are shown in Fig 4.1, where the M^2 is varied from 1 to 100. It is important to note that the wavelength, λ, is different in a laser medium, and is reduced by a factor of n, the refractive index of the medium, relative to its value in air. This means that the minimum average spot sizes derived from (4.3) will in fact be reduced by a factor of $\sqrt{n}$. For Nd:YAG, where $n \simeq 1.82$, the minimum average spot size will be reduced by 1.35 times. If we now consider a diode bar beam, where the M^2 value

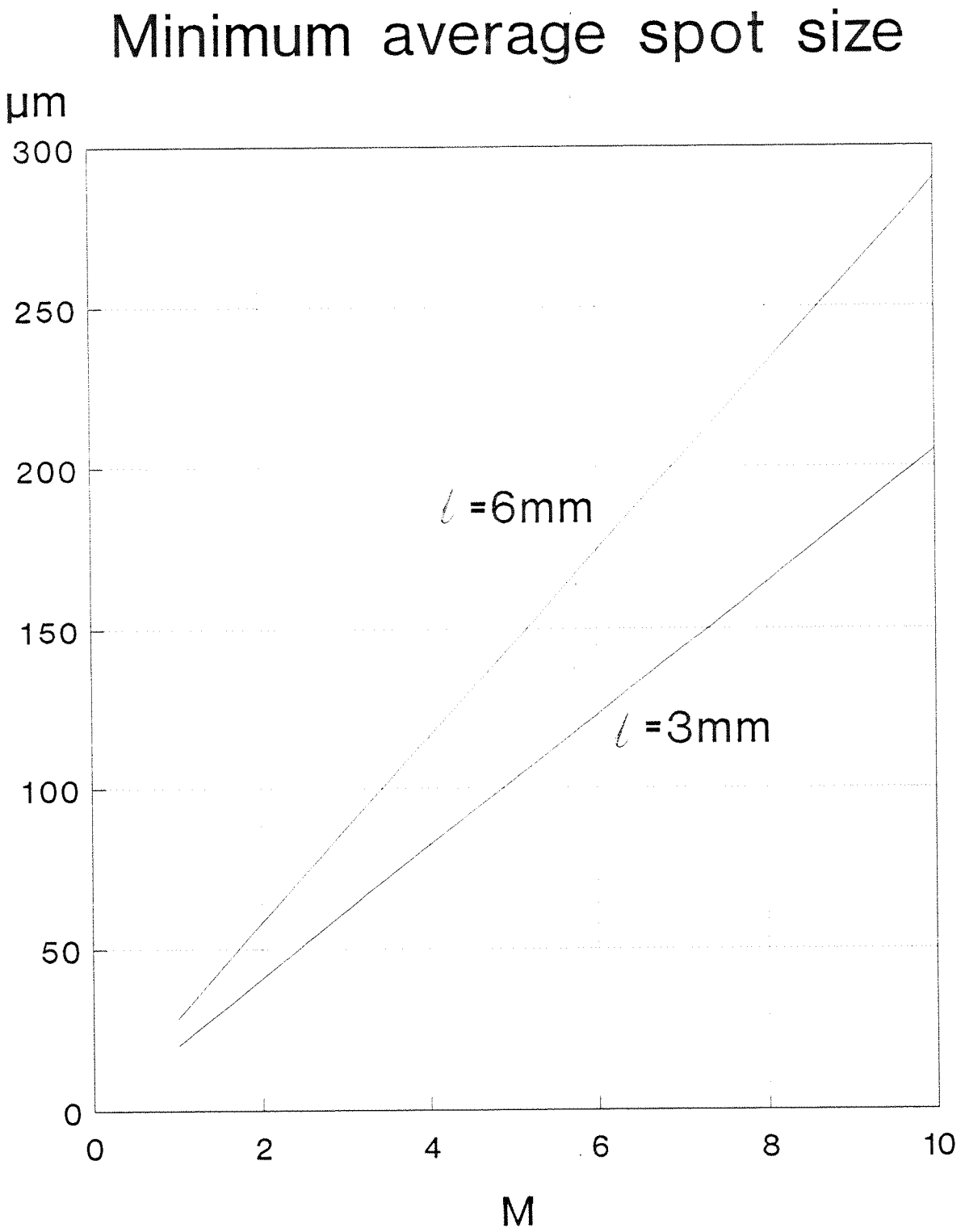

Fig 4.1 The minimum average spot size ($\bar{w}_{min}$) a pump beam at λ=807nm can be focused to over lengths of 3 and 6mm (in air) is shown here. $\bar{w}_{min}$ scales linearly with M.

in one plane can be >1000 times that in the perpendicular plane, we see that the minimum average spot size in the two planes differs by a factor of ~ 40 (e.g. over a 3mm length, for $M^2=1$, $\bar{w}_{min}=20.5\mu m$, whereas for $M^2=1500$, $\bar{w}_{min}=800\mu m$). Thus, conventional optics, which preserve the relative M^2 values in the perpendicular planes of emission will be restricted to producing highly asymmetric pump beams, which in turn restricts the choice of resonator design. If, for example, we simply try to focus the pump beam down to match its size at the focus to the laser waist size in the gain medium, we see from eq (4.1) that the average spot size produced over a given length will scale approximately with M^2, as shown in Fig 4.2, which again has important consequences for end-pumping with diode bars. In the example shown, if we tried to match a lasing mode waist size of $67.5\mu m$ by focusing to a waist size of $67.5\mu m$, an average beam radius over a length of 3mm of $67.58\mu m$ for $M^2=1$, and 4.3mm for $M^2=1500$ would result. To produce an acceptable beam from a diode bar, what we clearly need is some means of altering the respective M^2 values in the orthogonal planes, reducing it in the many times diffraction limited plane, while increasing the M^2 of the near diffraction limited plane by at least the same amount, to allow more symmetric beams to be produced. We shall now describe such a system.

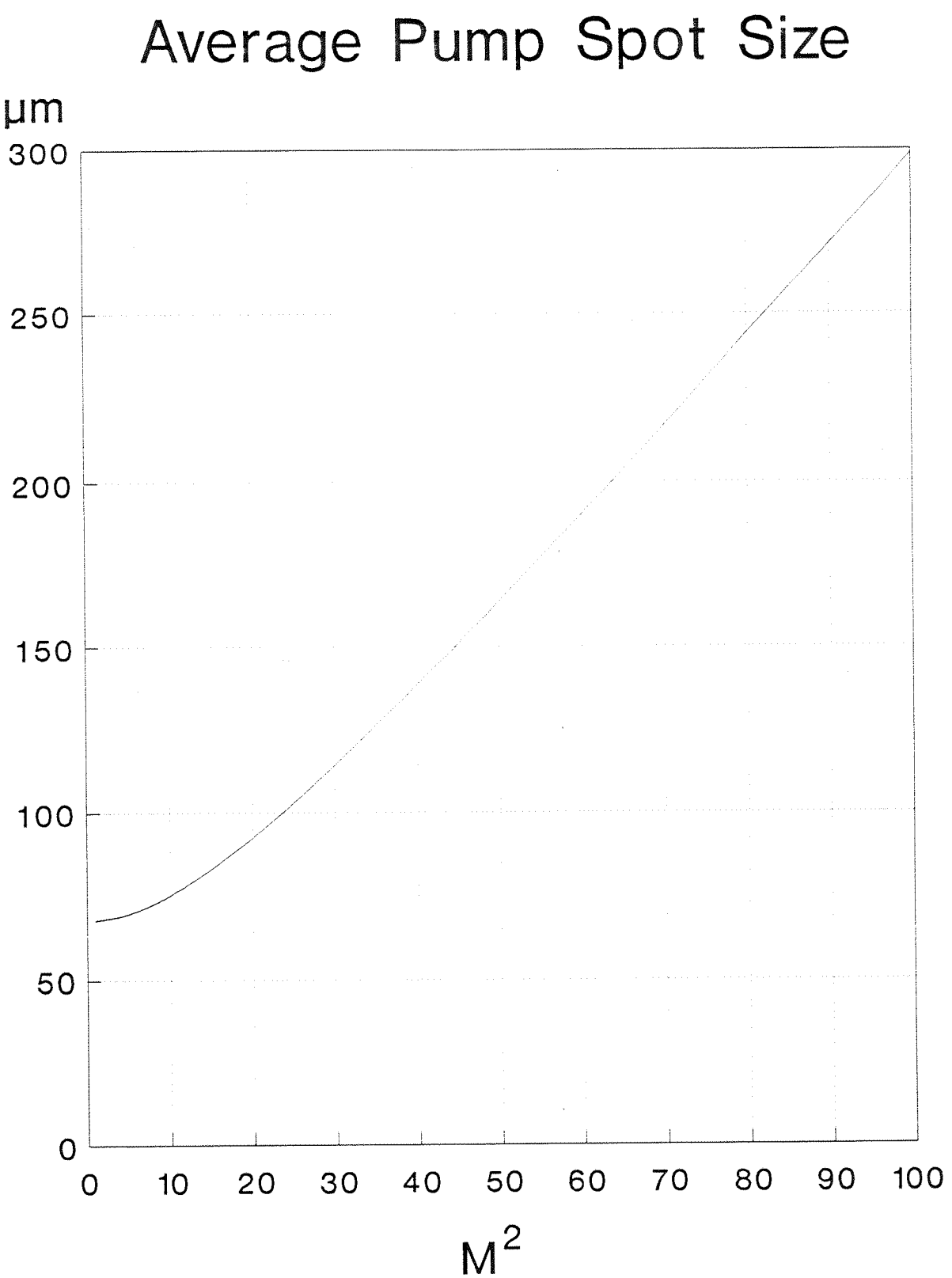

Fig 4.2 For a focused spot size of 67.5μm, the average spot size over a given length increases approximately linearly with M^2. In the example shown here, the average spot size over a 3mm length in air for λ=807nm is shown.

4.2 Beam Shaping Technique

In this section we describe a novel beam shaping technique which can be used to re-configure the transverse spatial intensity profile of a laser beam such that the M^2 in one plane is reduced, whereas in the orthogonal plane it is increased. This technique is also suitable for use with any other laser which produces a beam with highly asymmetric diffraction properties where, for many applications, it is desirable to obtain a final focused beam which has a nearly circular spot with far field beam divergences, in orthogonal planes, which are similar. Some of these additional applications are discussed in section 4.4.

In the description of this beam shaping technique, and in the rest of this chapter, two sets of axes are used to denote the orientation of the diode beam and the beam shaper. The principal set (x-y-z) is set in the plane of the diode beam, which is propagating along the z-axis, and whose x- and y-planes are as shown in Fig 4.3, which also shows a schematic of a typical diode bar and its emitting regions. The primed set of axes (x'-y'-z') is oriented to be orthogonal to the mirrors of the beam shaper, as shown in Figures 4.4 and 4.5, and is rotated at angle θ (x→x') and angle α (y→y') to the principle set of axes.

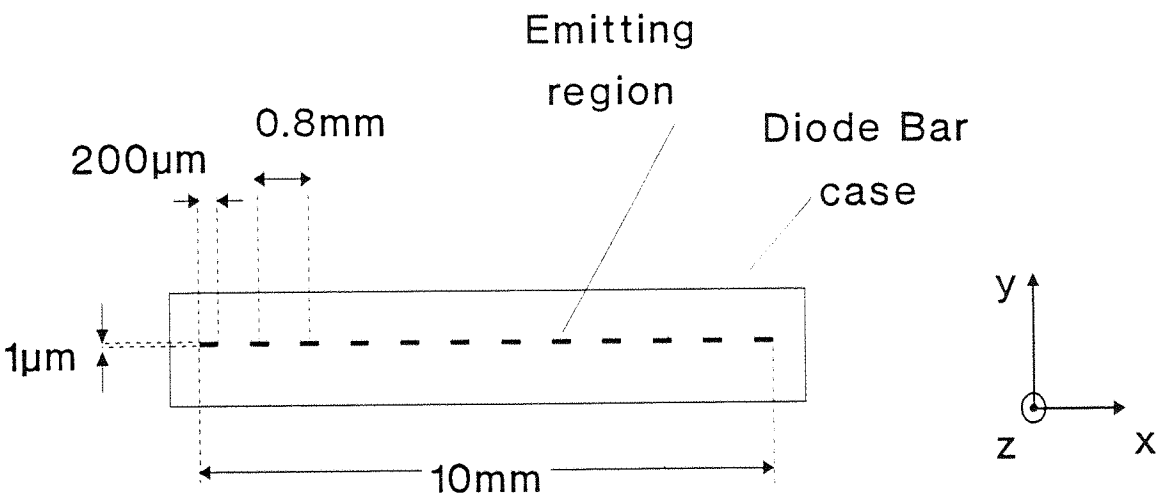

Fig 4.3 Diode bar schematic showing dimensions of the emitting regions and dead spaces, as well as the axes used to define the direction of diode beam propagation.

The method uses two parallel mirrors, facing each other, to chop up and rearrange the diode bar output to produce a more symmetric beam. The basic principles of operation are shown in Figures 4.4 and 4.5, where a beam from a diode bar is shown approaching the Multiple Reflection Beam Shaper (MRBS), inclined at angles θ and α to it. The diode bar beam here is assumed to have been collected and collimated by conventional optics (e.g. cylindrical and spherical lenses), and is approximately diffraction limited in the y-z plane and has an M^2 of >1000 in the x-z plane. The two mirrors of the MRBS (M1 and M2) are separated by a distance d (typically of the order of a few mm), and are offset from one another by small distances w and h in the orthogonal directions x' and y' respectively, so that small sections of both mirrors are unobscured by each other. The two mirrors are nominally aligned parallel to each other, but if required, can be angled slightly to each other, depending on the particular pump optics used and the divergence properties of the diode beam.

The main principle of operation of the MRBS can be explained by considering the incident laser beam to be made up of a number of adjacent beams. The number of beams depends on the width L of the incident beam, the mirror separation, d, and the incidence angle in the x'-z' plane, θ. We use $\theta=45°$ in our implementation of the MRBS, which means that the total number of beams is simply given by:

$$n=\frac{L}{\sqrt{2}d} \tag{4.4}$$

To simplify this discussion of the principle of operation of the MRBS, the incident beam has been arbitrarily chosen to consist of 5 parallel beams (labelled (1)-(5) in Fig 4.4 and 4.5). Beam (1) is not incident on either M1 or M2, since it passes above mirror M2 and by the side of M1, and so emerges from the MRBS with no change to its original direction. The width of this beam is set by the position of the MRBS relative to the incident beam, and should be chosen to match the widths of the other beams produced by the MRBS, which from eq.(4.4) can be seen to be:

$$s=\sqrt{2}d \tag{4.5}$$

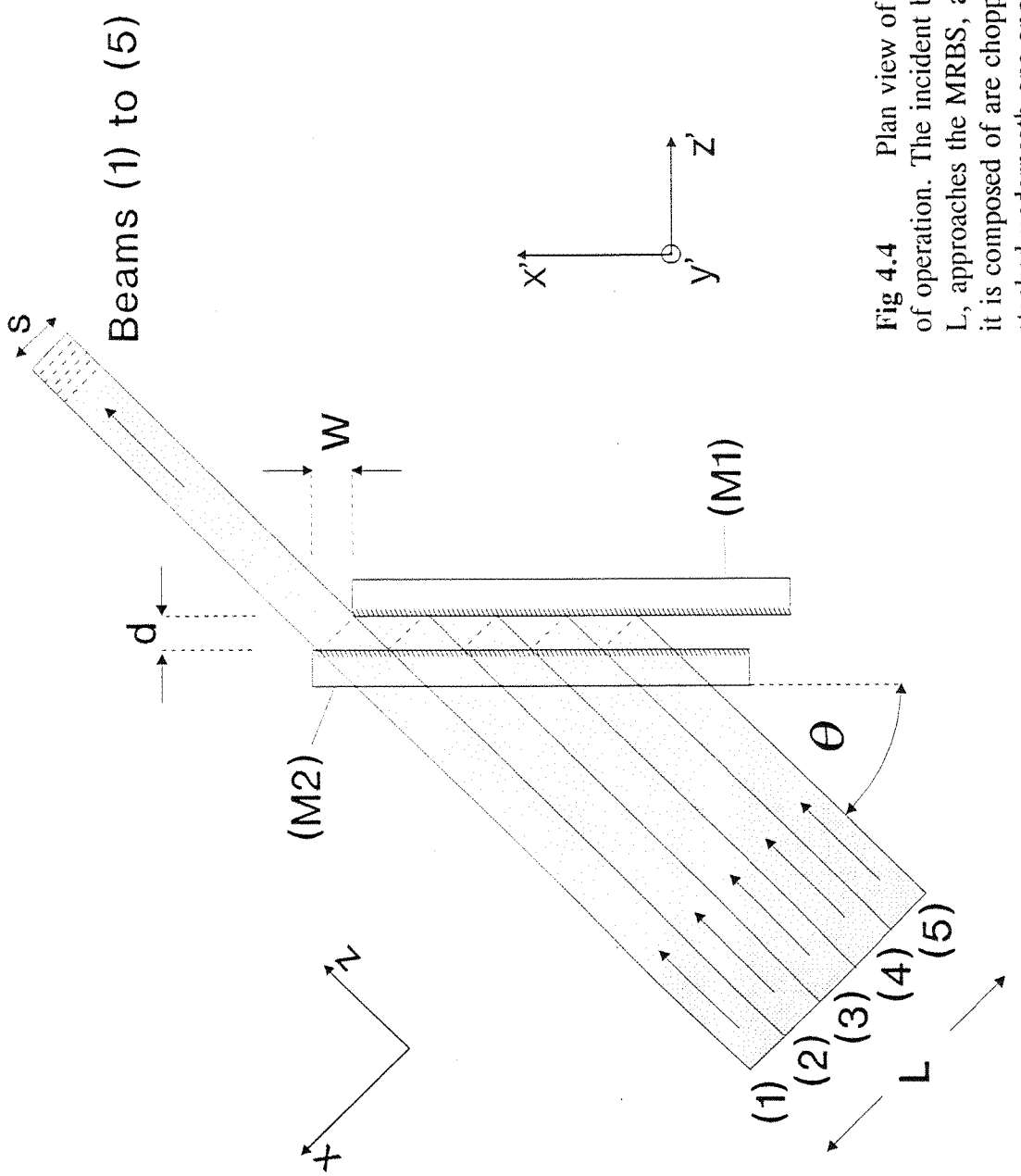

Fig 4.4 Plan view of MRBS principle of operation. The incident beam, of width L, approaches the MRBS, and the 5 beams it is composed of are chopped up and stacked underneath one another. Beam (1) is not incident on either mirror.

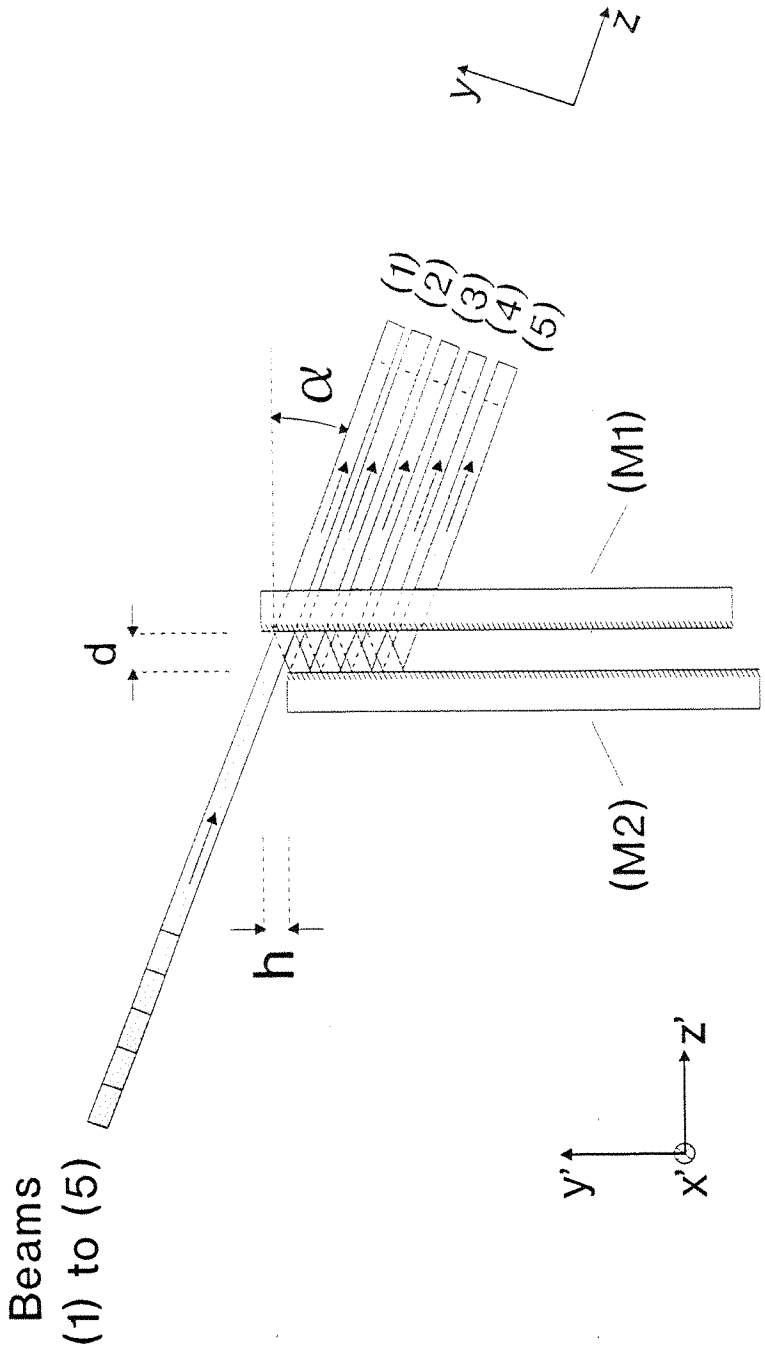

Fig 4.5 Side view of MRBS. Here we see each of the 5 incident beams being multiply reflected between mirrors M1 and M2 and stacked underneath one another.

Beam (2) however, passes above mirror M2 but is incident on mirror M1, where it is reflected at angles θ and α so that it strikes M1 immediately below beam (1). Beam (2) is then reflected from M1 and emerges from the MRBS underneath beam (1), and propagating parallel to it. The separation of beams (1) and (2) is determined by the mirror separation and inclination angle α in the y'-z' plane. If the mirrors are parallel, this separation will be maintained, after the beams emerge from the MRBS, and is given by:

$$\Delta y = d\tan 2\alpha \tag{4.6}$$

Beam (3) is also incident on M1 and is reflected onto M2, directly underneath the point where beam (2) was reflected onto M2. It is then reflected back onto M1 a second time, is again reflected onto M2, and then emerges from the MRBS parallel to beams (1) and (2), but separated vertically by a further factor Δy from beam (2). Beams (4) and (5) undergo similar multiple reflections between M1 and M2, eventually emerging from the beam shaper stacked underneath the other beams, but propagating parallel to them, as shown in Fig 4.5.

Thus the action of the MRBS is to effectively chop the incident laser beam into a specific number of equal sized beams and to re-arrange these beams so that they emerge from the beam shaper stacked on top of one another (i.e. with orthogonal displacements relative to their original displacements). If the original beam is initially many times diffraction limited in the x-z plane (i.e $M_x^2 \gg 1$), then the net effect of the MRBS is to decrease the beam width in the x-z plane, but without significantly increasing its divergence, thus reducing M_x^2. The amount by which M_x^2 is reduced is determined by MRBS parameters such as mirror separation d, angle of incidence θ, parallelism of the mirrors and position of the MRBS with respect to the incident beam. It should be noted, however, that significant reductions in the M_x^2 value of the incident beam can only be achieved if the initial M_x^2 value is much greater than 1. If this is not the case, then the beam emerging from the MRBS will experience significant diffraction effects at the edge of M1, and the divergence will increase so that the final M_x^2 value cannot be less than unity. In the y-z plane the beam size is effectively increased, but the divergence remains approximately the same, provided

that the mirrors are parallel, hence the emerging beam has its M_y^2 value increased. The factor by which M_y^2 is increased is approximately equal to the total width of the emerging beam in the y-direction, divided by the width of an individual beam (in the y-direction). To minimise this increase in M_y^2, it is necessary to choose the mirror separation d and inclination angle α to minimise the gap between adjacent beams (eq (4.6)), without degrading the transmission of the MRBS by clipping at the top edge of mirror M2. A satisfactory compromise is to set the beam separation Δy to be at least 3 beam radii at the input to the MRBS, as this reduces any clipping to less than 1%.

Clearly the MRBS can be used to chop the incident beam into an arbitrary number of beams to match the orthogonal M^2 properties of the emerging beam to any desired degree. However, as the number of beams produced increases, practical problems such as the reflectivities of the mirrors used becomes important, as the beams undergoing many multiple reflections will become progressively attenuated as they propagate through the MRBS. If a beam is chopped into n segments, then the total transmission of the MRBS will be

$$T=\frac{1}{n}\frac{(1-R^{2n})}{1-R^2} \qquad (4.7)$$

where R is the mirror reflectivity (assumed to be the same for both mirrors), and it is also assumed that the first beam segment is not incident on either mirror. If the mirrors have a 99% reflective coating, then chopping the beam into 12 segments will mean that the total transmission is around 90%. Clearly, we would want the mirrors to have as high a reflectivity as possible to maximise the transmission, and also to maintain a more equal distribution of power in the individual beam segments. In the system we describe in the next section, chopping the beam into 12 segments gave a transmission of only around 70%, implying that the mirror reflectivities were only of the order of 96.5%, a situation that can easily be improved by specifying higher quality dielectric coatings. With coatings of >99.8% reflectivity at the pump wavelength, it should be possible to achieve a transmission of around 98% (in the absence of any clipping), which would be considered negligible in almost all applications.

To summarise then, the MRBS re-configures the transverse intensity profile of a laser beam which is many times diffraction limited in one plane such that the number of times diffraction limited in that plane is reduced, and in the orthogonal plane is increased, without a significant loss of power. The factor by which the M^2 is reduced is approximately equal to the number of beams into which the incident beam is chopped (providing that the incident beam is greater than this number of times diffraction limited and that the emerging beams are of approximately equal width). In the orthogonal plane, the M^2 value is increased by at least the same factor. By appropriate selection of the parameters of the MRBS (e.g. d, h, w, θ, α), it should be possible to transform a laser beam with highly asymmetric diffraction properties to one with nearly symmetrical diffraction properties. The beam that is produced by the MRBS can then be simply focused using an appropriate arrangement of lenses (e,g, either a single spherical lens or a crossed pair of cylindrical lenses).

4.3 Experimental Implementation

4.3.1 Introduction

The principle of operation of the Multiple Reflection Beam Shaper (MRBS) which was outlined in the previous section can be implemented in a number of different ways. For a diode bar, there are two immediate possibilities for re-configuring the beam to have more equalised beam divergences and spot sizes. The first is not specific to the actual geometry of the diode bar, and treats the bar as a single emitter with dimension 10mm x 1μm, with M^2 values that differ by a factor of a thousand or so in these two planes. The output beam from such a diode bar would first be collimated in the diffraction limited plane, and then chopped into an arbitrary number of beams in the non-diffraction limited plane by the MRBS, the number of beams being determined by the degree by which one wishes to reduce the M^2 in the non-diffraction limited plane. This approach, which is non-specific to the diode architecture, has the advantage of being suitable for any type of linear diode bar, and is simple to implement. However, in our initial experiments we decided to exploit the geometry of the diode bar available to us in such a way as to improve the overall brightness of the diode as a whole, as will be explained in this section.

Diode bars consist of a linear array of smaller laser sources ("emitting regions") which are separated from each other by non-emitting regions ("dead-space"), this separation mainly being determined by thermal considerations. The diode bar which was available to us consisted of 12 emitting regions, each with dimensions of approximately 1μm by 200μm, with a centre to centre spacing of $\sim 800\mu$m, giving a total emitting region of 1μm x 10mm. A schematic of the emitting region of the 10W diode bar used is shown in Fig 4.3. Each of these emitting regions has a particular M_x^2 value, which we estimate to be of the order of 30-40. These individual emitters combine to give the diode bar an overall M_x^2 of >1000, as the overall divergence of the diode bar is the same as for an individual emitter, but the diode bar is 50 times the size of an individual emitter. Instead of treating the output from the

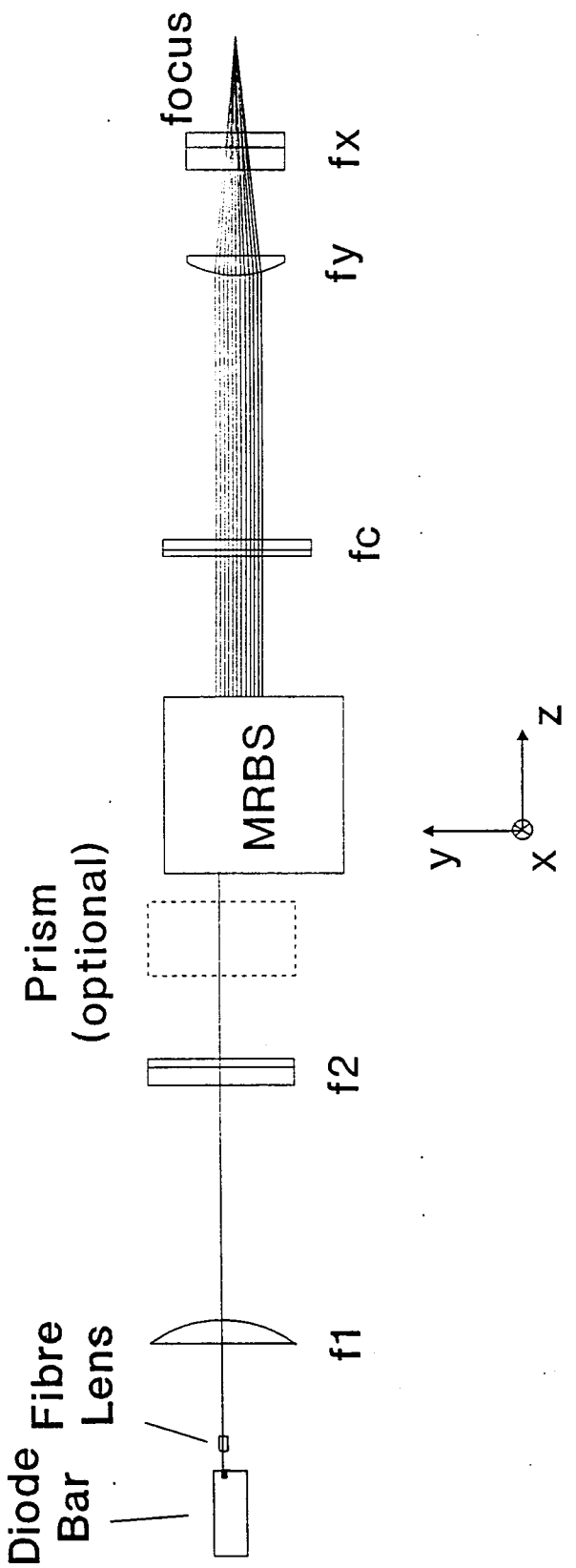

Fig 4.6 Side view of system used to individually chop up and stack the 12 emitting regions from a 10W diode bar. Twelve output beams are produced by the MRBS, which are then focused down by lens fy.

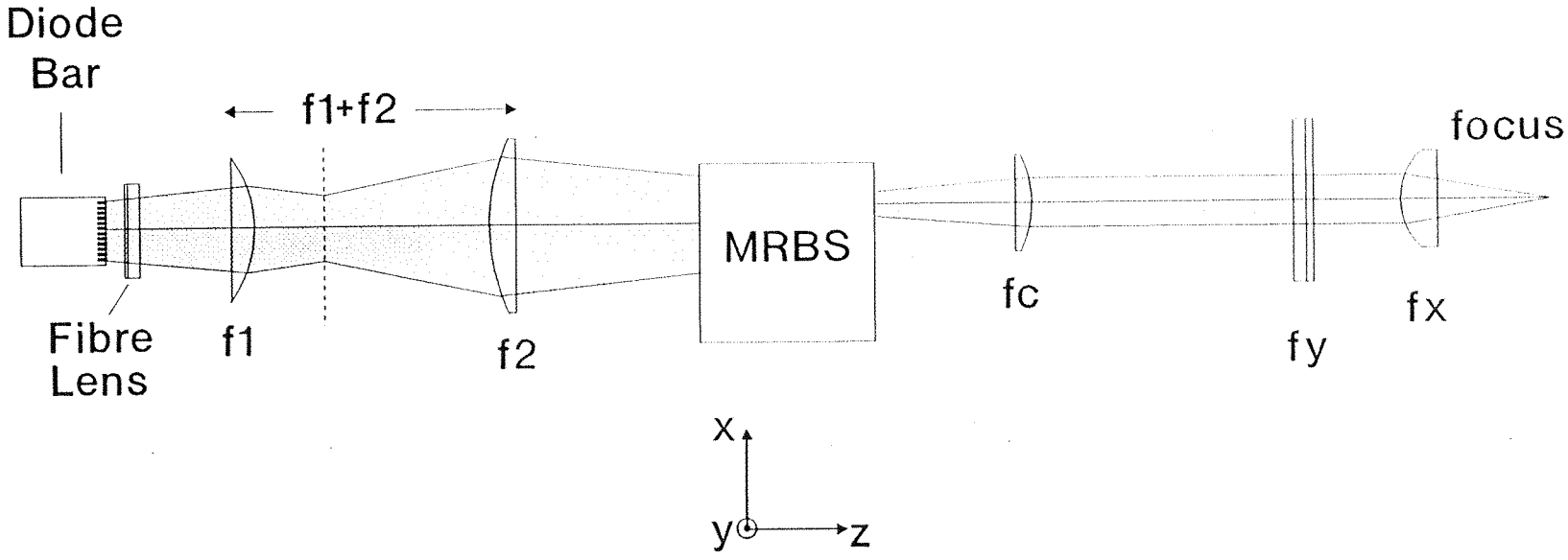

Fig 4.7 Plan view of experimental implementation of MRBS system. The individual beams produced by the MRBS are focused in the x-z plane by lens fx.

diode bar as a single beam >1000 times diffraction limited, in this situation it is advantageous to use the MRBS to chop up the output in such as way as to stack up each emitting region above one another, thereby effectively removing the dead-space between the emitters. In this way, by chopping the output up into only 12 beams, the M_x^2 value should be able to be reduced very significantly. In addition, as the emitting regions only occupy a fraction of the total emitting dimension, it should be possible to chop the beam up so that the edge of each "cut" falls in a dead space, reducing any diffraction effects from mirror M1. The system that we proposed to implement then, required that the diode bar emitting region be imaged onto the MRBS, which would then chop up and stack the emitting regions so that they were displaced vertically rather than horizontally, and with a much smaller amount of dead space between them.

4.3.2 Pumping scheme

A schematic of the system developed to end-pump a solid-state laser is shown in Fig 4.6 (side view) and Fig 4.7 (plan view). Here the MRBS is depicted in block form, with a more detailed view of its operation being shown in Figures 4.8 and 4.9. The 10W diode bar was mounted on a water cooled heat sink, the temperature of which could be altered to allow the output wavelength to be tuned to the peak of the solid-state laser absorption. As the temperature for matching to the Nd:YAG absorption was less than 10°C, the diode bar and mount were enclosed in a chamber purged with oxygen free nitrogen, to eliminate condensation. The first stage in the implementation of this system is to collimate and image the diode bar beam onto the MRBS. This is accomplished with a combination of fibre lens, spherical lens and cylindrical lens. The fibre lens used is the SAC900 lens described in section 3.1.3, and is positioned approximately 110μm from the output of the diode bar. When aligning this fibre lens, it was observed that the output from the diode bar could not be collimated to a single line, but appeared to have some degree of curvature relative to the fibre lens in the y-z plane. After verifying that the lens was indeed straight (by focusing a Helium-Neon laser onto the fibre lens and observing the direction of reflection), it was determined that the diode bar was curved by approximately 6μm (maximum displacement of one element relative to any other) along its length. We therefore needed to bend the fibre lens by the same amount to enable an essentially diffraction limited beam to be produced in this plane. An additional problem encountered was the thermal

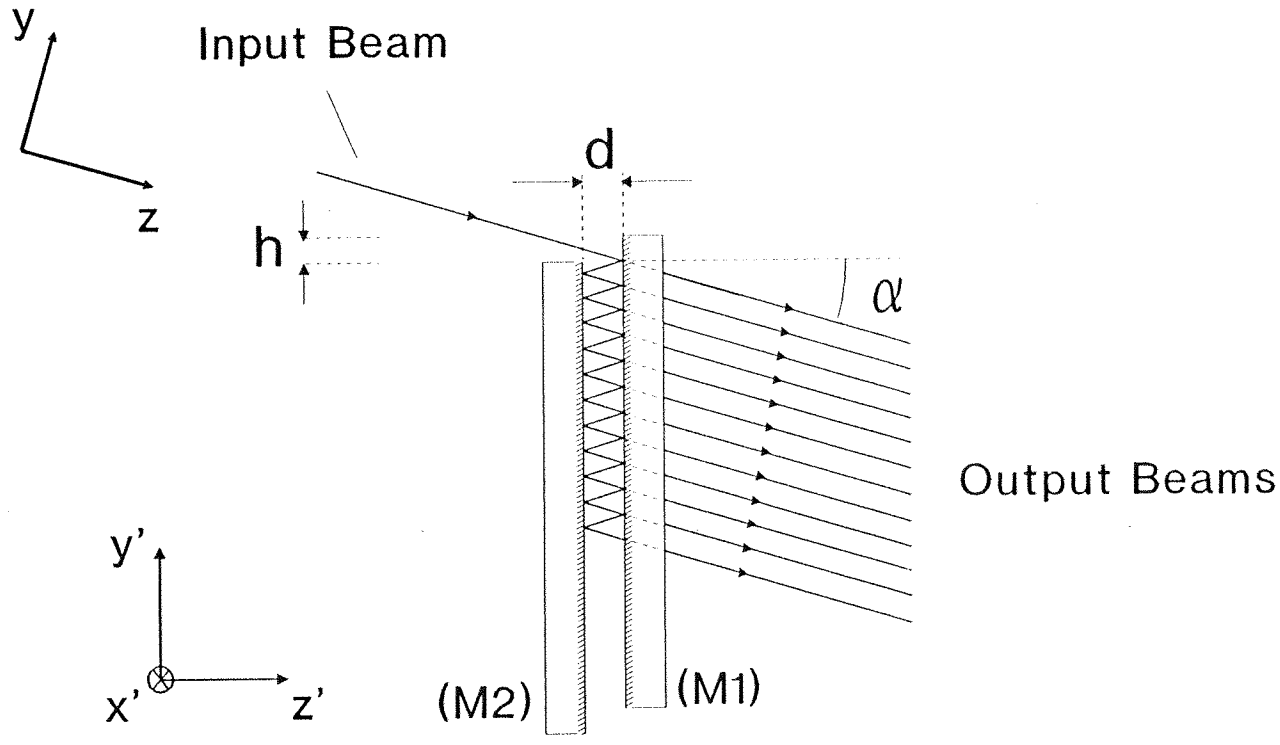

Fig 4.8 Detailed side view of MRBS being used to stack up the 12 emitting regions of a diode bar. For clarity, the output beams are shown separated to a much greater degree than they would be in practice.

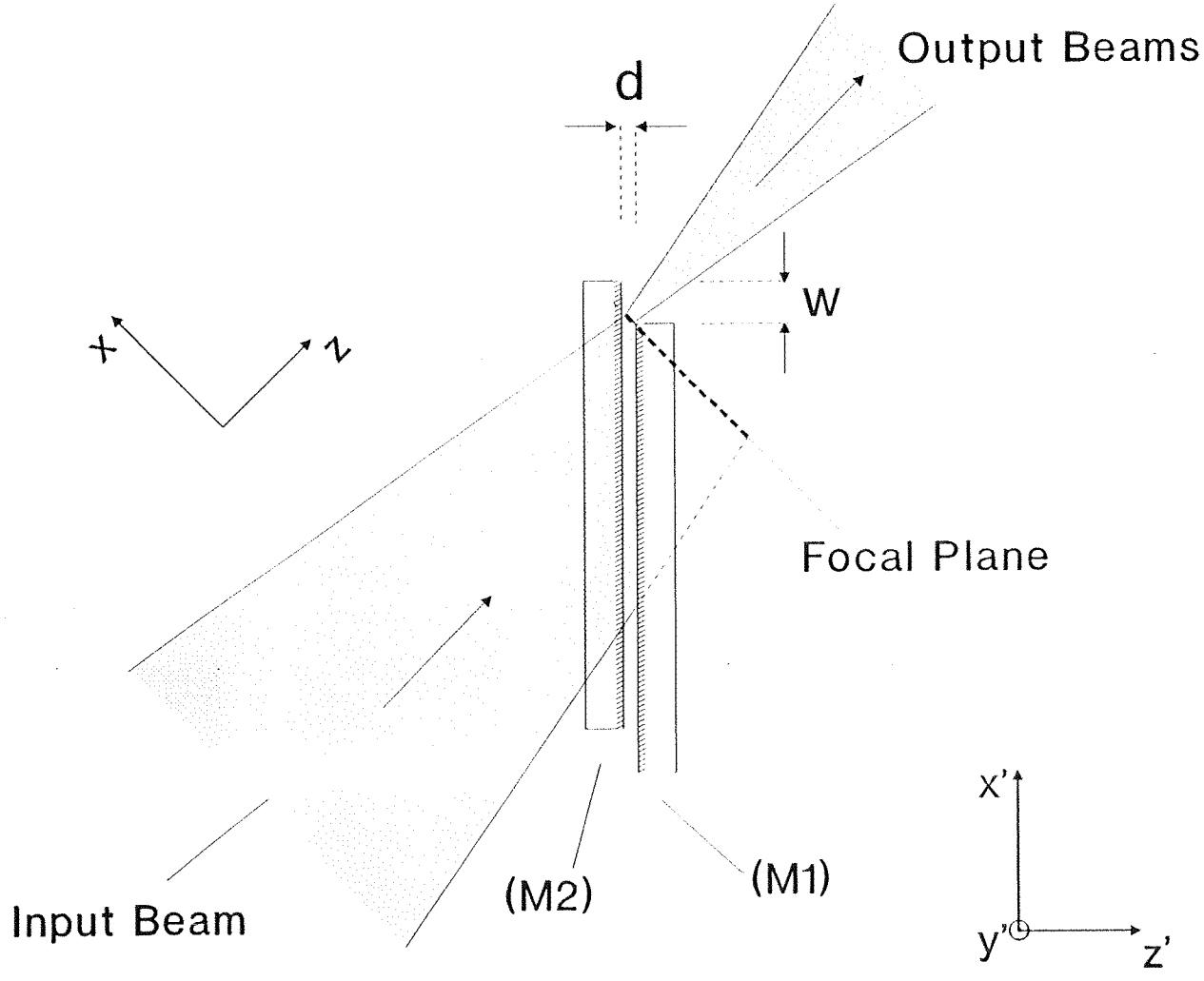

Fig 4.9 Plan view of MRBS, shown chopping up the 12 imaged emitting regions. The focal plane of these emitters is indicated, with the uppermost focus not being incident on either mirror.

expansion/contraction of the diode bar heat sink, which could easily alter the position of the fibre lens relative to the diode bar. Various heat sinking techniques were employed to minimise this effect so that the diode bar could be operated with minimal adjustments to the fibre lens position being necessary. Ultimately, the best solution would involve directly mounting the fibre lens onto the diode bar case, as all components would then share the same thermal variation. It is intended that we shall try to mount a fibre lens in such a way in future implementations of this experiment. When the fibre lens was positioned as accurately as possible, the far field divergence of the collimated beam suggested that the beam radius at the lens was $\sim 54\mu m$. As the fibre lens is $\sim 110\mu m$ away from the diode bar, and the output from the diode diverges at approximately 1 radian (full angle), we would expect the beam diameter at the point where it is collimated by the fibre lens to be $\sim 110\mu m$. The far field divergence from the fibre lens is therefore consistent with the beam being diffraction limited ($M^2 < 1.2$).

The beam emerging from the fibre lens is then collimated by a 40mm focal length plano-convex spherical lens (f1), positioned ~ 40mm from the diode bar. This re-collimates the beam in the y-plane, thus reducing the divergence in this plane, and collimates each individual emitting region of the diode bar. A 100mm focal length plano-convex cylindrical lens (f2), positioned at approximately the sum of its focal length and the focal length of the spherical lens away from the spherical lens (i.e. 140mm away), is then used to focus the beam in the x-z plane to form an image of the diode bar emitting regions approximately 100mm away from this lens. The individual emitting regions are magnified in the x-z plane by the ratio of the focal length of the cylindrical lens (f2) to the spherical lens (f1), i.e. by ~ 2.5 times. The MRBS is then placed close to the focal plane of the cylindrical lens, where the collimated beam from the diode bar is ~ 0.7mm wide (y-z plane), and each emitting region is focused to a diameter of around 0.5mm (x-z plane), with a dead space between these regions of ~ 1mm. It was also observed that three of the twelve emitting regions of the diode bar did not appear to be operating at all, thus reducing the maximum available output power. Fig 4.10 shows the diode beam at its focal plane, with the relative peak outputs of each emitting region being indicated. As the dead emitting regions were located near the centre of the diode bar, it was not thought that this would invalidate our initial test of the MRBS. This might have been the case if all the dead emitters were positioned

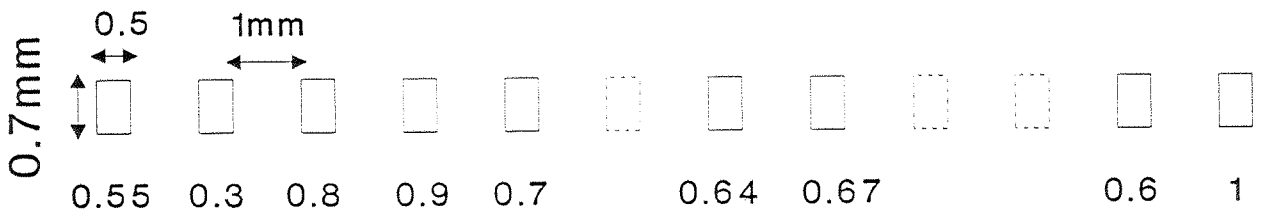

Fig 4.10 Diode bar emitting regions at the beam focus. The dashed emitters are those that did not appear to be working, and the numbers under each emitter represent the relative peak output of each emitter, as measured with a thin slit.

near one edge, as the effective size of the diode bar would be decreased, reducing the initial M^2 value. The results that we obtain with this particular diode bar should be no better than one with all emitters operating.

The action of the MRBS on the imaged beam is shown schematically in Figs 4.8 and 4.9, and in the experiment described here, used square plane mirrors that were 50mm along each side. The mirrors had a dielectric coating which was supposed to be highly reflecting around 800nm at a 45° angle of incidence, but in fact only seemed to be around 96.5%. This lower than expected reflectivity may have been due to the large angle we were operating the mirrors at ($\sim 50°$ overall angle of incidence) and losses due to the polarisation properties of the diode bar. Although these mirrors were designed be polarisation insensitive, it was found that the inclusion of a waveplate to rotate the diode polarisation could improve the throughput of the MRBS by $\sim 10\%$, and when tested on a polarised Ti:Sapphire output, a waveplate could make $>50\%$ difference to the overall transmission. Apart from the high reflectivity, two other features of the mirrors are important: the side edge of mirror M1, where the beam emerges from the MRBS, and the top edge of mirror M2, where the beam enters the MRBS, should be well-defined and straight, with the high reflectivity coating going right up to these two edges. This was achieved by polishing the edge of the mirrors down to the coating. This ensures that losses due to clipping are minimised and increases the throughput of the system. To chop up and rearrange the focused image of the diode bar, appropriate values of d, θ, α, w and h were chosen. The 1.5mm width of focused emitting region and accompanying dead space meant that the mirror separation was required to be 1.06mm (eq (4.5)) for a 45° incidence angle θ. In the y-z plane, we selected a spacing between adjacent stacked beams that was 3 times the radius of the collimated beam in the y-plane. For the given mirror spacing, d, and the input beam radius of ~ 0.35mm, this required that the MRBS be angled at 22° (eq. (4.6)). The mirror offset distances, w and h, were chosen to exceed the transverse width (in the x'-z' plane) of the output beam at mirror M2 and the depth (in the y'-z' plane) of the incident beams at mirror M1. In practice both w and h were at least 5mm, to allow a large margin of error.

The beam shaper is positioned so that the focused image of the uppermost

emitting region (as shown in Fig 4.9) is located at the output edge of mirror M1. Each subsequent emitting region from the diode bar will then be stacked underneath this first emitting region (Fig 4.8), with a centre-to-centre spacing of around 3 beam radii, producing a stack of twelve beams. The M^2 values for the vertical (y-z) plane should increase by approximately the total beam width divided by the individual beam width (i.e. by a factor of 1.5 x 12), which assuming the collimated input beam was essentially diffraction limited, would give rise to an emerging M^2 of 18-20. In the horizontal plane, the M^2 should be approximately the same as for that of an individual emitting region, of the order of 30-40. If we define the effective M^2 value of the total beam to be the geometric mean of the M^2 values for the orthogonal planes, i.e.

$$M^2=\sqrt{M_x^2\ M_y^2} \tag{4.8}$$

then the effective M^2 for the output from the MRBS is approximately $\sqrt{800}$, i.e. 28. This is a significant improvement over the initial total M^2 of the diode bar, which is of the order of $\sqrt{1500}$, i.e. 39. This improvement is possible only because we have effectively removed the dead-space between the individual emitting regions, increasing the effective brightness of the diode bar source.

The output beams from the MRBS are collimated in the x-z plane with a plano-convex cylindrical lens (fc) of focal length ~80mm. This beam is then focused separately in the x-z and y-z planes by a pair of crossed cylindrical lenses (fx and fy, respectively, as shown in Figures 4.6 and 4.7). This enables the focused waist sizes to be matched more exactly than with using a single lens, giving an extra degree of flexibility in these initial investigations. Separate lenses also allow the waist positions in the two planes to be positioned more accurately. Using final lenses with f_y=20mm, f_x=12mm, we were able to obtain a focused spot with dimensions w_{px}=45μm, w_{py}=40μm, but with a divergence which we considered to be too large to be suitable for end-pumping. Whilst producing small focused beams may be useful in some applications, for solid-state laser end-pumping, it the average spot size over a given length that is more important, as discussed in section 4.1. A more suitable combination of lenses was found to be f_y=60mm, f_x=20mm, which produced a focused ($1/e^2$) spot size of 67.5μm in both planes. The spot profiles are shown in Fig 4.11, where it can

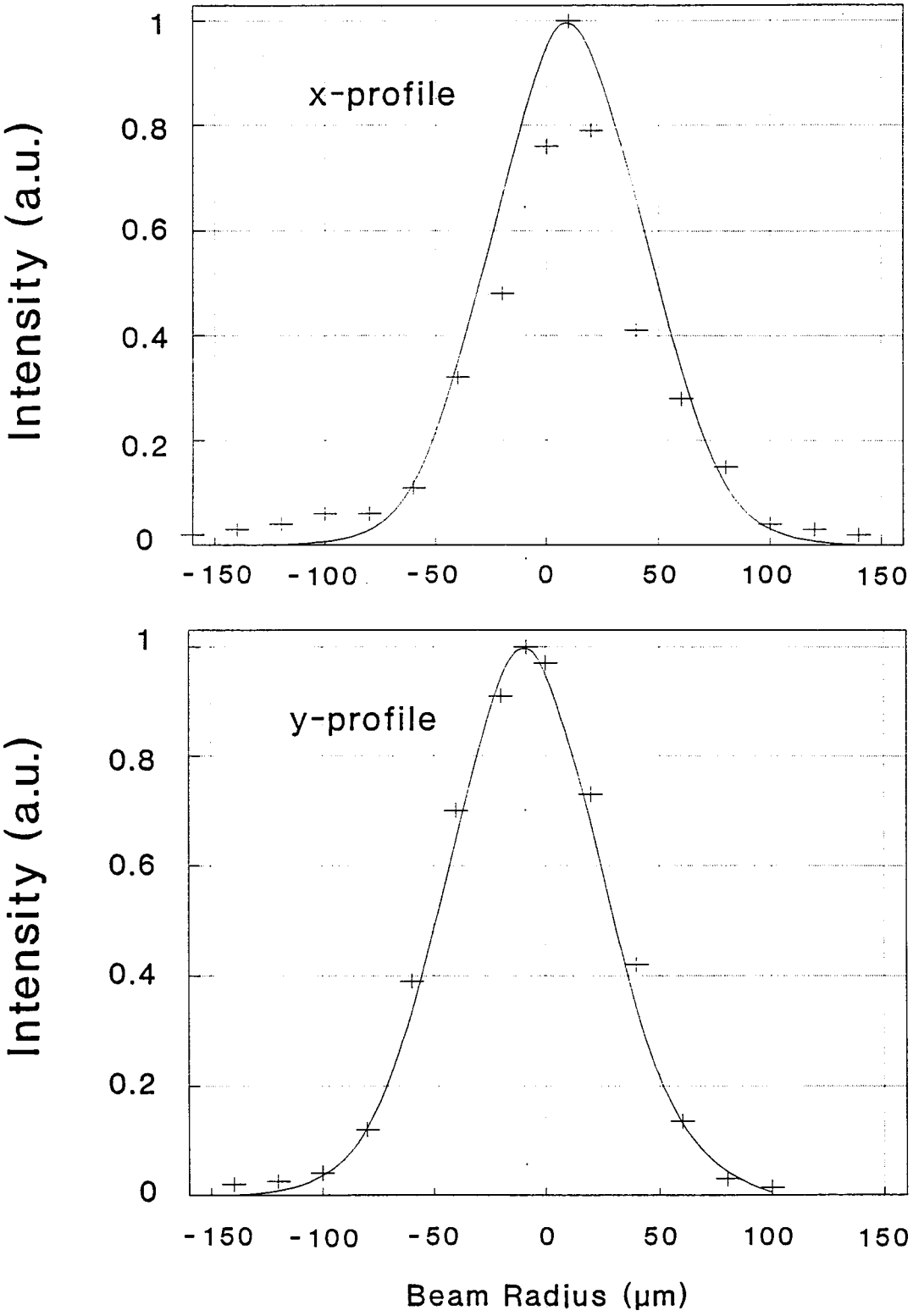

Fig 4.11 Profiles of the focused beam from the MRBS system in the x-plane (upper diagram) and y-plane. In both cases a gaussian curve with $1/e^2$ radius of 67.5μm is fitted to the measured profile points (+).

be seen that the beam in the y-plane is a much closer approximation to a Gaussian than the beam in the x-plane.

The beam size in both planes was measured at a number of positions around the focal point, and from these the M^2 values for both planes could be calculated. This is shown in Fig 4.12, where best-fit values of $M_x^2=40$ and $M_y^2=19.2$ were obtained, which are the values that might be expected when chopping the beam up into the individual emitting regions as we have done. This demonstrates that we are able to achieve M^2 values close to the theoretical limit for this particular implementation of the MRBS, and that little extra diffraction is produced by it. Over a 3mm path length in air, these M^2 values would produce average beam diameters of $\sim 190\mu$m and 280μm in the y-z and x-z planes respectively. Such beam sizes can be readily matched to the mode size of simple solid-state laser cavities, as we now describe.

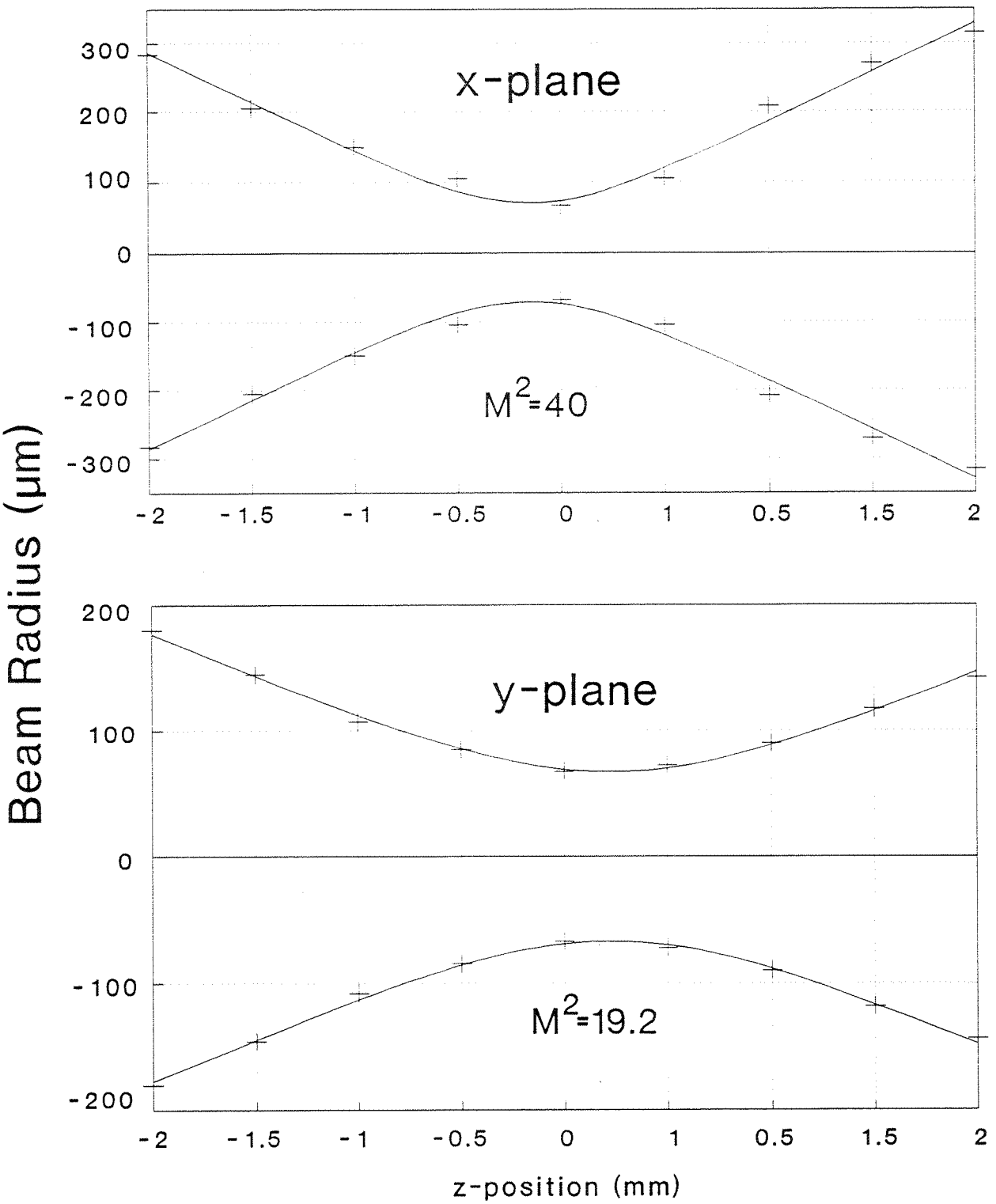

Fig 4.12 Beam radii measured around the focal plane of the beam from the MRBS. In both the x- and y-planes, the solid line is a fitted curve for the propagation of a beam with waist size w_0=67.5μm with the M^2 values shown.

4.3.3 End-Pumping Performance

With the focused beam produced using the system described above, we constructed a number of simple Nd:YAG lasers to demonstrate the effectiveness of this system for end-pumping. The first laser used a Nd:YAG rod 5mm long, 4mm in diameter, which was coated to be highly reflecting at 1.064μm at one end and antireflection coated at the other (Fig 4.13). The laser cavity was completed with a concave mirror as the output coupler. A variety of output couplers were used, with the best results in terms of mode quality being obtained for a mirror with a 25cm radius of curvature and 10% output coupling. The laser cavity was ~8cm long, which means that the calculated lasing mode size at the HR end of the Nd:YAG rod was ~200μm (radius).The pump power threshold for lasing was 320mW, with a 40% slope efficiency being obtained (Fig 4.14). As we have already mentioned, the diode bar we were using had a number of its emitting regions not lasing, reducing its output power to under 7W. For the maximum available input power of 3.4W (the 50% throughput is due to the coating loss on the mirrors of the MRBS and some non-anti-reflection coated lenses used in the system), we obtained 1.16W of output, in a beam that appeared to be TEM_{00}. At higher pump powers, there appeared to be a slight degree of non-TEM_{00} structure in the wings of the lasing mode, which may have been due to thermal deformation on the HR end of the laser rod. At the pump powers available to us, we may be just on the border of experiencing significant thermal lensing effects with the Nd:YAG rod. A detailed study of this thermal lensing will require higher pump powers than we currently have available.

We next used a Nd:YAG rod that was antireflection coated at 1.06μm at both ends and employed a high reflector that was separated from the rod, to determine if the mode quality could be improved. Now the input face of the Nd:YAG rod will not be a cavity mirror, and it was expected that any thermal abberations would be less pronounced. Again, a 25cm radius of curvature output coupler with 10% transmission was used, and the laser power performance was virtually identical to that of the HR-AR rod shown in Fig 4.14. The output beam was focused down with a 10cm focal length lens, and the beam profile measured at a number of points to determine the M^2 value of the beam. Within the measurement error of the focused spot size (which was

measured with a 5μm pinhole), the beam had an M^2 of < 1.05, i.e. it was entirely diffraction limited and TEM_{00}.

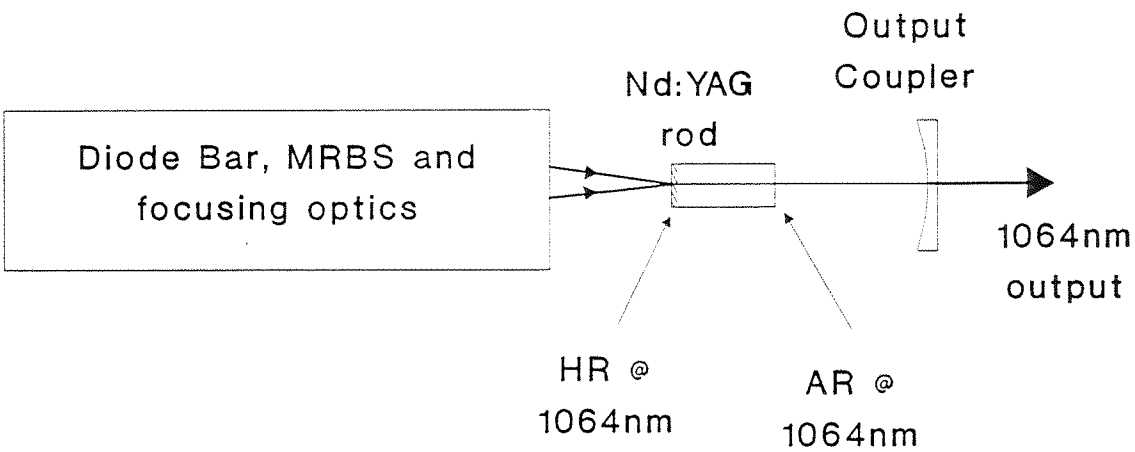

Fig 4.13 End-pumping of a simple Nd:YAG laser using a diode bar beam shaped by the MRBS and focused to a spot size of 67.5μm.

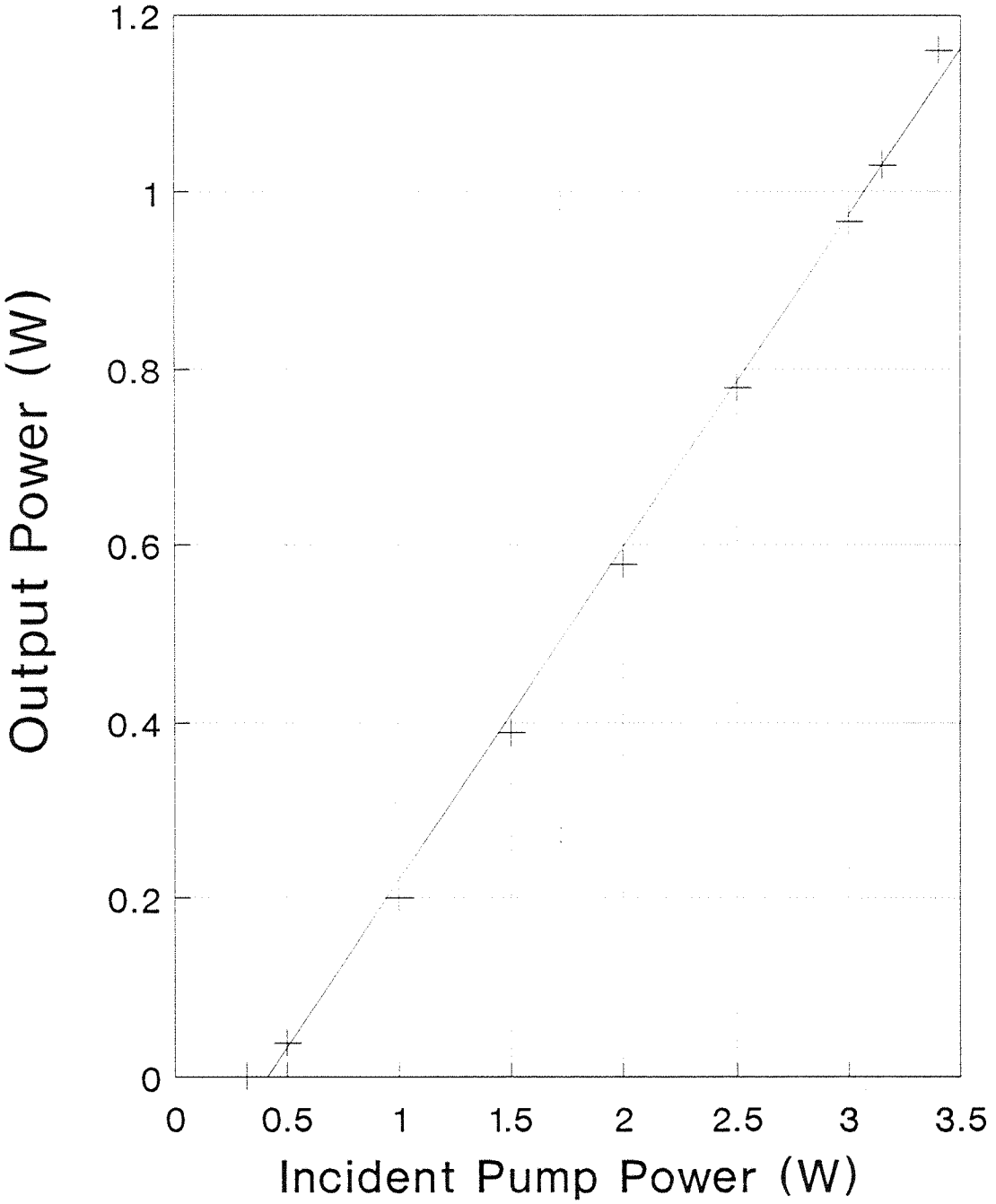

Fig 4.14 Performance of Nd:YAG laser when end-pumped by the MRBS system. A slope efficiency of ~40% is obtained for an essentially diffraction limited beam.

4.3.4 System Improvements

The focused spot size that we produce from the MRBS (67.5μm) with the current arrangement of lenses, may in fact be smaller than is desirable. As noted, the laser cavity produced a waist size of 200μm, so we may have been better off with a larger pump spot size, as this would have better matched the lasing mode size, and would not have diverged as rapidly. For example, the pump beam that we have produced with a waist size of 67.5μm will have an average spot size (over 3mm in air) in the x-plane of 138.3μm and in the y-plane will be 92μm. On the other hand, a focused spot size of 200μm with the same M^2 values would produce a beam with average beam radii of 205μm and 201μm over a 3mm length, which obviously would give a much better match to the lasing mode in the cavity we have constructed, and would be less likely to produce problems with excitation of higher-order transverse modes. At the time of performing these experiments, we did not have suitable cylindrical lenses to produce such a focused spot, but it is anticipated that these lenses will be available shortly, allowing a much more suitable beam for end-pumping to be produced.

There are a number of other simple improvements that can be made to the performance of this system. The first is in the area of diode heatsinking, as in the present experimental set-up, we have difficulty in cooling the diode to properly match the peak of the Nd:YAG absorption. We have an pump absorption length of ~3mm, which should be able to be improved to around 2.5mm, based both on previous experience with diode-pumped lasers, and on reported values from other diode-bar pumped systems [Tidwell, 1992]. A second issue to be addressed is that of cross-talk between adjacent emitting regions. This could occur if adjacent regions overlap as they emerge from the beam shaper and is exacerbated by the fact that the laser beams from individual emitting regions travel different distances to reach the output of the MRBS. In the system we have described, each emitting region will be defocused to a different amount as they propagate through the lasing MRBS, and may spread enough to overlap with adjacent beams. As shown in Fig 4.4, beam (1), which is not incident on either of the MRBS mirrors, travels the least distance, and as each subsequent beam undergoes more multiple reflections they will travel a progressively greater distance to

reach the exit of the beam shaper. The effect of cross-talk is to increase the M^2 value in the x-z plane for a particular output beam relative to its value without cross-talk, as the output beam may be composed of more than one emitting region in each x-z segment. A simple solution to the problem of cross-talk would be to insert a prism between the focusing lens and MRBS, as shown in Fig 4.15, which is designed to equalise the effective optical paths of all the laser beams in the x-z plane (i.e. the effective path length for diffraction, where the wavelength in the prism is reduced to λ/n, with n the refractive index of the prism) at the exit of the beam shaper. This would place the focus of each individual emitting region at the same z-position as that of the emitter which is not incident on either of the two mirrors, so that all beams will have the same propagation properties when they reach the focusing lenses.

Thus, at the diode pump powers available to us, we were able to demonstrate efficient, low threshold, TEM_{00} operation of an end-pumped Nd:YAG laser with a simple resonator design. With better coatings on the lenses and mirrors used, it should be possible to pump the laser with $>80\%$ of the output from the diode bar. As we move to higher powers, however, thermal problems will become more pronounced, and our laser rod and cavity will need to be modified to reduce these effects. With a 20W bar used as the pump source, at least 6W of TEM_{00} output at $1.06\mu m$ should be possible, which would allow other applications such as frequency doubling to be considered. Other possibilities such as polarisation-coupling two diode bars together and then using a single MRBS to re-configure their beams are also envisaged for the future. The pumping scheme we have described here allows great flexibility in pump sizes and divergence properties, and with optimised coatings should allow great versatility in the design of diode bar end-pumped solid-state lasers.

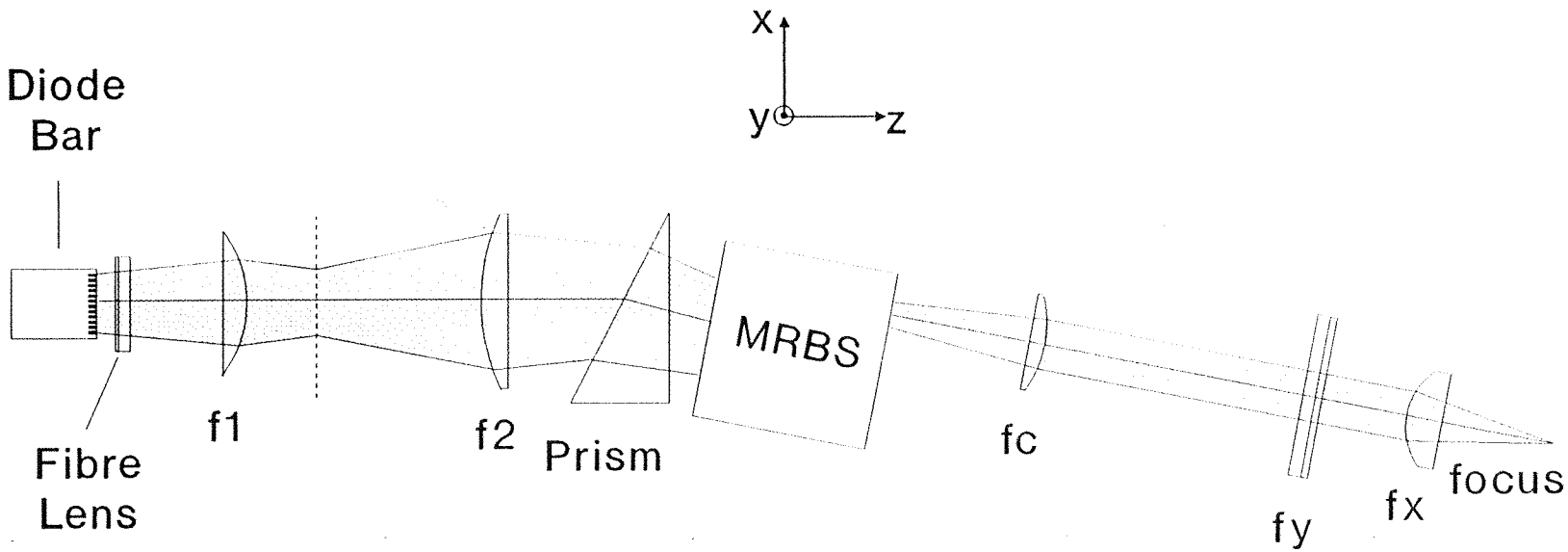

Fig 4.15 Inserting a prism between the focusing lens f2 and the MRBS can help to equalise the effective optical lengths of adjacent beams and reduce the effect of cross-talk.

4.4 Discussion

The beam shaping technique which we have described in this chapter should prove to be very useful for altering the beam from a diode bar to produce a more useful pump distribution for end-pumping solid-state lasers. In this way it will help in the development of efficient, moderately high power ($\sim$ 10W) diode pumped lasers. In addition to this important application, there are a number of other possible applications for the MRBS in a variety of laser systems [Clarkson, 1993]. Any laser which produces a non-diffraction limited beam may have its spatial properties changed by the MRBS, and in particular lasers such as laser diode arrays, broad stripe laser diodes, planar waveguides or thin slab lasers, which all have output beams with one plane that is many more times diffraction limited than the other, could be made more symmetrical with the MRBS. The ability to improve the beam quality from non-diffraction limited lasers in this way would allow them to be used in a number of applications where previously difficulties may have been encountered. Particular examples of this include end-pumping of bulk solid-state lasers, and being able to more efficiently couple light into a fibre, either for remote delivery of high powers for medical or machining applications, or as a pump source for a fibre laser or amplifier.

Another range of applications could use the MRBS in the reverse direction, i.e. taking a stack of laser outputs and converting them into a single beam, and then using a second MRBS to stack up the beam again, but with a different vertical spacing. In high power quasi-cw diode lasers, a commonly used architecture is to stack up a number of diode bars in a single physical unit (e.g. 5 bars to produce 500W quasi-cw), with the spacing between the individual bars being restricted be thermal and mechanical limitations, 400μm spacing being typical. Using the MRBS in the reverse direction would allow a single elongated beam to be produced, which could then be re-configured with a second MRBS (with different d and α parameters) to produce a stack of beams with much closer spacing, thus increasing the effective brightness of the original source, as the "dead space" between the individual bars has been much reduced. This is shown schematically in Fig 4.16. This same technique can be used on any stack of lasers that have a large physical separation compared to beam diameter, to reduce the spacing of the output beams. Increasing the brightness of a collection of sources in this manner may be attractive for both side-pumped slab lasers and end pumped lasers.

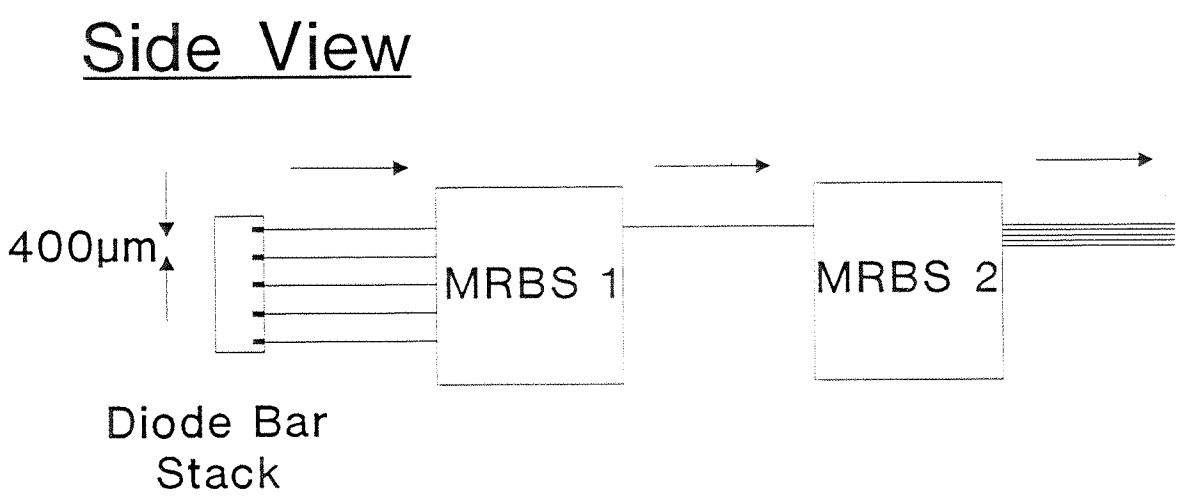

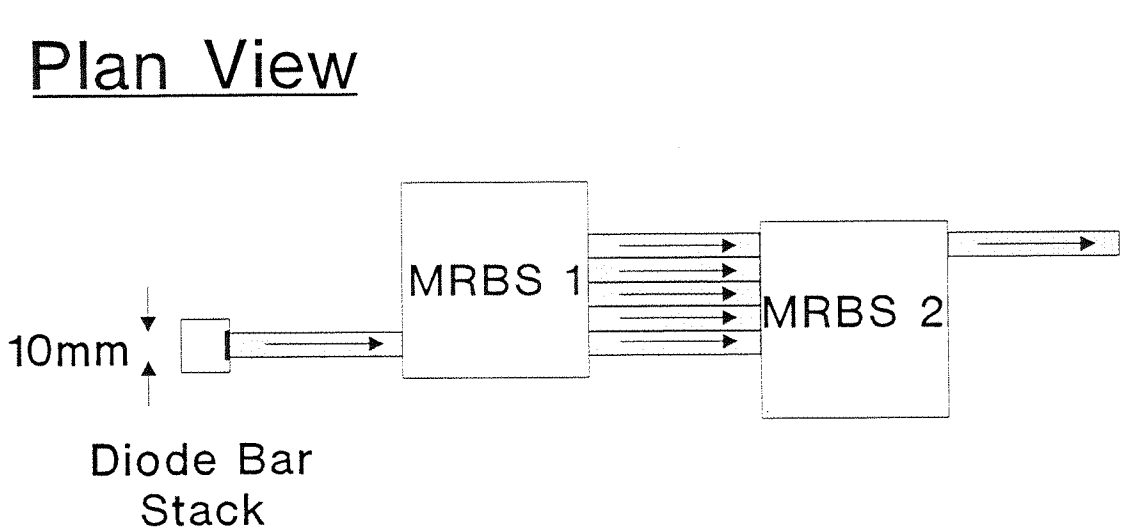

Fig 4.16 Schematic of system using 2 MRBS units to rearrange the outputs from a quasi-cw diode bar stack to be much closer together. MRBS 1 converts the vertical stack of diode emitters to a single plane of emission, which is then chopped up and stacked much closer together by MRBS 2.

An additional important advantage of the MRBS system, with its ability to produce small focused spots, is in the area of thermal effects at higher pump powers. As yet, we have not experienced severe thermal problems, but as we upgrade to higher pump powers, this will have to be considered more carefully. An analysis of thermal effects in diode end-pumped Nd:YAG lasers [Tidwell, 1992], shows that in almost all respects, smaller pump beam sizes are better. For situations where the laser cavity is assumed to a half-symmetric stable resonator (i.e. g=0.5 in the nomenclature of eq (3.6)), and where the pump size is matched to the lasing mode size in the gain medium, it is theoretically shown that the round-trip losses in the cavity from thermal aberrations increase quadratically for pump powers up to ~ 10W, and then increase at around $P^{1.4}$ for pump powers from 15W-40W, in both cases the loss increasing faster than the gain, which increases linearly. This effect dominates the extraction efficiency of the laser (i.e. pump power converted into lasing output), but it is shown that the effect is less severe for high gain (i.e. small spot-size) lasers. The spot sizes that we have been discussing here for the MRBS are in fact smaller than any discussed in [Tidwell, 1992], and should allow much higher slope efficiencies than is typically possible with high power end-pumped lasers. As the pump power is increased, the slope efficiency decreases, and above a certain power, which depends on the gain of the system, the output power will actually decrease for increased pump power. However, for the small spot sizes possible with our system, this point is not expected to be reached at pump powers up to the fracture limit of Nd:YAG, which corresponds to around 70W of pump power absorbed at one end of the rod. In addition, as the pump power increases, the M^2 value of the solid-state laser beam increases due to thermal aberrations, but again this effect is less severe for smaller pump sizes, due to the strong guiding effects of the gain region. Tidwell[1992] suggests that the M^2 from an end-pumped laser pumped with a 20W pump focused to a radius of 250μm should be less than 1.2, and as we anticipate smaller mode sizes than this, the beam quality should be correspondingly better. In this discussion, it is assumed that the pump spot is as large as possible with respect to the laser rod used, to limit the temperature rise of the rod. We would therefore have to consider using smaller laser rods to reduce thermal effects, with the suggested rod radius being around three times the pump radius (i.e. three times the average spot size over the length of the rod). Thus, the high gains possible with the

MRBS system are not only beneficial for producing efficient operation and allowing low gain transitions to be accessed, but help to reduce thermal effects, and may enable us to avoid having to actively compensate for thermal distortion by placing additional components in the laser cavity. If this expectation is realised, then efficient, high power, diffraction limited beams should be able to be produced from relatively simple laser cavities.

References

Clarkson, W.A., Neilson, A.B., and Hanna, D.C., *Beam Shaping Device*, United Kingdom Patent Application, Filed November 1993.

Tidwell, S.C., Seamans, J.F., Bowers, M.S. and Cousins, A.K., IEEE J. Quantum Electron., **28**, 997 (1992)

Chapter 5
CONCLUSIONS AND FUTURE WORK

In this thesis I have addressed two main areas of research, single frequency ring lasers and diode bar end-pumped solid-state lasers. Both these areas are ongoing research topics, and in this section I will discuss some of the future directions that this research may take.

In the field of acousto-optically induced unidirectional operation of ring lasers, the explanation of the mechanisms presented in Chapter 2 is important, as it for the first time allows optimisation of such ring lasers, and exploration of other acousto-optic materials that may be more suited to particular applications. Thus we can now specify the most suitable material for either cw or Q-switched single frequency operation, design cavities to take advantage of one or the other of the two techniques described in Chapter 2, or use laser materials as acousto-optic elements in ring cavities. Laser media usually do not have very good acousto-optic properties, and hence in the past have been thought unsuitable for use as modulators. However, as we have shown, using the feedback mechanism, large loss-differences can be produced for only very small diffraction losses, and so laser media could be used as acousto-optic unidirectional devices, with an appropriate choice of resonator design. Such work has already been carried out in Nd doped phosphate glass, and is currently being extended to Nd:YAG, which has a very low acousto-optic figure of merit. Monolithic designs for acousto-optically induced unidirectional operation of ring lasers have been devised where the laser medium is the acousto-optic modulator, and such devices would be useful in areas such as injection seeding of high power single frequency lasers.

Thus far, we have not attempted to frequency stabilise or tune the output from our ring lasers, but this can be important in a number of applications, and it is anticipated that we shall begin to work on these areas in the coming year. Developments in the theory of residual spatial hole burning can also be expected to reveal new ways of operating our ring lasers to obtain higher levels of single frequency output, and it will be necessary to understand fully these effects as we progress to pumping ring lasers with high power diode bars.

In the area of diode-bar end-pumping of solid-state lasers, there are a number of immediate improvements to be made to the system we have outlined in Chapter 4. The dielectric coatings on the two mirrors used to rearrange the diode beam need to be better optimised for the tilt angles used, and be more highly reflecting for all polarisations. This should increase the MRBS transmission from around 70% to more than 95%. We now have available a new fibre microlens with larger numerical aperture and better optimised antireflection coatings which should allow an improved collection efficiency of the diode bar output, and which, because of its dimensions, should be less sensitive to alignment with respect to the diode bar. Obvious improvements such as antireflection coatings for all the cylindrical lenses are also planned. Practical difficulties in mounting the fibre lens so that it does not need continual adjustment are also being addressed, with the aim being to mount the fibre lens so that it is directly mechanically and thermally coupled to the diode bar to reduce the effects of thermal variations and vibrations.

As yet, we have not had sufficiently high powers available to make thermal effects a major consideration with the performance of our end-pumped lasers. As we improve the transmission of our system and upgrade to higher power diodes, attention will need to be paid to the thermal handling of the laser rod. Issues such as rod dimensions, heatsinking, pump spot size, modematching, etc will have to be considered to reduce the thermal distortions that can impair the mode quality and efficiency of the laser. As we have already discussed in Section 4.4, the higher gain that we are able to produce with our end-pumping scheme helps to reduce the effects of thermal aberrations, which may prove to be extremely useful at higher pump powers. We also need to address the issue of diode heatsinking, as we believe that we have not been able to adequately temperature tune the diode bar output to match the peak of the Nd:YAG absorption. This results in longer absorption lengths which can impair mode quality, as more pump light will be absorbed in the wings of the lasing mode, and reduces the overall efficiency of the laser.

There are a number of experiments which should be ideally suited to this end-pumping scheme, in particular low gain transitions in laser media such as Nd:YAG. The high gains possible with the small pump sizes our system produces should allow

wavelengths such as 1.3μm, 940nm, 1.8μm, and other low gain transitions to be operated as lasers relatively efficiently. With higher power diode pump sources (e.g. 20W diode bars, either used on their own or polarization coupled together), the prospects for frequency doubling, either intracavity or in an external cavity, look promising.

It is also hoped that we will be able to construct a unidirectional ring laser pumped by a laser diode bar, giving a high power single frequency source. Attention will have to be paid to residual spatial hole burning, as this may place upper limits on the maximum single frequency output power possible. It may be necessary to construct a ring laser where the gain medium does not lie in the overlap region of the laser mode. A stable, single frequency high power source such as this could be used as a source for frequency doubling. The eventual aim would then be to pump a cw optical parametric oscillator with this frequency doubled output, resulting in a compact, efficient, stable, tunable source of coherent radiation.

Appendix A
FABRY-PEROT ANALYSIS OF FEEDBACK MECHANISM

A feedback cavity for a ring laser (Fig A1 and section 2.5) can be considered to be equivalent to the Fabry-Perot ring cavity shown in Fig A2. In this analysis we shall examine the behaviour of the Fabry-Perot ring cavity and relate it to the manner in which the feedback cavity can produce a non-reciprocal effective diffraction loss different to the applied diffraction loss that depends on the phase shift in the cavity.

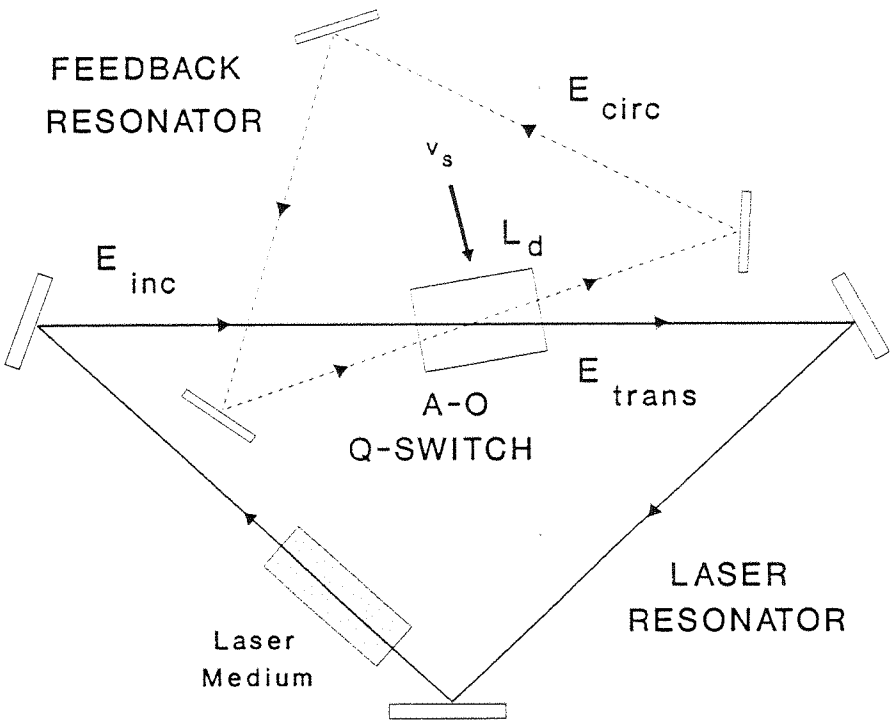

Fig A1. Ring laser with feedback cavity. Only one direction of propagation is shown for clarity. E_{inc} is the beam from the main laser cavity that enters the A-O modulator, E_{circ} is the diffracted circulating beam in the feedback cavity and E_{trans} is the total transmission through the modulator.

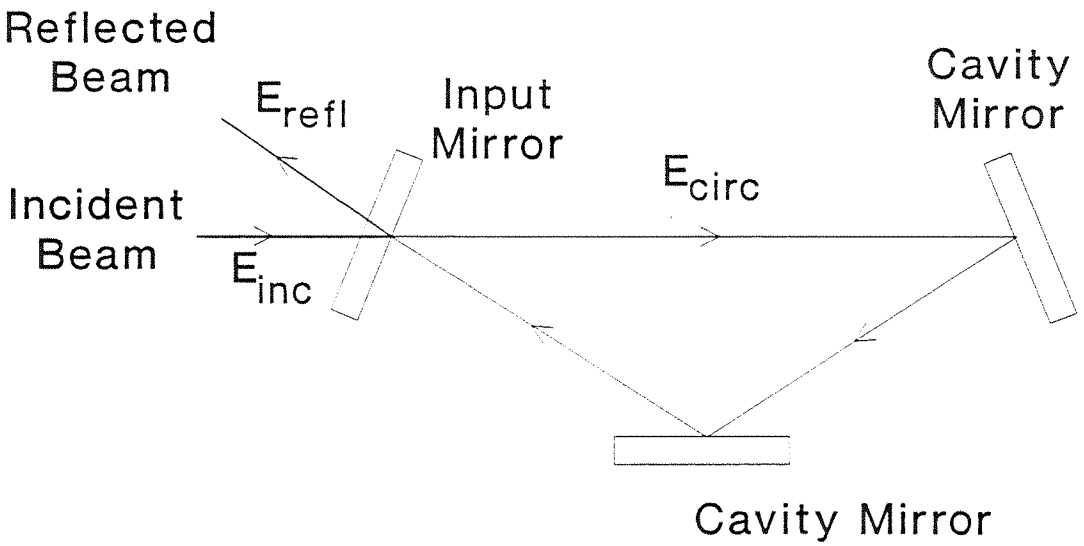

Fig A2. Equivalent Fabry-Perot ring cavity to the feedback cavity in Fig A1. E_{inc} and E_{refl} denote the incident and reflected amplitudes just outside the input mirror. E_{circ} is the circulating signal amplitude just inside the mirror.

We begin the analysis by noting that the single pass diffraction loss of the A-O modulator, L_d, can be related to the reflectivity of the Fabry-Perot input mirror, R_d, by

$$R_d = 1 - L_d \tag{A1}$$

where we assume that we have a lossless acousto-optic modulator (i.e. all incident light is either transmitted or diffracted into a first order beam). In this situation $L_d = T_d$, the Fabry-Perot mirror transmission, where $T_d = t_d^2$.

The amplitude reflectivity from the input Fabry-Perot mirror is given by $r_d = \sqrt{R_d}$, and is equivalent to the amplitude transmission of the laser beam through the A-O Q-switch. What we are seeking here is the effective diffraction loss, L_{eff}, at the output of the acousto-optic modulator (AOM). By analogy, this is found from the effective total reflection at the input mirror of the Fabry-Perot cavity:

$$R_{eff} = \frac{I_{refl}}{I_{inc}} = \frac{E_{refl} \cdot E_{refl}^*}{E_{inc}^2} = 1 - L_{eff} \tag{A2}$$

To complete the analogy between the feedback cavity and the Fabry-Perot cavity we recognize that:

(i) The amplitude of the laser beam that is diffracted and hence enters the feedback cavity is the same as the amplitude transmission of the incident beam entering the Fabry-Perot cavity, i.e. t_d

(ii) The amplitude of the resonated diffracted beam transmitted through the A-O modulator on re-entry to the modulator after one round-trip is equivalent to the amplitude reflectivity of the beam in the Fabry-Perot cavity reflected by the output mirror on each round trip, i.e. r_d'

(iii) The amplitude of the resonated diffracted beam being diffracted on re-entry to the A-O modulator and hence re-entering the main laser cavity is equivalent to the amplitude transmission of the recirculating beam that leaves the Fabry-Perot cavity after each round trip, i.e. t_d'.

With these reference points between the feedback resonator and a Fabry-Perot

cavity, we shall now examine the behaviour of the Fabry-Perot cavity to determine the effective total reflection from the input mirror of the Fabry-Perot. We shall use the notations and conventions of Siegman [1986], and assume that there is no internal attenuation of the beam in the Fabry-Perot cavity (i.e. $\alpha_0=0$ in his notation). The circulating amplitude just inside the Fabry-Perot cavity (and hence the feedback cavity) is given by

$$E_{circ}=jt_dE_{inc}+g_{rt}(\omega)E_{circ} \tag{A3}$$

where $g_{rt}(\omega)$ is the net complex round-trip gain (or loss) of the Fabry-Perot cavity. The net loss in this case is given by the reflectivity of the output mirror, r_d', the reflectivities of other mirrors completing the Fabry-Perot cavity, r_f, and the round-trip phase shift, $\exp(-i\omega\ell_f/c)$. In this phase shift term, ℓ_f is simply the length of the cavity, and the frequency takes on one of two values, depending on the direction of propagation considered. As the frequency in the feedback cavity is up- (or down-) shifted by the acoustic frequency ν_S, we can write the net round-trip gain term (changing from ω to ν) as

$$\begin{aligned} g_{rt}^{\pm}(\nu)&=r_d'r_f\exp\left(\frac{-j2\pi\ell_f(\nu\mp\nu_s)}{c}\right) \\ &=r_d'r_f\exp(-j\delta^{\pm}) \end{aligned} \tag{A4}$$

For ease of presentation δ will be used in future equations instead of $\delta^{\pm}$ until the final result is obtained. We can now calculate that the circulating field after one round trip of the Fabry-Perot cavity is

$$E_{circ}^{(1)}=E_{inc}t_dr_d'r_f\exp(-j\delta) \tag{A5}$$

and after n round trips:

$$E_{circ}^{(n)}=E_{inc}t_d(r_d'r_f)^n.\exp(-jn\delta) \tag{A6}$$

We now consider the total reflected electric field just outside the Fabry-Perot cavity, which is given by

$$E_{refl}=r_d E_{inc}+\frac{t_d g_{rt}(\nu)}{r_d'}E_{circ} \tag{A7}$$

where we divide by r_d', because the circulating beam is passing through the output mirror, rather than being reflected by it. Expanding (A7) we find

$$\begin{aligned}E_{refl}=&E_{inc}r_d+E_{inc}t_d t_d' r_f \exp(-j\delta)\\&+E_{inc}t_d t_d' r_f \exp(-j\delta)[r_f r_d'.\exp(-j\delta)]+...\end{aligned} \tag{A8}$$

and summing up all terms gives

$$E_{refl}=E_{inc}r_d+\frac{E_{inc}t_d t_d'}{r_d'}\sum_{n=0}^{\infty}(r_f.r_d')^n.\exp(-jn\delta)-\frac{E_{inc}t_d t_d'}{r_d'} \tag{A9}$$

where the summation can be reduced to

$$E_{refl}=E_{inc}r_d-\frac{E_{inc}t_d t_d'}{r_d'}+\frac{E_{inc}t_d t_d'}{r_d'}.\frac{1}{(1-r_d' r_f.\exp(-j\delta))} \tag{A10}$$

With this expression for E_{refl} we can calculate R_{eff} from (A2). Eventually we obtain:

$$R_{eff}=r_d^2-\frac{t_d t_d' r_d}{r_d'}+\frac{(t_d t_d' r_f)^2}{\gamma(\delta)}+\frac{t_d t_d' r_d}{r_d'\gamma(\delta)}.(1-(r_d' r_f)^2) \tag{A11}$$

where

$$\gamma(\delta)=1+(r_d' r_f)^2-2r_d' r_f\cos\delta \tag{A12}$$

We are now in a position to calculate the effective diffraction loss of the feedback cavity. The losses in the feedback cavity, L_f, are due to leakage through the feedback mirrors, material losses through the modulator, and can be expressed as

$$L_f=1-R_f=1-r_f^2 \tag{A13}$$

Clearly, $r_d = r_d' = \sqrt{R_d}$ as the input mirror must have the same reflectivity for beams passing in and out of the cavity, and likewise $t_d = -t_d'$. Using the fact that $L_{eff} = 1 - R_{eff}$ we obtain from (A11) that

$$L_{eff} = \frac{L_d(1-(1-L_d)(1-L_f)) - L_d^2(1-L_f)}{\gamma(\delta)} \tag{A14}$$

which, for L_d, $L_f \ll 1$ approximates to

$$L_{eff} \simeq \frac{L_d L_f}{\gamma(\delta)} \tag{A15}$$

$\gamma(\delta)$ can be simplified using the approximations that:

(i) $L_d L_f/4 \simeq 0$

(ii) $(L_d + L_f) \ll 16$

to give

$$\gamma(\delta) \simeq \frac{(L_d+L_f)^2 + 16\sin^2(\delta/2)}{4} \tag{A16}$$

If we now allow for counter-propagating beams with phase shifts δ^+ and δ^- we obtain the final expression for effective diffraction loss in the presence of a feedback cavity:

$$L_{eff}^{\pm} = \frac{4L_d L_f}{(L_d+L_f) + 16\sin^2\left(\frac{\pi \ell_f(\nu \mp \nu_s)}{c}\right)} \tag{A17}$$

L_d being the applied diffraction loss, and L_f the loss in the feedback cavity, excluding the diffraction loss.

Reference:

Siegman, A.E., *Lasers*, University Science Books, Chapter 11. (1986)

Appendix B

PUBLISHED PAPERS

The following papers have arisen from the work carried out in the course of this PhD, and have been written in collaboration with co-workers from the Optoelectronics Research Centre.

Journal Papers:

"*Explanation of the mechanism for acousto-optically induced unidirectional operation of a ring laser*", W.A. Clarkson, A.B. Neilson and D.C. Hanna, Optics Letters **17**, 601 (1992)

"*Acousto-optically induced unidirectional operation of a ring laser: A feedback mechanism*", W.A. Clarkson, A.B. Neilson and D.C. Hanna, Optics Communications **91**, 365 (1992)

"*Single Frequency CW and Q-Switched operation of a diode-pumped Nd:YAG 1.3μm ring laser*", A.B. Neilson, W.A. Clarkson and D.C. Hanna, Optics Letters, **18**, 1426 (1993)

Patent Applications:

"*A Stable Two Frequency Laser*", W.A. Clarkson, D.C. Hanna and A.B. Neilson, United Kingdom Patent Application No. 9304076.4 (1993)

"*Beam Shaping Device*", W.A. Clarkson, A.B. Neilson and D.C. Hanna, United Kingdom Patent Application, Filed November 1993.

Conference Papers:

"*Acousto-Optically Induced Single Mode and Q-Switched Operation of a Miniature Diode-Pumped Nd:YLF Ring Laser*", W.A. Clarkson, D.C. Hanna and A.B. Neilson, European Quantum Electronics Conference and Tenth UK National Quantum Electronics Conference, Edinburgh, 1991, Paper PLTu8.

"*Unidirectional ring laser operation via the acousto-optic effect: an explanation of the mechanism*", W.A. Clarkson, A.B. Neilson and D.C. Hanna, Advanced Solid-State Lasers Topical Meeting, Santa Fe, New Mexico, 1992, Paper TuA3.

"*Explanation of the mechanism for acousto-optically induced unidirectional operation of a ring laser*", W.A. Clarkson, D.C. Hanna and A.B. Neilson, Conference on Lasers and Electro-Optics (CLEO) '92, Anaheim, California 1992, Paper CMI1

"*Unidirectional operation of a ring laser by resonating the diffracted beams in a travelling-wave acousto-optic modulator*", W.A. Clarkson, D.C. Hanna and A.B. Neilson, CLEO '92, Paper CMI3

"*Stable Two-Mode Operation of a Unidirectional Ring Laser via Controlled Spatial Hole Burning*", W.A. Clarkson, D.C. Hanna, D.M. Kane, K.I. Martin and A.B. Neilson, CLEO '93, Baltimore, Maryland, Paper Cths15.

"*The effect of residual spatial hole burning in unidirectional ring lasers*", K.I. Martin, W.A. Clarkson, A.B. Neilson and D.C. Hanna, Eleventh UK National Quantum Electronics Conference, Belfast, 1993, Paper 1054.